

A Hybrid-Structure Offset-QAM Filter-Bank Multi-Carrier MIMO System

Aya Tarek Abou-Elkheir

School of Science, Engineering and Environment

Submitted in Partial Fulfilment of the Requirements of the Degree of Doctor of Philosophy

“To my parents, my role models, who are and will always be the reason for any success I achieve in life.”

TABLE OF CONTENTS

TABLE OF CONTENTS	III
ACKNOWLEDGEMENT	VI
LIST OF FIGURES	VII
LIST OF TABLES	X
LIST OF ACRONYMS	XI
LIST OF SYMBOLS	XV
ABSTRACT	XVII
1 INTRODUCTION	1
1.1 Introduction to OQAM/FBMC	1
1.2 Research Motivation & Problem Statement	3
1.3 Research Aim & Objectives	4
1.4 Research Process & Methodology	5
1.5 Thesis Contribution	5
1.6 Thesis Organization	6
2 RELATED WORK	7
2.1 Different OQAM/FBMC Implementation Techniques.....	7
2.1.1 Frequency Spreading (FS) FBMC.....	7
2.1.2 Polyphase Network (PPN) FBMC	9
2.1.2.1 Modified PPN FBMC.....	10
2.1.3 Other Complexity Reduction Methods.....	11
2.1.4 Reflection.....	12
2.2 Alamouti coding OQAM/FBMC	13
2.2.1 Reflection.....	14
2.3 PAPR Reduction of OQAM/FBMC signals.....	14
3 OVERVIEW OF MULTI-CARRIER WAVEFORMS	19
3.1 Why New Waveforms?.....	20
3.2 Candidate Multi-carrier Waveforms	23
3.2.1 Filter-Bank Multi-carrier (FBMC)	24

3.2.2	Universal Filtered Multi-carrier (UFMC).....	25
3.2.3	Filtered OFDM (f-OFDM)	28
3.2.4	Generalized Frequency Division Multiplexing (GFDM)	28
3.2.5	Non-orthogonal Multiple Access (NOMA).....	31
3.3	Multi-carrier Waveforms Comparison	33
3.4	FBMC in Literature	37
3.4.1	OQAM/FBMC Discrete System Model.....	38
3.4.2	Prototype Filter.....	39
3.4.3	Overlapping Factor	44
4	PROPOSED HYBRID OQAM/FBMC MIMO SYSTEM	46
4.1	FS-OQAM/FBMC SM/SFBC MIMO Model	47
4.1.1	Transmitter	47
4.1.2	Receiver	49
4.2	Hybrid OQAM/FBMC SFBC MIMO Model	51
4.2.1	PPN Transmitter	52
4.2.2	FS-FDE Receiver	54
4.2.3	PPN-TDE Receiver	58
4.3	BER Analysis.....	59
4.4	Computational Complexity Comparison	62
4.5	Simulation and Results.....	66
4.5.1	Channel Model	67
4.5.2	Analytical vs. Simulated BER performance.....	68
4.5.3	Power Spectral Density & Spectral Efficiency	69
4.5.4	BER performance of the proposed hybrid OQAM/FBMC MIMO System	72
4.5.4.1	<i>Effect of increasing the modulation order</i>	<i>73</i>
4.5.4.2	<i>Effect of increasing the MIMO order</i>	<i>74</i>
4.5.5	BER performance of the proposed PPN-TDE OQAM/FBMC System	77
4.5.6	BER performance of the proposed SM OQAM/FBMC vs. SFBC MIMO systems	78
4.5.6.1	<i>Effect of available bandwidth</i>	<i>80</i>
4.5.7	BER performance of the proposed OQAM/FBMC SFBC system in Rician channel	80
5	PROPOSED SC-OQAM/FBMC SYSTEM.....	83

5.1	SC-OQAM/FBMC MIMO System Model	83
5.1.1	Transmitter	83
5.1.2	Receiver	86
5.2	Additional Complexity	87
5.3	Simulation & Results	87
5.3.1	PAPR.....	88
5.3.2	PSD.....	90
5.3.3	BER.....	92
6	CONCLUSION	95
6.1	Summary	95
6.2	Conclusions.....	96
6.3	Future Work	97
	REFERENCES	98
	APPENDIX A: PUBLICATIONS	115
	APPENDIX B: ATTENDED TRAINING SESSIONS	116
	APPENDIX C: SAMPLE MATLAB CODE	117
1.	Hybrid OQAM/FBMC SFBC MIMO FDE vs. OFDM BER (Chapter 4)	117
2.	Hybrid SC-OQAM/FBMC MIMO BER (Chapter 5).....	120

ACKNOWLEDGEMENT

First and foremost, I must thank Allah the Almighty for giving me the strength and perseverance to complete this work, despite the circumstances which forced me to interrupt my study more than once.

I would like to thank my supervisor Dr. Omar Alani for his help, guidance, valuable feedback and continuous support throughout the research journey. I would also like to thank my local supervisor Prof. Ehab Badran (AAST) for his help, guidance, valuable feedback and our fruitful scientific discussions, which added to the value of my research. I could not have done it without them.

I would like to thank the Arab Academy for Science and Technology for sponsoring my PhD study at the University of Salford. I would also like to thank my colleagues at the department of Electronics and Communication Engineering (AAST) Dr. Tamer Badran and Dr. Nour Medany who have been my mentors. I would also like to thank Dr. Eman Galal for her help guiding me around the processes in Salford and in Manchester in general.

Finally, I would like to thank my family for their help, support and patience. First, special thanks to my mother who is my role model engineer, for her continuous prayers, encouragement, and help. Second, I would like to thank my young kids Alia and Abdelrahman, who endured a lot with me during the research journey and gave me the motive to continue to make them proud. And finally, my husband Hussein who is my number one supporter, I could not have done it without him.

LIST OF FIGURES

Figure 2-1: Explicit operation of the FS FBMC transmitter [5].	8
Figure 2-2: Explicit operation of the FBMC Frequency de-spreading FBMC receiver [5],[28].	9
Figure 2-3: FBMC transceiver using PPN.	10
Figure 2-4: Modified implementation of the PPN FBMC transmission for $K=4$ [39].	11
Figure 2-5: OQAM FBMC (a) without coding (b) with coding [52].	14
Figure 3-1: Multiple access techniques of cellular network generations.	19
Figure 3-2: CP-OFDM transceiver.	21
Figure 3-3: PSD of different neighbouring applications illustrating the effect of localized spectrum [105].	21
Figure 3-4: Alternative modulation and waveform requirements.	23
Figure 3-5: Waveform design trade-offs.	24
Figure 3-6: UFMC Transmitter block diagram.	26
Figure 3-7: PSD of (a) OFDM with 200 subcarriers. (b) UFMC with 8 blocks each with 25 subcarriers.	27
Figure 3-8: Filtered-OFDM transceiver structure.	28
Figure 3-9: GFDM modulator block diagram [117].	29
Figure 3-10: GFDM filtering operation illustration [117].	30
Figure 3-11: Cyclic prefix insertion in OFMD vs. GFDM.	30
Figure 3-12: OMA vs. power-domain NOMA for two UEs [123].	32
Figure 3-13: NOMA Downlink for two users [122].	32
Figure 3-14: PSD of the transmitted signals using different MC techniques.	34
Figure 3-15: CCDF of the PAPR of the transmitted signal of different MC techniques.	35
Figure 3-16: OQAM/FBMC system transceiver model [27].	38
Figure 3-17: Normalized time and frequency response of PHYDYAS and Hermite filters	41
Figure 3-18: PSD of OQAM/FBMC transmitted signal using different prototype filters	42
Figure 3-19: Normalized power over symbol duration of OQAM/FBMC with different prototype filters for $K = 4$	43
Figure 3-20: CCDF of PAPR of OQAM/FBMC system with different prototype filters with an overlapping factor of 4.	43

Figure 3-21: PSD of OQAM/FBMC transmitted signal using different K	44
Figure 3-22: PAPR of OQAM/FBMC transmitted signal using PHYDYAS prototype filters with different K	45
Figure 4-1: The proposed FS-OQAM/FBMC MIMO system transmitter.....	47
Figure 4-2: The proposed FS-OQAM/FBMC MIMO system receiver.....	50
Figure 4-3: The proposed hybrid OQAM/FBMC $P \times P$ MIMO system transmitter	52
Figure 4-4: The proposed FS-OQAM/FBMC $P \times P$ SFBC MIMO FDE receiver.....	55
Figure 4-5: The proposed PPN OQAM/FBMC $P \times P$ SFBC MIMO TDE receiver.....	58
Figure 4-6: Order of computational complexity for different OQAM/FBMC systems for $K = 2$	64
Figure 4-7: Number of real multiplications for different OQAM/FBMC systems for $K = 4$	65
Figure 4-8: (a) Random sample of the PDP of 7-tap Rayleigh fading channel (b) Random sample of the normalized frequency response of 7-tap Rayleigh fading channel.....	68
Figure 4-9: Analytical vs. simulated BER for hybrid OQAM/FBMC MIMO system using ZF-FDE in 7-tap Rayleigh fading channel.....	69
Figure 4-10: Normalized PSD of the proposed hybrid OQAM/FBMC system vs. CP-OFDM.	70
Figure 4-11: Percentage of enhancement in throughput efficiency FBMC over OFDM with variable $N_{cp}N$	71
Figure 4-12: BER of 4-QAM hybrid OQAM/FBMC 2×2 MIMO system vs. OFDM in 3-tap Rayleigh fading channel.	72
Figure 4-13: BER of 4-QAM hybrid OQAM/FBMC 2×2 MIMO system vs. OFDM in 7-tap Rayleigh fading channel.	73
Figure 4-14: BER of 16-QAM hybrid OQAM/FBMC 2×2 MIMO system vs. OFDM in 3-tap Rayleigh fading channel	74
Figure 4-15: BER of 4-QAM hybrid OQAM/FBMC 2×2 vs. 4×4 MIMO systems in 7-tap Rayleigh fading channel.	75
Figure 4-16: BER of M -ary QAM hybrid OQAM/FBMC 2×2 vs. 4×4 MIMO systems with MMSE in 7-tap Rayleigh fading channel.....	76
Figure 4-17: BER of OQAM/FBMC using hybrid-FDE vs. PPN-TDE structures in pedestrian channel A.	77
Figure 4-18: BER of 4-QAM OQAM/FBMC SM MIMO vs SM CP-OFDM in 3-tap Rayleigh fading channel.....	79

Figure 4-19: BER of 4-QAM OQAM/FBMC SM MIMO vs SFBC MIMO in 3-tap Rayleigh fading channel.....	80
Figure 4-20: BER of hybrid OQAM/FBMC 2×2 MIMO vs CP-OFDM in 5-tap Rician fading Channel.	81
Figure 5-1: Proposed SC-OQAM/FBMC MIMO transmitter model	84
Figure 5-2: Transfer function of HPA for different <i>Asat</i>	86
Figure 5-3: Proposed SC-OQAM/FBMC MIMO receiver model.....	86
Figure 5-4: PAPR of 4-QAM OQAM/FBMC vs. SC-OQAM/FBMC for IM and LM for $N=128$	89
Figure 5-5: PAPR of 16-QAM OQAM/FBMC vs. SC-OQAM/FBMC for IM and LM for $N = 128$. .	90
Figure 5-6: PSD of SC-OQAM/FBMC system vs. OQAM/FBMC with $K=4$, $N=128$, no HPA.	91
Figure 5-7: PSD of SC-OQAM/FBMC system vs. OQAM/FBMC with $K = 4$, $N = 128$, with HPA.	91
Figure 5-8: BER of 2×2 SFBC SC-OQAM/FBMC vs. OQAM/FBMC with MMSE FDE in 3-tap Rayleigh fading channel.	92
Figure 5-9: BER of 2×2 SFBC SC-OQAM/FBMC vs. OQAM/FBMC with MMSE FDE in 20-tap Rayleigh fading channel.	93
Figure 5-10: BER of 2×2 SFBC SC-OQAM/FBMC vs. OQAM/FBMC with MMSE FDE in 20-tap Rayleigh fading channel.	94

LIST OF TABLES

Table 2-1 Different OQAM/FBMC implementation techniques in literature	12
Table 2-2 OQAM/FBMC PAPR reduction methods in literature	16
Table 3-1 Multi-carrier Waveforms Simulation parameters	33
Table 3-2 Candidate Multi-carrier Waveforms Comparison	36
Table 3-3 Coefficients of the PHYDYAS prototype filter for different overlapping factors	40
Table 4-1 Total number of real multiplications of different OQAM/FBMC system structure.....	64
Table 4-2 Number of real multiplications for different number of subcarriers.	66
Table 4-3 OQAM/FBMC Simulation Parameters.	67
Table 5-1 SC-OQAM/FBMC Simulation Parameters	88

LIST OF ACRONYMS

3GPP	Third Generation Partnership Project
ACLR	Adjacent Channel Leakage Ratio
AWGN	Additive White Gaussian Noise
BER	Bit Error Rate
BS	Base Station
CCDF	Complementary Cumulative Distribution Function
CDMA	Code Division Multiple Access
CP	Cyclic Prefix
CS	Cyclic Suffix
CSI	Channel State Information
D2D	Device To Device
DAC	Digital-To-Analog Converter
DCT	Discrete Cosine Transform
DFT	Discrete Fourier Transform
EE	Energy Efficiency
FBMC	Filter-Bank Multi-Carrier
FDE	Frequency Domain Equalization
FDMA	Frequency Division Multiple Access
FFT	Fast Fourier Transform
FIR	Finite Impulse Response
FM	Frequency Modulation
f-OFDM	Filtered OFDM
FS	Frequency Spreading

GFDM	Generalized Frequency-Division Multiplexing
HPA	High Power Amplifier
ICI	Inter-Carrier Interference
IFFT	Inverse Fast Fourier Transform
IID	Independent Identically Distributed
IM	Interleaved Mapping
IMT	International Mobile Telecommunications
IoT	Internet Of Things
ISI	Inter-Symbol Interference
KPI	Key Performance Indicator
LM	Localized Mapping
LOS	Line Of Sight
LTE	Long Term Evolution
MC	Multi-carrier
MIMO	Multiple Input Multiple Output
MMSE	Minimum Mean Square Error
mmWave	Millimeter Wave
MTC	Machine Type Communications
NOMA	Non-Orthogonal Multiple Access
OFDM	Orthogonal Frequency Division Modulation
OFDMA	Orthogonal Frequency Division Multiple Access
OMA	Orthogonal Multiple Access
OOB	Out Of Band
OQAM	Offset Quadrature Amplitude Modulation

P/S	Parallel-To-Serial
PAPR	Peak To Average Power Ratio
PDP	Power Delay Profile
PHYDYAS	Physical Layer for Dynamic Access
PN	Phase Noise
PPN	Polyphase Network
PSD	Power Spectral Density
QAM	Quadrature Amplitude Modulation
RC	Raised Cosine
RF	Radio Frequency
RRC	Root Raised Cosine
S/P	Serial-To-Parallel
SC	Single Carrier
SE	Spectral Efficiency
SFBC	Space Frequency Block Coding
SI	Side Information
SIC	Successive Interference Cancellation
SISO	Single-Input Single Output
SLM	Selective Mapping
SM	Spatial Multiplexing
SNR	Signal-To-Noise Ratio
STBC	Space Time Block Coding
TDE	Time Domain Equalization
TDMA	Time Division Multiple Access

UE	User Equipment
UFMC	Universal Filter Multi-carrier
UHDTV	Ultra-High Definition Television
URLLC	Ultra-Reliable Low Latency Communications
V2X	Vehicle-to-everything
WSN	Wireless Sensor Networks
ZF	Zero Forcing
ZP	Zero Prefix

LIST OF SYMBOLS

N	Number of subcarriers
K	Overlapping factor
H_k	Prototype filter coefficients
$h(t)$	Prototype filter impulse response
$h(k)$	Sampled Prototype filter impulse response
T	Multicarrier symbol Duration
β	Equalization matrix
N_{CP}	Cyclic prefix length
P	Number of transmitting/receiving MIMO antennas
L_F	Prototype filter length
\mathcal{F}	Isometric Fourier transform matrix
L	$N \times K$
\mathbf{I}	Identity matrix
\mathbf{G}	MIMO multipath channel frequency response
\mathcal{H}	Prototype filter convolution matrix
η	Noise vector at the receiver input
L_H	Number of multipath channel taps
\mathbf{c}_{ji}	MIMO multipath channel coefficients
\mathbf{a}_{ji}	Time domain equalizer coefficients
P_b	Theoretical probability of error

m	Subcarrier index
M	QAM modulation order
n	Discrete-time index
N_c	Number of complex modulated symbols
$\mathbf{0}_K$	A $K \times K$ matrix of zeros
\mathbf{k}_n^M	A column vector of length M , with all-zero elements except the n^{th} element equal to one
\mathbf{CN}	Complex normal random variable
\mathbf{M}	Subcarrier mapping matrix
N_s	Length of symbol after subcarreir mapping
Q	Number of users

ABSTRACT

Offset quadrature amplitude modulation (OQAM) filter-bank multi-carrier (FBMC), has great potential for boosting the spectral efficiency (SE) and energy efficiency (EE) of future communication systems. This is due to its superior spectral localization, CP-less transmission and relaxed synchronization requirements. Our research focuses on three main OQAM/FBMC research problems: the computational complexity reduction taking equalization into consideration, its integration with multiple-input multiple-output (MIMO) and its high peak-to-average power ratio (PAPR). OQAM/FBMC systems are mainly implemented either using frequency spreading (FS) or polyphase network (PPN) techniques. The PPN technique is generally less complex, but when using frequency domain equalization (FDE) to equalize multipath channel effects at the receiver, there is a computational complexity overhead when using PPN. A novel hybrid-structure OQAM/FBMC MIMO space-frequency block coding (SFBC) system is proposed, to achieve the lowest possible overall complexity in conjunction with FDE at the receiver in frequency selective Rayleigh fading channel. The Alamouti SFBC block coding is performed on the complex-orthogonal signal before OQAM processing, which resolves the problems of intrinsic interference when integrating OQAM/FBMC with MIMO. In better multipath channel conditions with a line-of-sight (LOS) path, a zero-forcing (ZF) time domain equalization (TDE) is exploited to further reduce the computational complexity with comparable performance bit-error-rate (BER). On the other hand, to tackle the high PAPR problem of the OQAM/FBMC system in the uplink, a novel single carrier (SC)-OQAM/FBMC MIMO system is proposed. The system uses DFT-spreading applied to the OQAM modulated signal, along with interleaved subcarrier mapping to significantly reduce the PAPR and enhance the BER performance over Rayleigh fading channels, with relatively low additional computational complexity compared to the original complexity of the FBMC system and compared to other FBMC PAPR reduction techniques.

The proposed hybrid-structure system has shown significant BER performance in frequency-selective Rayleigh fading channels compared to OFDM, with significantly lower OOB emissions in addition to the enhanced SE due to the absence of CP. In mild multipath fading channels with a LOS component, the PPN OQAM/FBMC MIMO using TDE has a comparable BER performance

with significantly less computational complexity. As for the uplink, the SC-OQAM/FBMC MIMO system significantly reduces the PAPR and enhances the BER performance, with relatively low additional computational complexity.

1 INTRODUCTION

1.1 Introduction to OQAM/FBMC

Multi-carrier (MC) modulation is a key factor in meeting the enormous data rates and the massive connectivity promised by future communication networks [1]. Orthogonal frequency division multiplexing (OFDM) has been the dominating MC modulation in most wireless networks, due to its robustness in frequency-selective channels and ease of implementation [2], [3]. However, to address some drawbacks of OFDM, including the need for CP and the strict synchronization requirements, research is ongoing for alternative MC techniques, to succeed or co-exist with OFDM in future networks. The research towards spectrum localized MC waveforms which enhance the systems SE, enable the exploitation of fragmented spectrum, and relax the synchronization requirements, resulted in multiple OFDM-based waveforms. These waveforms include filtering-based techniques such as filter-bank multi-carrier (FBMC), universal filtered multi-carrier (UFMC), filtered-OFDM (f-OFDM) and generalized frequency division multiplexing (GFDM), which were all considered candidate 5G waveforms [4].

In FBMC, each subcarrier is individually filtered using a frequency-shifted version of a prototype filter. As a result of filtering, the subcarriers become strictly band-limited but the mutual complex-orthogonality is lost. However, real-orthogonality is retained when using offset quadrature amplitude modulation (OQAM) with FBMC [5]. OQAM/FBMC has immense potential for boosting the SE of communication systems, due to its superior spectral localization and CP-less transmission [6]. Unlike OFDM, which uses rectangular pulses with high out-of-band (OOB) emissions, OQAM/FBMC uses specially designed localized time-frequency filters to shape the subcarriers, resulting in extremely low OOB emission [7], [6]. This makes it especially suitable for applications which exploit fragmented spectrum [8], [9], such as internet-of-things (IoT) applications in FM radio bands and TV white spaces [10], [11]. In addition, the low OOB emission reduces the required guard bands thus increasing the SE [12], and efficiently supporting different usage scenarios within the same frequency band [13].

In addition to its ability to increase the SE, OQAM/FBMC is particularly suitable for asynchronous transmission scenarios [14], [15], [16]. Due to its highly localized subcarriers, OQAM/FBMC is more robust against synchronization errors and carrier frequency offsets (CFO) and thus has relaxed synchronization requirements compared to OFDM [2], [17], [14]. The complexity of the synchronization process and the energy involved can thus be reduced enhancing the energy efficiency (EE). This makes OQAM/FBMC suitable for usage in scenarios which involve simple energy-constrained devices, sporadically transmitting data with no sophisticated synchronization capabilities as in some Internet of things (IoT) scenarios [2]. The use of OQAM/FBMC in such scenarios enhances the EE and increases the robustness against timing and frequency offsets [18], [19], [20].

Considering compatibility with other current and future networks technologies, OQAM/FBMC was investigated for implementation in millimeter (mm)-wave MIMO systems [21], [22]. Furthermore, studies show the ability of FBMC to co-exist with existing OFDM-based networks [4], [23], [22]. On the other hand, it has been studied in the context of massive MIMO [24], [25], [26], [27]. In brief, OQAM/FBMC is a robust MC modulation candidate, suitable for deployment in various scenarios of future heterogeneous wireless networks.

In OQAM/FBMC systems, the FBMC modulation is implemented using either frequency spreading (FS) or polyphase network (PPN) techniques [5], [28]. In the frequency spreading (FS) method, filtering is performed in the frequency domain on the upsampled signal before the inverse fast Fourier transform (IFFT) operation at the transmitter [5]. In the PPN FBMC method, filtering is performed in the time domain after the IFFT transmitter operation. The PPN implementation is generally less complex than FS, since filtering is performed on the lower rate signal and an IFFT of size N is required, where N is the number of subcarriers. On the other hand, in FS an IFFT of size NK is required, where K is the upsampling and the overlapping factor.

When using FDE to equalize multipath channel effects, the received signal needs to be first converted to frequency using NK -point FFT. When using the PPN receiver where filtering is performed in the time domain, the signal after equalization must be converted back to the time domain using an additional NK -point FFT, before PPN-FBMC demodulation. Thus, when using FDE with PPN receivers, there is an overhead of two NK -point FFTs. The proposed hybrid-

structure OQAM/FBMC FDE transceiver resolves this issue, where the transmitter is implemented using the PPN technique, and the receiver is implemented using the FS technique, thus reducing the overall complexity in conjunction with FDE.

1.2 Research Motivation & Problem Statement

The research motivation stems from the importance of MC waveform design in the evolution of communication networks. There is still a research gap before new MC waveforms could succeed or co-exist with OFDM in future networks. We identified the research problems concerning OQAM/FBMC, and our work focuses on three points summarized as follows.

First, as multiple-input multiple-output (MIMO) and massive MIMO are an integral part of current and future mobile communication networks, the research for integrating OQAM/FBMC in MIMO systems is of crucial importance. Integration of MIMO and OQAM/FBMC systems has always been a challenge, due to the imaginary interference in the OQAM/FBMC symbols, since the signal is only real-orthogonal, while the Alamouti space-time block coding (STBC) MIMO requires complex orthogonality. Our first research problem was finding an efficient method for implementing Alamouti coding with OQAM/FBMC.

Second, although PPN FBMC is less complex, frequency domain equalization (FDE) required to efficiently equalize multipath channel effects is easier to perform on FS-FBMC signal [29], and FS-FBMC is considered an extension to OFDM [5], [30]. Our second research problem was to exploit this point in the structure of the proposed hybrid-structure OQAM/FBMC MIMO system, where the transmitter is implemented using the PPN technique, and the receiver is implemented using the FS technique. Thus reducing the overall complexity in conjunction with FDE and obtaining the best BER performance in frequency-selective Rayleigh fading channels. Furthermore, in multipath channels where a LOS path exists, which is the case for some IoT applications and device-to-device D2D communication [15], [31], [32], a PPN-TDE system is proposed to further reduce the complexity of the system.

Third, OQAM/FBMC systems, just like all MC signals suffer from a high peak-to-average power ratio (PAPR) due to the summation of independent information carried on different subcarriers [33]. In the uplink scenario at battery-operated UE, the high PAPR transmitted signal

is energy inefficient due to the high power required by the high-power amplifier (HPA), as the last stage of the transmitter, to operate in the linear region. Our third research problem was finding a method to reduce the PAPR of the OQAM/FBMC MIMO signal with relatively low additional computational complexity.

1.3 Research Aim & Objectives

Our research aims at finding a comprehensive novel solution for OQAM/FBMC efficient implementation, integration with MIMO, and PAPR reduction, which bridges the research gap enabling future communication networks from benefitting from its underlying potential of boosting the SE and EE.

The research objectives include:

- Investigating and comparing different OQAM/FBMC realization methods and prototype filter designs.
- Comparing OQAM/FBMC to OFDM using key performance indicators (KPI) including OOB emission, PAPR, SE and complexity.
- Testing the efficiency of the proposed hybrid OQAM/FBMC system in different multipath channels using FDE and TDE.
- Finding the optimum solution to integrate OQAM/FBMC with MIMO and minimizing the intrinsic interference problem.
- Obtaining an analytical BER formula for OQAM/FBMC ZF-FDE MIMO system with M-ary QAM modulation.
- Finding the best possible realization for the OQAM/FBMC MIMO system in terms of overall complexity and BER via the proposed hybrid system.
- Reducing the PAPR of OQAM/FBMC via the proposed SC-OQAM/FBMC structure.
- Preparing a robust MATLAB code to simulate and test different aspects and realization techniques of the OQAM/FBMC MIMO system at the signal processing level.

1.4 Research Process & Methodology

Our research used a scientific quantitative research methodology, which utilizes mathematical models based on hypotheses, theories, and simulations. Our methods are mathematical analysis and computer simulation using MATLAB software. Initially, the Vienna 5G Link Level simulator [34], which is a MATLAB-based toolbox, was used for simulation and comparisons of OFDM-based MC waveforms in chapter 2. Afterwards, in chapters 4 and 5, our MATLAB codes were developed and continuously modified to simulate the OQAM/FBMC system and control all its various aspects and parameters on a signal processing level, to test the proposed solutions according to KPIs. A sample of the MATLAB scripts used for each chapter is provided in the appendix.

The research process started with reviewing all 5G modern technologies and building a comprehensive overview and comparison of all new MC waveforms. After OQAM/FBMC was chosen, its major research gaps were identified, before determining the research problems and suggesting the proposed solutions via the proposed models. Finally, the proposed models were tested to see if the desired gains were achieved.

1.5 Thesis Contribution

The thesis contributions can be summarized as follows:

- Proposing a novel structure for implementing Alamouti space-frequency block coding (SFBC) MIMO with OQAM/FBMC, avoiding the effects of the intrinsic interference and obtaining promising results compared to other Alamouti application techniques to OQAM/FBMC.
- Reducing the complexity of the OQAM/FBMC MIMO system using the proposed hybrid structure, which exploits a novel aspect of complexity reduction, in which the transmitter uses the PPN structure, and the receiver uses the FS structure in conjunction with FDE.

- Providing two equalization options including FDE and TDE for the OQAM/FBMC system depending on the operation scenario and the multipath channel conditions, thus maintaining the least complexity for the desired application.
- Finding a novel effective method to apply the SC concept within the OQAM/FBMC signal in the uplink scenario, via the proposed SC-OQAM/FBMC system, thus reducing the PAPR and enhancing the BER performance.

1.6 Thesis Organization

The thesis is divided into six chapters, which are organized as follows:

- **Chapter 1** presents an introduction to OQAM/FBMC and its importance in future networks, followed by the thesis motivation and problem statement, our research objectives, research methodology, contribution and finally thesis organization.
- **Chapter 2** presents the literature review of the related work to the three OQAM/FBMC research problems identified: Different implementation structures and complexity reduction techniques, integration with MIMO and PAPR reduction.
- **Chapter 3** presents an overview of new waveform-design aspects and a brief system description of new MC waveforms. In addition, MC OFDM-based waveforms are simulated and comparison from various aspects. This chapter is concluded with a detailed description of different OQAM/FBMC system aspects.
- **Chapter 4** presents the proposed hybrid OQAM/FBMC SFBC MIMO system and its mathematical model, followed by BER and complexity analysis, and concluded with the simulation results. It also presents the spatial multiplexing (SM) system model and the PPN-OQAM/FBMC TDE system model.
- **Chapter 5** presents the proposed SC-OQAM/FBMC system for uplink along with its mathematical model, complexity analysis and results.
- **Chapter 6** presents the thesis summary, conclusions and possible future work.

2 RELATED WORK

This chapter presents a summary of the literature review and recent related work on the addressed research problems of OQAM/FBMC systems. It is divided into three sections each dedicated to one of the three main aspects tackled by the proposed systems presented in the following chapters. First, different structures for implementing the OQAM/FBMC modulation are discussed including FS, PPN and other techniques which aim at reducing the computational complexity. Second, a review of MIMO implementation methods with OQAM/FBMC is described. Finally, different techniques for PAPR reduction in OQAM/FBMC systems are discussed. At the end of each section, the differences between the existing methods and our proposed solutions are highlighted.

2.1 Different OQAM/FBMC Implementation Techniques

The main implementation methods for FBMC are the FS and the PPN approaches. In the PPN method, the filtering is performed in the time domain after the N -IFFT block, where N is the number of subcarriers. In the FS method, filtering is performed first, in the frequency domain before the KN -IFFT block, where K is the FBMC symbol overlapping factor. The PPN approach is generally less complex, while the FS approach shows better performance when combined with FDE. This section demonstrates both methods and their variants present in literature.

2.1.1 Frequency Spreading (FS) FBMC

The FS technique was first introduced by the PHYDYAS project in [5]. The FS name comes from the spreading of the input data, which is carried by one subcarrier in OFDM, over a number of points equal to the prototype filter length of $2K - 1$, where K is the overlapping and the upsampling factor as well. This spreading is achieved by applying the prototype filters' frequency coefficients on the upsampled input signal $d(nM)$, then applying the output to an IFFT of length NK , thus filtering is applied in the frequency domain signal before the IFFT. Afterwards, the symbols are overlapped and added according to the overlapping factor K , to generate the transmitted FBMC symbol. Figure 2-1 displays the operation of the FS transmitter approach for $K = 4$ [5], [28], which is adopted in the initial system in section 4.1.1.

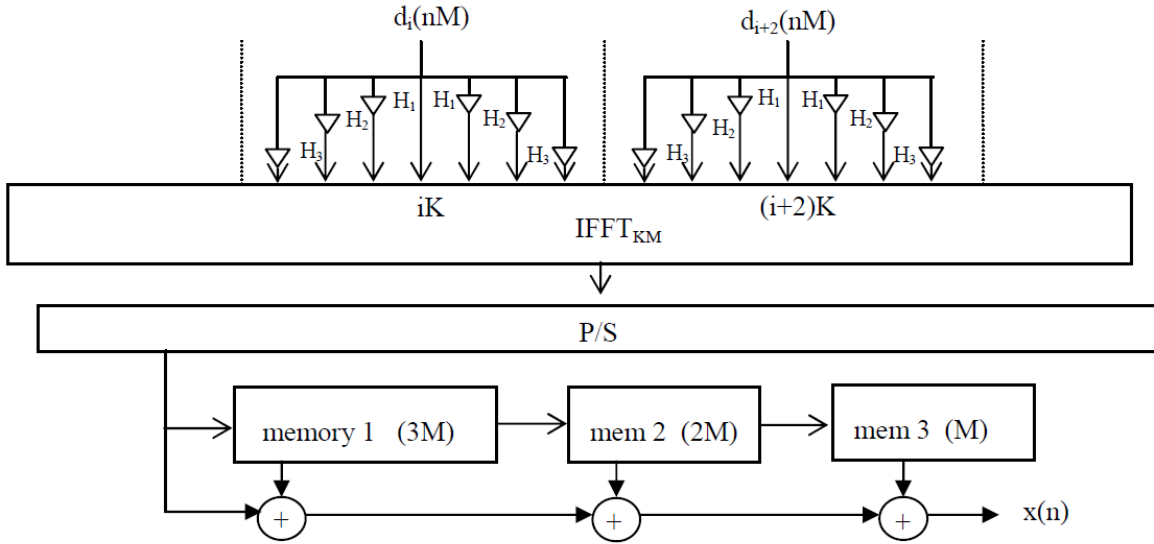


Figure 2-1: Explicit operation of the FS FBMC transmitter [5].

In the figure, M is the number of subcarriers. The even symbols $d_i(nM)$ and $d_{i+2}(nM)$ are the even data symbols upsampled by K , therefore they are $2K$ -points spaced therefore there is no overlap between them. Each symbol only overlaps with its immediate neighbour, ie. $d_i(nM)$ overlaps with $d_{i+1}(nM)$ and so forth. This is why OQAM processing is used, where a phase shift is introduced between the even and odd symbols, keeping them orthogonal in the real domain. For example, the even symbols $d_i(nM)$ and $d_{i+2}(nM)$ are real while the odd ones $d_{i+1}(nM)$ and $d_{i+3}(nM)$ are imaginary. This method needs $K - 1$ memory elements to perform the overlap-and-add operations.

An additional feature of the FS technique is the flexibility to change the overlapping factor K , for a constant FFT length of NK . For example, we can implement a $K = 4$, $N = 64$ FS-FBMC system using the same FFT as a $K = 2$, $N = 128$ system. The real and imaginary parts of the OQAM modulated symbols can either be processed together using a $2NK$ -point IFFT, or are separately treated on two separate branches each with an NK -point FFT, and added at the transmitter end [35], [36].

The corresponding frequency de-spreading receiver operation is demonstrated in Figure 2-2. After the serial-to-parallel (S/P) conversion, the reverse FS operations are performed to recover the upsampled symbols $d_i(nM)$, which are next downsampled by K to recover the transmitted symbols.

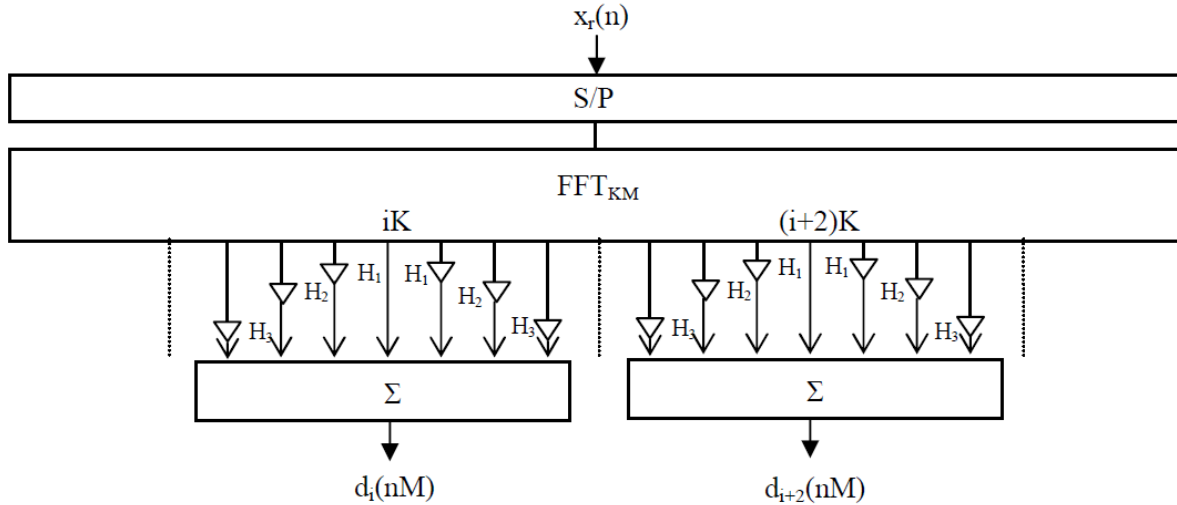


Figure 2-2: Explicit operation of the FBMC Frequency de-spreading FBMC receiver [5],[28].

As can be seen from the figure, the first step of the FS receiver is the FFT converting the signal to the frequency domain. Therefore, in frequency-selective multipath channels, equalization can be easily performed in the frequency domain (FDE). The problem of the FS FBMC technique lies in the complexity of the NK -point IFFT in the transmitter and the corresponding FFT at the receiver, this is reduced by the PPN approach.

2.1.2 Polyphase Network (PPN) FBMC

The PPN FBMC approach efficiently exploits the redundancy in the FS filtering operation to reduce the computational complexity. The PPN implementation of the FBMC transceiver was first proposed in [37]. Unlike the FS method, the N -point IFFT is performed first on the OQAM modulated symbols, then filtering is performed using an N -component polyphase filter network. The polyphase filter network consists of N frequency shifted versions of the prototype filter, each centered at the frequency of the n^{th} subcarrier. Since all the filters have the same transfer function, with only frequency shifts which translate into phase shifts, this filter structure is called a polyphase filter network (PPN). The PPN FBMC implementation forms a synthesis filter-bank at the transmitter and an analysis filter-bank at the receiver, which is the original filter-bank idea, as displayed in Figure 2-3.

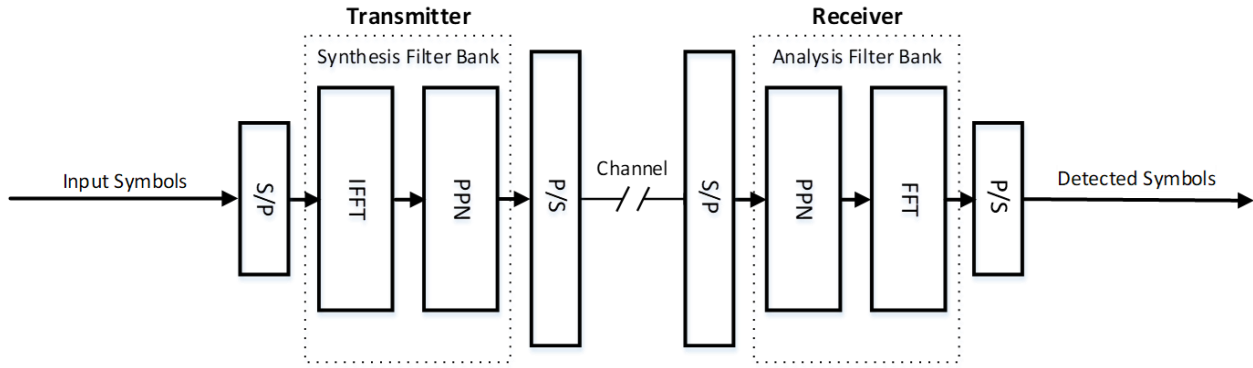


Figure 2-3: FBMC transceiver using PPN.

The main advantage of the PPN implementation is that the NK -point FFT of the FS technique is replaced by N -point FFT, since it is performed on the lower rate signal before filtering and upsampling, and thus the computational complexity is significantly reduced. However, the application of FDE at the receiver, when the signal is transmitted over frequency-selective multipath fading channels, on the received signal is not straightforward. This is due to that the PPN is the first block of the PPN-FBMC receiver, as shown in the transceiver block diagram of the PPN-FBMC in Figure 2-3. The same figure also shows another main merit of the PPN implementation, that it is an extension to the original OFDM system, with the PPN filtering block added and the CP-insertion/removal blocks removed.

2.1.2.1 Modified PPN FBMC

Modifications to the FS and the PPN FBMC methods have been proposed in literature to further reduce the FBMC implementation complexity. The most important modification was that proposed in [38], [39], and [21] for PPN FBMC implementation. Figure 2-4 illustrates the operation of the modified PPN method for $K = 4$, which is adopted in the transmitter of our proposed model with slight modification. After the N -point IFFT, which is the first block of the PPN-FBMC transmitter, the N -point frame is duplicated and appended K -times, forming an NK -point symbol. Afterwards, the filter is applied through point-by-point scalar multiplication of the duplicated symbol by the oversampled impulse response of the prototype filter of length NK . Afterwards, the resulting filtered symbol is shifted by N (overlapped), and added to the previously obtained symbol, producing the current FBMC symbol and so forth.

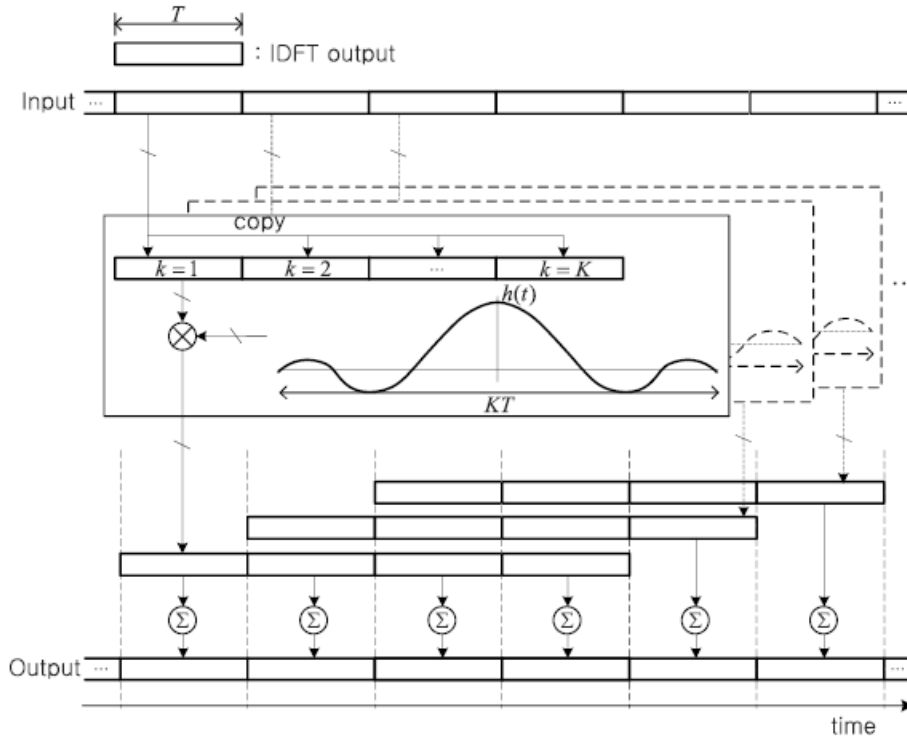


Figure 2-4: Modified implementation of the PPN FBMC transmission for $K=4$ [39].

This method reduces the computational complexity of the PPN network to only that of an N -point FFT plus the complexity of the NK multiplication. Furthermore, the memory elements required are reduced to only one element. On the other hand, the latency is reduced as well since each symbol is demodulated at the transmitter with the knowledge of the previous symbol only, instead of $K - 1$ symbols.

2.1.3 Other Complexity Reduction Methods

In [41], [42] and [43], a comparison of the computational complexity of the previously mentioned implementations is presented. Other techniques for complexity reduction of the FBMC systems were proposed in literature. In [44] the conjugate symmetry between the FFT outputs was exploited to reduce the complexity of PPN-FBMC by half using pruned FFT, which was later adopted in [45]. In [35], hopping discrete Fourier transform (DFT) is proposed for FS-FBMC to reduce complexity, but at the expense of an introduced processing delay. In [46], [36], the real and imaginary parts of the FS-OQAM/FBMC signal are processed in parallel on two branches each with a separate FFT, to reduce the FFT size and thus reduce the required complex

multiplications. A summary of the OQAM/FBMC modulation transceiver implementation and complexity reduction techniques in literature is presented in Table 2-1.

Table 2-1 Different OQAM/FBMC implementation techniques in literature

Method	References	Technique	Year
FS	[28] , [43]	Original FS	2012, 2014
	[47] , [35]	Hopping DFT instead of FFT	2019, 2021
PPN	[38] , [39]	Modified-PPN	2013, 2018
	[38]	Recursive DFT instead of FFT	2013
	[44] , [45] , [39], [46]	Two-branch PPN	2011, 2016, 2018, 2021

2.1.4 Reflection

All of the previous work used the same implementation for both the transmitter and receiver. In fact, all the complexity reduction techniques of OQAM/FBMC tackled the issue from the aspect of reducing the complexity of the FFT/IFFT process itself. In our model, we tackle the problem from a different point of view. In the proposed model, a hybrid implementation of the OQAM/FBMC MIMO system is proposed in which the transmitter is implemented using the less complex PPN approach and the receiver using FS. The hybrid implementation reduces the overall computational complexity when using FDE in Rayleigh fading channel. This way the transmitter benefits from the PPN's lowest possible computational complexity, and the FS receiver has the lowest computational complexity when combined with FDE, in addition to the enhanced performance, without additional processing or delays. Moreover, in better channel conditions with a LOS path, a simple TDE equalizer is suggested with the all PPN-OQAM/FBMC system, to significantly reduce the overall complexity by benefiting from the less complex PPN approach in both the transmitter and receiver, without sacrificing performance. The FFT complexity reduction techniques which don't introduce additional delays are compatible and suitable for use in our proposed systems.

2.2 Alamouti coding OQAM/FBMC

One challenge for OQAM/FBMC systems is the effect of the intrinsic ICI upon integration with MIMO. OQAM/FBMC maintains real orthogonality for subcarriers and the interference of the overlapped symbols becomes pure imaginary. By proper filter design, interference is simply removed at the receiver by taking the real part of the received symbols. On application with MIMO, inter-antenna ICI occurs as ICI between the subcarrier transmitted from one TX antenna and the adjacent subcarriers transmitted from others. Alamouti coding as a spatial diversity (SD) technique [48], aims at reducing the BER by sending dependent (coded) data streams from the transmitting antennas. On the other hand, SM aims at increasing the data rate by sending independent data streams on different transmitting antennas [49].

The Alamouti-coded FBMC was proposed in [50] and [150]. The combination of FBMC with Alamouti space-time block coding (STBC) has been first studied in [150], which proposed a block-wise Alamouti coding scheme with 2 transmitting and 1 receiving antennas. The transmission blocks were separated in frequency by inserting guard bands, and in time by inserting a guard interval. In [51], the block-wise scheme proposed in [150] was further examined and extended to a 2x2 MIMO system. Another approach was proposed in [52], which suggested spreading blocks of FBMC symbols in time or frequency using Hadamard matrices, to eliminate the imaginary interference. The FBMC symbols were divided into blocks with guard intervals inserted to avoid interference between blocks. More recently in [53], Discrete Fourier Transform (DFT) spreading was combined with Alamouti FBMC to reduce the PAPR. In [54], a receiver for Alamouti FS-FBMC was proposed in which Alamouti decoding is performed before frequency de-spreading. As for the OQAM/FBMC SM system, it was presented in [55] which suggested an MMSE and maximum likelihood receiver for 2×2 MIMO. In [56] the performance of soft decision linear receivers for SM OQAM/FBMC was examined. More recently in [p38], a block-wise Alamouti code was proposed for OQAM/FBMC, but with repeated blocks to remove the imaginary interference.

An iterative interference cancellation approach was proposed in [57] while in [58] several IDFT/DFT blocks are added to the transceiver to eliminate the intrinsic interference. These approaches significantly increase the complexity of the system [50].

More recently, a low complexity MIMO solution was proposed in [52], using Hadamard matrix spreading, cancelling the intrinsic interference. In [59] the MSE performance of linear receivers for MIMO FBMC is investigated. In [60], [61] multi-tap equalizers are suggested to enhance the performance, which in turn has an increased complexity.

Another method to solve the intrinsic interference problem in OQAM/FBMC MIMO is that proposed in [52] and [62]. It suggests spreading the FBMC symbols in time or in frequency to make them orthogonal in the code domain, thus eliminating the intrinsic interference between OQAM/FBMC symbols, therefore enhancing the performance when integrated with massive MIMO systems. Figure 2-5 shows the basic idea of the approach plotted through a 3D plot of FBMC symbols in time and frequency with spreading (a) compared to the original FBMC (b).

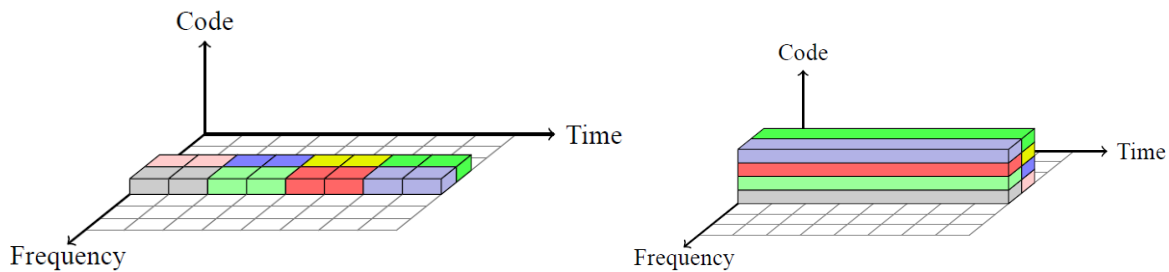


Figure 2-5: OQAM FBMC (a) without coding (b) with coding [52].

2.2.1 Reflection

All of the previous methods which suggest methods for implementing Alamouti MIMO coding with OQAM/FBMC systems solve the real-orthogonality problem either by introducing guard intervals in time, guard subcarriers in frequency, or introducing a new orthogonality dimension such as code. Others deploy time reversal of symbols blocks, which essentially introduces additional latency at both the transmitter and receiver. These processes alter the nature of the OQAM/FBMC signal and consequently sacrifice some main advantages of OQAM/FBMC modulation including superior spectral localization and high spectral efficiency.

2.3 PAPR Reduction of OQAM/FBMC signals

All MC modulation techniques result in inevitably high PAPR signals compared to SC techniques. This is due to the summation of independent information carried on different

subcarriers, resulting in high power fluctuations. A simulated comparison of the PAPR of various OFDM-based MC modulation techniques, including OQAM/FBMC was presented in Section 3.3, showing that OQAM/FBMC has a slightly higher PAPR compared to CP-OFDM, due to the overlapping of symbols in time, according to the overlapping factor K . As K increases, this means more symbols overlap in time resulting in higher PAPR. However, compared to the original PAPR of OFDM, the increase in the PAPR due to increasing K is small.

The problem with the high PAPR signal lies in the non-linearities of the practical HPA and the limited dynamic range (resolution) of digital-to-analog converters (DAC), which are the last parts of the transmitter, leading to transmitted signal clipping or distortion. The power efficiency of the HPA is inversely proportional to the PAPR [63]. In other words, as the PAPR of the transmitted signal increases, the power required to operate the HPA in the linear region increases, thus degrading the system's EE. This forms a major problem for the battery-limited UE in the uplink, where the output power is limited. For a high PAPR signal, the non-linearities of the HPA cause cross-modulation distortion for the subcarriers in the MC modulation technique, thus degrading the system performance. The effects of the HPA on the system performance increase as communication systems head towards operation in the mmWave bands [64], [65], [66], [67].

There are various techniques when it comes to the PAPR reduction of OQAM/FBMC signals, which are similar to the techniques used for PAPR reduction of OFDM but modified to suit the real-orthogonal, overlapped, pulse-shaped nature of the OQAM/FBMC signal [68]. These methods include traditional methods like clipping and companding [69], [70]. Other side information (SI)-based techniques like selective mapping (SLM) [71], [72], [73] and partial transmit sequence (PTS) [74], [75]. Recent techniques involve precoding using matrices such as DFT or discrete cosine transform (DCT). Some techniques involve a combination of the previous methods as in [76], [77], [78], [59], [79], [80], [81] and [82]. The following table shows a categorized summary of all the different OQAM/FBMC PAPR reduction techniques presented in literature.

Table 2-2 OQAM/FBMC PAPR reduction methods in literature

Technique	References	Highlight	Year
Clipping	[83]	Cancel peak by band-limited cancel pulse EVM and ACLR	2016
Companing	[69], [70]	Nonlinear companing transform	2018
SI - based	[71], [72]	Trellis based SLM	2018
	[73]	conversion vector-based low-complexity SLM	2020
	[74]	Cuckoo search optimization algorithm PTS	2017
DFT - spreading	[84]	SC-FDMA for FBMC	2010
	[85]	Error Performance of precoded FBMC/OQAM	2012
	[86]	Pruned DFT-spreading	2018
	[39]	Low PAPR FBMC	2018
	[87]	Alamouti Coding for Low PAPR FBMC	2019
	[88]	Generalized DFT for FBMC	2019
	[89]	Decision Feedback Equalizers and Alamouti Coded - DFT Spread	2020
	[90]	single sideband (SSB) pruned (DFT)-spreading	2020
[91]	Generalized DFT for FBMC	2022	
Hybrid Techniques	[78]	Tone Injection + Companing	2015
	[77]	Hadamard Transform + randomly assigning prototype filters.	2017
	[76]	DST + A-law nonlinear companing	2017
	[92]	DFT spreading with SI	2020
	[59]	DST/DCT +Clipping/Companing	2020
	[79]	Hybrid SLM and PTS	2021
	[81]	DFT spreading + SLM	2021
	[82]	Shaping code in conjunction with DCT	2021

The various techniques for PAPR reduction described in the above table each has its merits and drawbacks. The techniques like SLM and PTS, which depend on searching for the best candidates over the overlapped FBMC symbols, have the overhead of SI which reduces the SE and ruins one of the main FBMC merits of CP-less transmission by adding another overhead. Furthermore, the application of these techniques to the OQAM/FBMC signal requires more complex systems due to the overlapped FBMC symbol nature.

Other DFT-spreading-based approaches for PAPR reduction of OQAM/FBMC signal which depend on precoding are generally less complex than the previous techniques, without the overhead of SI. However, directly applying the SC concept to the FBMC signal does not achieve the same results as applying it to OFDM [39]. The enhancement in the PAPR was only marginal as in [84], due to the overlapping structure of the in-phase and quadrature neighbouring subcarriers, which makes the FBMC signal only real-orthogonal [85], [88]. Solutions for this problem have been proposed in recent literature, but they mainly come at the expense of computational complexity.

The most referenced solution is the low PAPR OQAM/FBMC proposed in [39]. Variants of the same system were proposed in [87] for Alamouti coding system, [92] for additional embedded SI and [89] with decision feedback equalizers. The basic idea of the low PAPR FBMC is to apply a special condition for the phase shift for each subcarrier $\theta_{m,n}$, to make use of the SC effect of DFT spreading. However, the PAPR reduction gain achieved by applying the phase shift condition alone is not significant, offering only a gain of $2dB$ at a BER of 10^{-4} as per Fig.3 in [39]. To improve the PAPR, a further candidate selection scheme is applied, where 4 versions of the FBMC symbol are generated and compared to pick the one with the lowest power for transmission. Although the phase shift pattern does not add any additional complexity to the FBMC system, the candidate selection approach significantly increases the complexity of the system, which compares to the complexity of SLM and PTS. Furthermore, the overall PAPR gain is $3dB$ at a BER of 10^{-4} as per Fig.7(a) and (b) in [39], which is less than the gain offered by our proposed approach, as will be shown in the results section of chapter 5.

Another solution is the generalized DFT (GDFT) proposed in [88], in which a GDFT, which is a DFT with a phase shaping function, is applied to the signal to reduce PAPR. The GDFT is applied to the real and complex parts of the signal separately. An additional candidate selection algorithm is combined to enhance the PAPR reduction gain, which in turn increases the system complexity. The overall gain is 4 dB at 10^{-4} for 64 subcarriers as per Figure 4. Despite the increased complexity, this gain is still inferior to the gain of our proposed SC-OQAM/FBMC model.

The last DFT-based approach is the pruned DFT proposed in [86] and deployed in [90]. This scheme achieves a PAPR reduction gain of almost 4 dB at 10^{-4} with no CP, and a gain of 5.5 dB when using a CP of length 26. However, this scheme forfeits the main advantage of FBMC systems with the increased OOB emission as a result of the filtering effect of pruned DFT and the decreased overlapping factor. In addition, the CP added to enhance the PAPR gain in cases where the number of the allocated subcarriers is small, reduces the SE.

3 OVERVIEW OF MULTI-CARRIER WAVEFORMS

The evolution of cellular communication generations has always been driven by the need for increased data rates. The physical layer of successive generations of cellular networks can be marked by its MA technique. From Frequency Division Multiple Access (FDMA), Time Division Multiple Access (TDMA), Code Division Multiple Access (CDMA) to Orthogonal Frequency Division Multiple Access (OFDMA) and SC-FDMA of LTE. Figure 3-1 shows the evolution of MA techniques in successive cellular network generations.

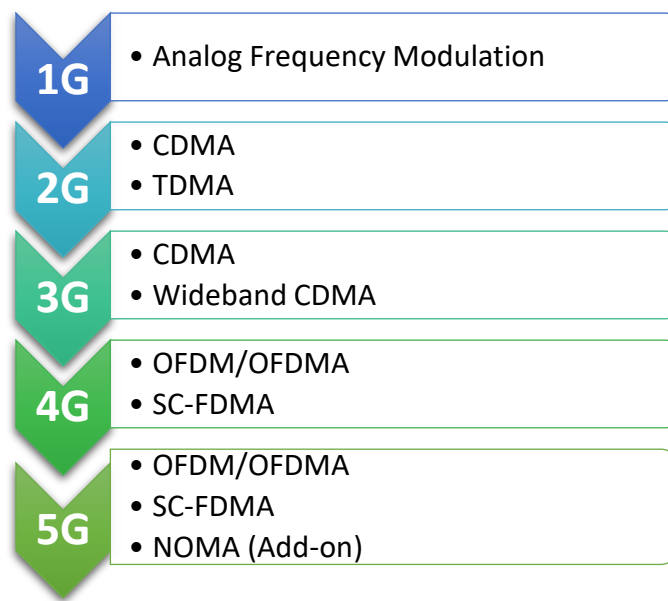


Figure 3-1: Multiple access techniques of cellular network generations.

As for 5G, although several other candidate waveforms were proposed in literature as OFDM successors, the last 3GPP release supports cyclic prefix CP-OFDM as the main modulation technique [93]. However, the massive connectivity and the diverse scenarios and applications of 5G networks and beyond, leave the door open for research towards new SE and EE waveforms to succeed or coexist with OFDM in future communication networks. Orthogonal techniques that are based on OFDM with additional filtering; FBMC, GFDM, UFMC and f-OFDM are the candidates most addressed in literature [4], [94], [95]. A different approach is non-orthogonal multiple access (NOMA) in which orthogonality between users is forfeited [94].

This chapter begins with a discussion of the need for new waveforms, followed by an overview of the OFDM-based MC techniques suggested as waveform candidates for 5G networks and beyond. This includes FBMC, UFMC, f-OFDM, GFDM and NOMA, a complete literature review about the waveforms is presented.

3.1 Why New Waveforms?

Future communication networks promise massive wireless connectivity and enable a wide range of high data rate applications [1]. Therefore, the research for spectral and energy-efficient modulation and signal processing techniques is a necessity. Moreover, in IoT which is an essential part of future communication networks a multitude of devices are connected throughout the network [96]. Since the connected devices may have simple capabilities, limited battery life and small amounts of randomly transmitted data, the modulation scheme must be power efficient, robust to synchronization errors and suitable for short-range communications [97], [98], [18]. Furthermore, the modulation techniques for future systems should be able to efficiently exploit fragmented spectrum. In addition to the mmWave frequency bands, cognitive spectrum access is suggested to deliver broadband wireless access to remote areas with unused licensed frequency bands. Moreover, the communication service must be reliable and have low latency to enable real-time ultra-reliable low latency communications (URLLC) applications such as online gaming and vehicle-to-everything (V2X) communications [104].

The main revolutionary feature in the physical layer of 4G systems was the deployment of MC techniques which greatly enhanced the data rate enabling a range of high data rate applications. OFDM and OFDMA are adopted in 4G network standards instead of CDMA of 3G networks downlink, along with SC-FDMA in the uplink. The main advantages of OFDM include the ability to minimize multipath distortion and combat the delay spread of wireless channels using simple equalization methods. This is achieved by splitting the available bandwidth into orthogonal subcarriers each with a narrow band, such that the channel response is considered flat over the subcarrier width, thus allowing simple one-tap FDE [43]. Furthermore, the orthogonality of subcarriers eliminates ICI, in addition to its compatibility with adaptive

modulation techniques and ease of integration with MIMO. A block diagram illustrating the OFDM transceiver is shown in Figure 3-2.

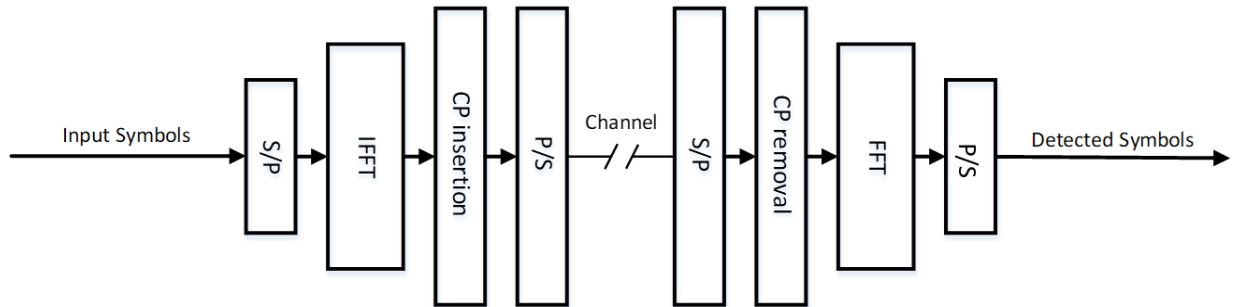


Figure 3-2: CP-OFDM transceiver.

Despite its numerous advantages, OFDM has some limitations. First, the use of rectangular pulses which slowly decay in the frequency domain makes it difficult to implement OFDM in limited fragmented spectrum. The need for efficient spectrum localization in 5G is demonstrated in Figure 3-3.

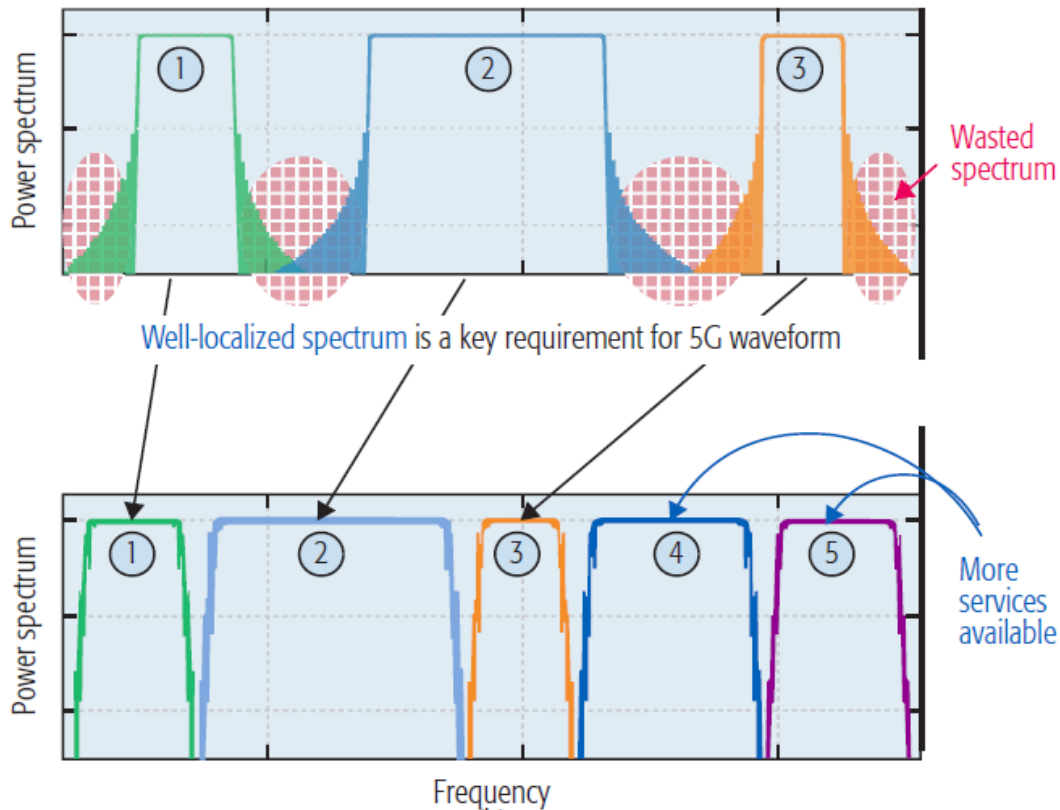


Figure 3-3: PSD of different neighbouring applications illustrating the effect of localized spectrum [105].

The well-localized spectrum enhances the SE of the system by decreasing the guard band required. Also, the high spectrum localization enables accommodating different applications in the same bandwidth and exploiting spectrum holes.

In addition, the need for a long CP in heavy multipath environments to avoid inter-symbol interference (ISI), decreases the system SE. Another problem is the large PAPR, which decreases the efficiency of the HPA, especially in the mmWave bands. Besides, OFDM needs strict synchronization to maintain the orthogonality of subcarriers. At ideal transmission conditions (perfect synchronization and sufficient CP length) the subcarriers are orthogonal to each other. However, if the transmission conditions become imperfect, severe performance degradation occurs due to the spread of inter-carrier interference (ICI) over a wide subcarrier range due to the poor spectrum localization causing OOB leakage. The synchronization issue is considered the main challenge for OFDMA, especially in the uplink which requires full synchronization between the user and the base station (BS) [99].

For example, a typical IoT application which is expected to benefit from the 5G machine type communication (MTC) platform, is wireless sensor networks (WSN) [100]. WSNs are part of many applications including health care, industry, and agriculture. WSNs typically transmit small amounts of data (low data rate) randomly [101], therefore highly localized waveforms with loose synchronization requirements will be efficient in such scenarios. The loose synchronization requirements simplify the synchronization process required in IoT devices with simple capabilities.

In brief, the previously mentioned scenarios for 5G systems and beyond imply that the modulation techniques and waveforms used must be energy and spectral-efficient, reliable, suitable for short-range communication, robust to synchronization errors and of very low latency. Furthermore, backwards compatibility with previous systems is a plus in addition to low complexity. All these requirements, summarized in Figure 3-4, inspire research towards alternative modulation and waveforms, which can succeed or co-exist with OFDM, to make all future networks scenarios and expectations possible.

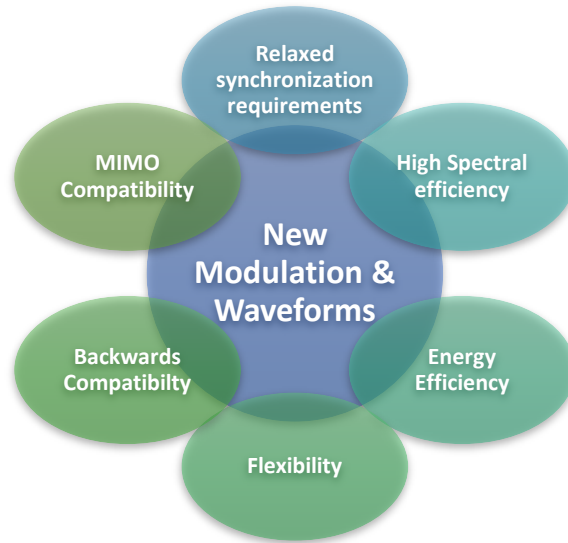


Figure 3-4: Alternative modulation and waveform requirements.

3.2 Candidate Multi-carrier Waveforms

The limitations of OFDM, are research topics for future waveforms. Different approaches have been attempted to reduce the OOB leakage of traditional OFDM and improve its SE, including filtering, pulse shaping and precoding [95], [98]. The modifications to OFDM resulted in several candidate MC waveforms including FBMC, UFMC, GFDM and f-OFDM. A different approach is NOMA in which orthogonality is forfeited for increased capacity.

Among the candidate waveforms, trade-offs are considered. According to the Balian-Low theorem [102], no waveform can perfectly satisfy all three conditions: mutual orthogonality of symbols, high symbol density, and high time-frequency localization. Mutual orthogonality means the absence of ICI and ISI in ideal transmission conditions. The symbol density is defined as $1/TF$ where T is the symbol duration and F is the subcarrier spacing, it can be seen as the number of symbols per unit time-frequency. The trade-off is displayed in Figure 3-5. Many waveforms including OFDM satisfy the orthogonality condition but have poor spectrum localization. On the other hand, Gaussian pulses for example satisfy the localization criteria but do not meet the orthogonality condition.

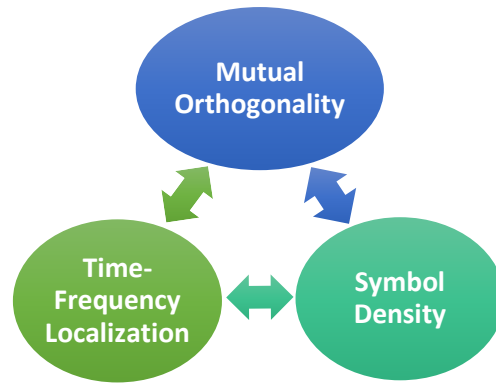


Figure 3-5: Waveform design trade-offs.

New waveforms and multiple access for 5G networks and beyond, and their related signal processing techniques are extensively addressed in recent literature. The following sub-sections provide an overview of the main OFDM-based MC waveforms proposed for 5G networks. The first three FBMC, UFMC and f-OFDM are based on linear filtering, while other techniques including GFDM are based on pulse shaping and circular filtering. Afterwards, a brief about NOMA is presented.

3.2.1 Filter-Bank Multi-carrier (FBMC)

FBMC is considered a generalization of the MC waveform concept, where OFDM can be considered a special case of FBMC, which rectangular prototype filter. To improve the spectrum localization and increase the SE, each subcarrier is individually filtered to suppress side lobes, making each subcarrier band-limited. Traditionally, OFDM counters ISI by introducing a CP longer than the channel's delay spread. This allows simple transceiver implementations using IFFT/FFT, at the expense of a time overhead leading to a loss in SE. Conversely, FBMC keeps the symbol duration unchanged and counters ISI by additional filtering.

Each output of the IFFT is filtered by a frequency-shifted version of a low pass prototype filter $h(k)$, where k is the discrete time index. The prototype filter performs the pulse shaping and is designed to band-limit the subcarriers so that each subcarrier only overlaps with its neighbour [5]. In addition, it must satisfy the Nyquist criterion. With N subcarriers, the synthesis filter-bank (at the transmitter end) is regarded as N exponentially modulated (frequency shifted) prototype transfer functions. The transfer function of the prototype filter at the m^{th} subcarrier

is given by the z-transform of the shifted impulse response as in 3-1, Where L_F is the length of the prototype filter of the sampled impulse response $h(k)$.

$$G_m(z) = \sum_{k=0}^{L_F} h(k) e^{j\frac{2\pi m}{N}(k - \frac{L_F-1}{2})} z^{-k} \quad 3-1$$

The additional filtering along with the IFFT/FFT operation, form a synthesis-analysis filter-bank structure [103]. The filter-bank of the frequency-shifted prototype filters can be efficiently realized using PPN, as shown in Figure 2-3. It can be noted from the figure that the FBMC transceiver is similar to that of OFDM with the removal of CP and the addition of PPN.

The prototype filter introduces additional coefficients between the FFT coefficients in the frequency domain. The number of introduced coefficients between two consecutive FFT coefficients is called the overlapping factor of the filter (K), which is the ratio between the filter impulse response duration and the MC symbol period. Thus, the overlapping factor determines the number of MC symbols which overlap in the time domain. An example of the prototype filters used for FBMC is the Physical Layer for Dynamic Access (PHYDYAS) filter [5], and the Hermite filters [104], both of which satisfy the half-Nyquist criteria.

FBMC is traditionally combined with OQAM modulation to preserve orthogonality while keeping the same sampling rate [5]. However, in later literature, the combination with QAM was proved possible [104]. For offset QAM, only a real or an imaginary symbol is transmitted per subcarrier [106]. Consequently, the throughput for an OQAM system would be half that of a QAM system. However, the OQAM FBMC system transmits at a symbol duration of $\frac{T}{2}$ where T is conventional OFDM symbol duration, thus compensating for halving the throughput due to the use of OQAM. Unlike OQAM/FBMC, there are multiple definitions and implementations for QAM-FBMC [13], [107]. The different realizations for the filter-bank are discussed in detail in the following section.

3.2.2 Universal Filtered Multi-carrier (UFMC)

UFMC is an MC modulation format that has been proposed by the European Union-funded research project 5GNOW [108], [109]. While in FBMC each subcarrier is individually filtered by a

frequency-shifted version of the prototype filter, in UPMC subcarriers are divided into groups (sub-bands), and each sub-band is filtered independently. The block diagram of the transmitter of UPMC is shown in Figure 3-6. The sub-band filters $h_i(k)$ are the frequency shifted version of the prototype filter, designed to attenuate side-lobe levels in the frequency domain. The N -point IFFT of each sub-band contains the relevant columns of the IFFT matrix according to the respective sub-band position [109]. The filtered signals $s_i(k)$ are then added.

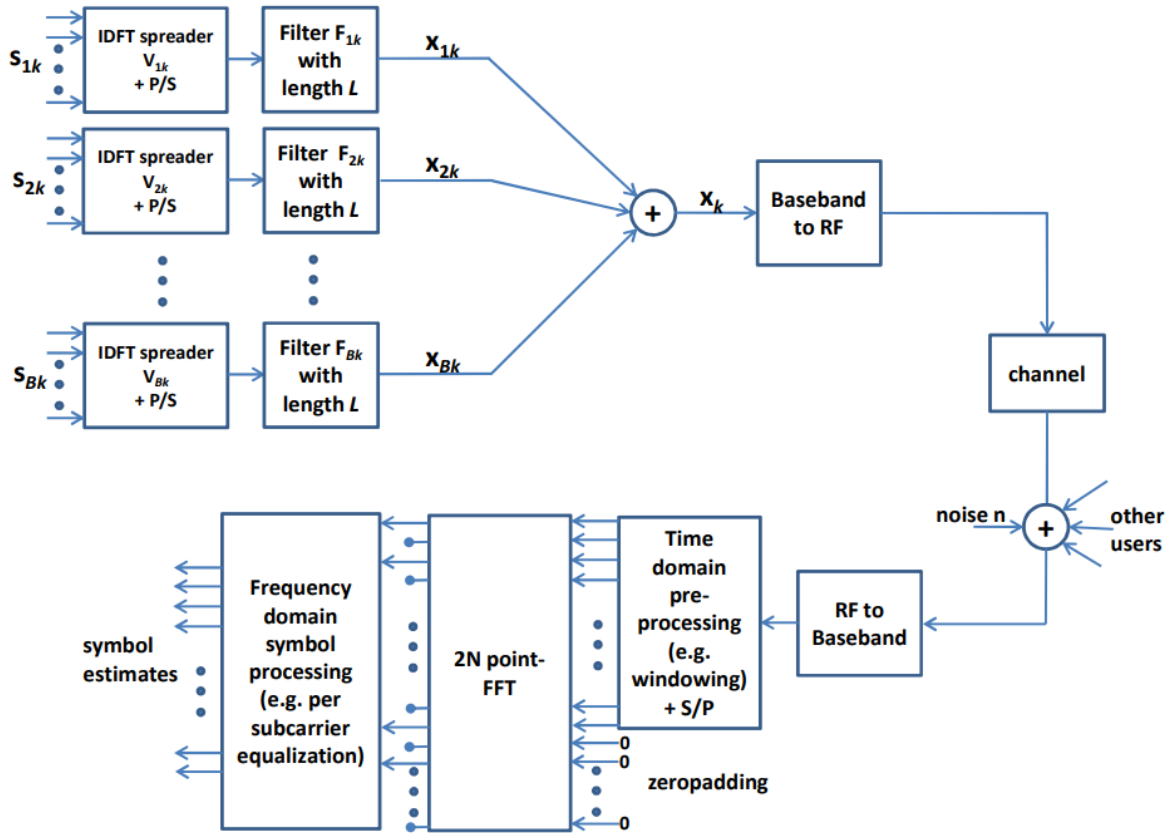


Figure 3-6: UPMC Transmitter block diagram.

The bandwidth of the sub-band filter is wider than that of FBMC as it is equal to the bandwidth of multiple subcarriers. Consequently, the length of the filter in the time-domain is much shorter close to the length of CP-OFDM [110]. The shorter length causes less interference by the pulse tails, which can be easily combated by inserting a zero-padding prefix (ZP) [94]. UPMC generally doesn't use a CP, however, a CP can be inserted to further enhance the robustness against ISI [109]. UPMC represents a generalization of the principle of OFDM and FBMC, targeting to gather the advantages and avoid the disadvantages by choosing the suitable

number of blocks S and the length of each block W . Since UFMC blocks keep complex-orthogonality, QAM may be efficiently used with UFMC instead of OQAM preferred with FBMC [108], [110].

Figure 3-7 shows the PSD of OFDM with 200 subcarriers carrying QAM modulated symbols versus the PSD of the corresponding 8 UFMC blocks each with 25 subcarriers. The blocks are filtered using the Dolph-Chebyshev prototype filter.

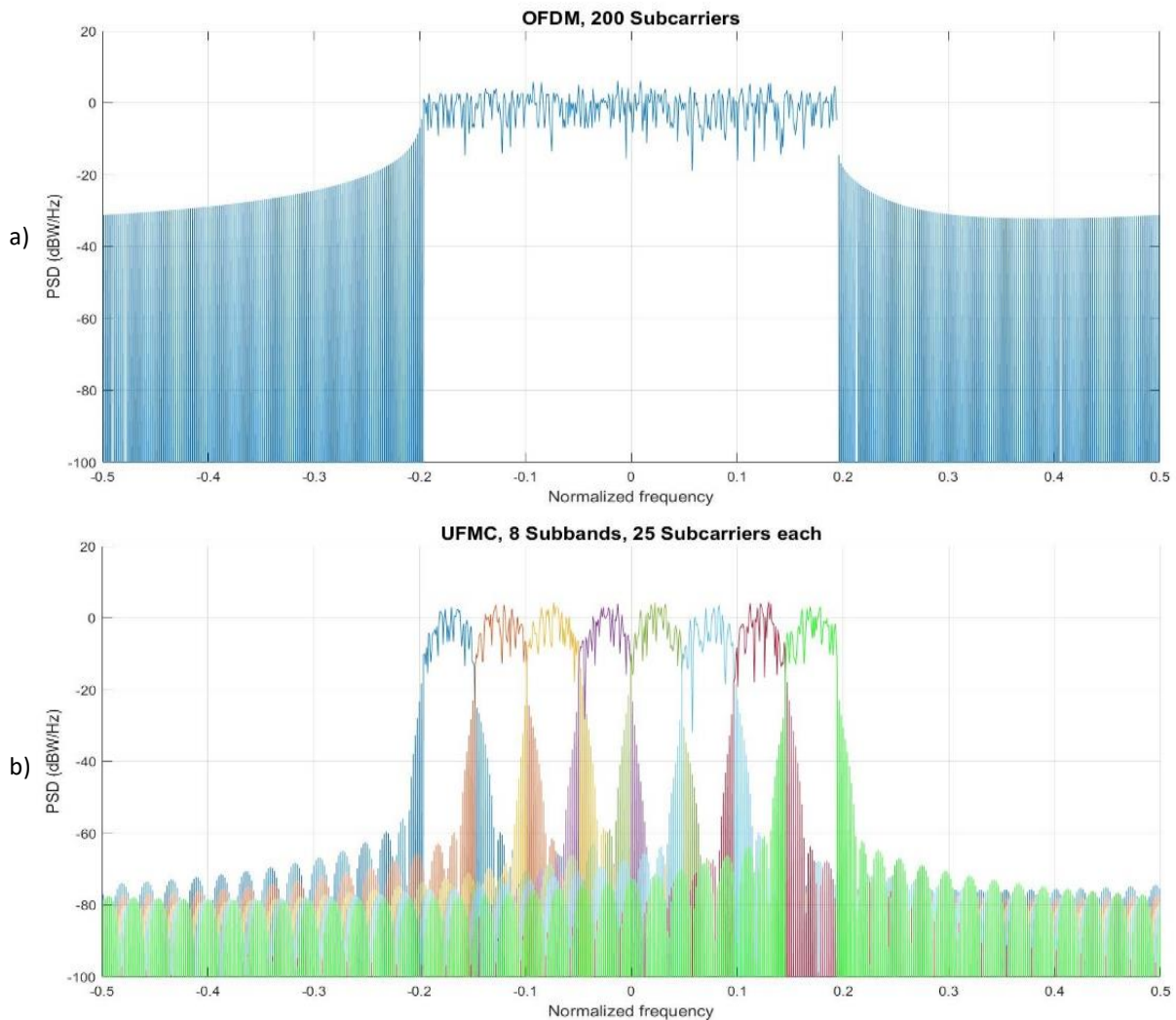


Figure 3-7: PSD of (a) OFDM with 200 subcarriers.
(b) UFMC with 8 blocks each with 25 subcarriers.

It can be noted that UFMC exhibits lower OOB side lobes than traditional OFDM leading to a more localized spectrum. Therefore, narrower guard bands are required thus enhancing SE.

However, FBMC still provides lower OOB emission and better SE as will be shown later. In addition, due to sub-band filtering, the orthogonality of the subcarriers is destroyed causing aliasing and ICI.

3.2.3 Filtered OFDM (f-OFDM)

Filtered OFDM is like UFMC in the manner that filtering is done per each group of subcarriers (sub-band) [111]. However, the main difference is that in f-OFDM the prototype filter usually has a longer length, providing better spectrum localization. While in FBMC controlled ISI is allowed, and in UFMC, ZP is used to eliminate any ISI, f-OFDM permits limited ISI due to its longer filter length compared to UFMC. In addition, f-OFDM uses CP instead of ZP like traditional OFDM as shown in the transceiver structure in Figure 3-8. The use of CP facilitates the equalization process and makes PAPR reduction techniques designed for OFDM applicable.

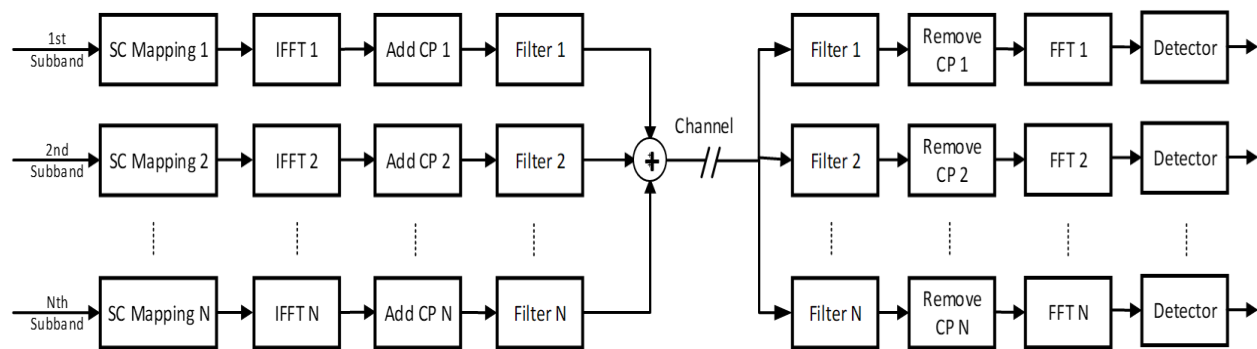


Figure 3-8: Filtered-OFDM transceiver structure.

Another difference is that in f-OFDM the number of subcarriers per sub-band does not have to be the same, instead, the available bandwidth can be divided according to the application and the transmission channel. In each sub-band, according to the type of service and the channel characteristics, the suitable parameters are chosen including the number of subcarriers, subcarrier spacing, and CP length [112]. Generally, a soft-truncated sinc-shaped filter is used.

3.2.4 Generalized Frequency Division Multiplexing (GFDM)

GFDM was first introduced in [113] as a modification to OFDM in which each subcarrier is filtered to minimize the overlap between subcarriers, thus relaxing the synchronization requirements [114]. Like FBMC, GFDM performs per subcarrier filtering but in a block and circular

manner [115], [116]. Figure 3-9 shows the block diagram of the GFDM transmitter based on [117]. The GFDM transmits parallel data streams on carrier frequencies f_1 to f_k , which do not have to be adjacent. The basic idea is to transmit a block frame composed of M time slots, each with K subcarriers [118].

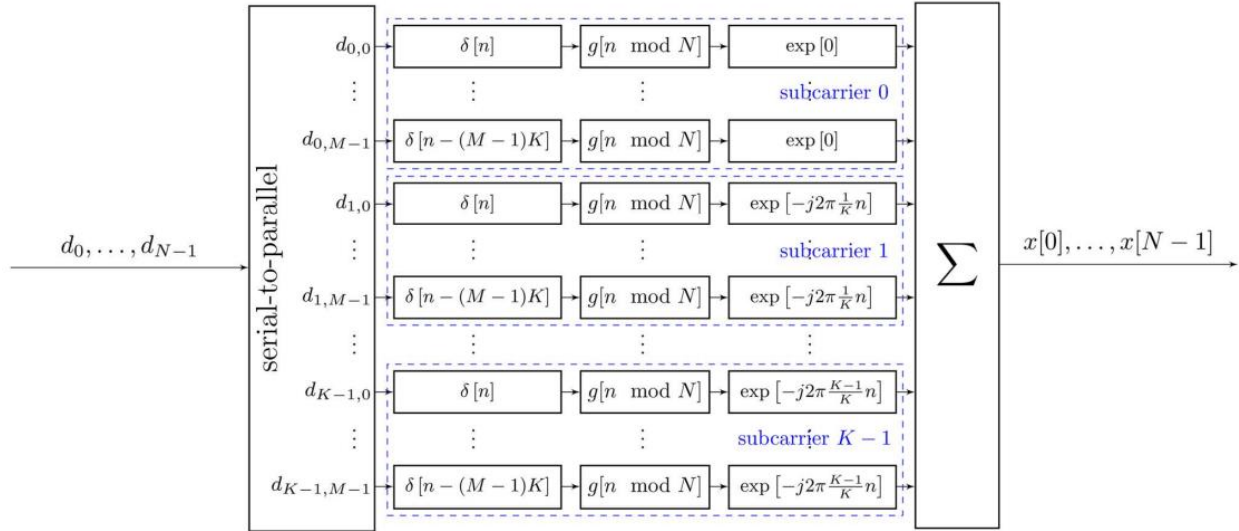


Figure 3-9: GFDM modulator block diagram [117].

Each subcarrier is individually filtered within a GFDM block. The filter for each branch is a circularly shifted version of the prototype filter $g[n]$. Regularly, raised cosine (RC) and root RC (RRC) prototype filters are used. In the block diagram, $d_{k,m}$ represents the modulated symbol which is to be transmitted onto the k^{th} subcarrier and the m^{th} sub-symbols. The impulse response of the shaping filters is given by:

$$g_{k,m}(n) = g[(n - mK) \bmod N] e^{j2\pi \frac{k}{K} n} \quad 3-2$$

The $\bmod N$ operator makes $g_{k,m}(n)$ a circularly shifted version of $g_{k,0}(n)$ and the complex exponential performs the shifting operation in frequency [117]. A diagram illustrating the circularly shifted filters of GFDM is shown in Figure 3-10 using an RC prototype filter, with $N = 28$, $K = 4$ and $M = 7$.

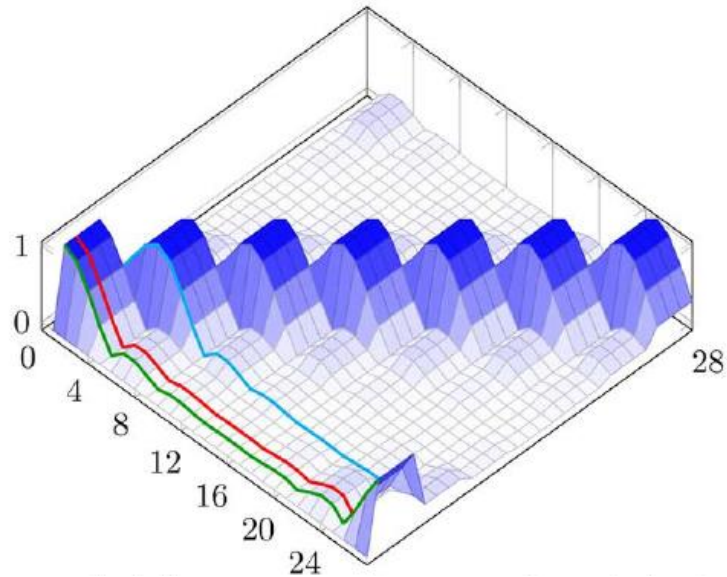


Figure 3-10: GFDM filtering operation illustration [117].

A CP and a cyclic suffix (CS) are added per block to combat time dispersion, which makes it more spectral-efficient compared to OFDM whose CP is added per symbol. An illustration of the CP insertion difference between OFDM and GFDM is shown in Figure 3-11. Unlike OFDM where the CP length is longer than the channel impulse response, in GFDM the CP length should be longer than the sum of lengths of the impulse responses of the transmitter shaping filter, the channel and the receiver filter.

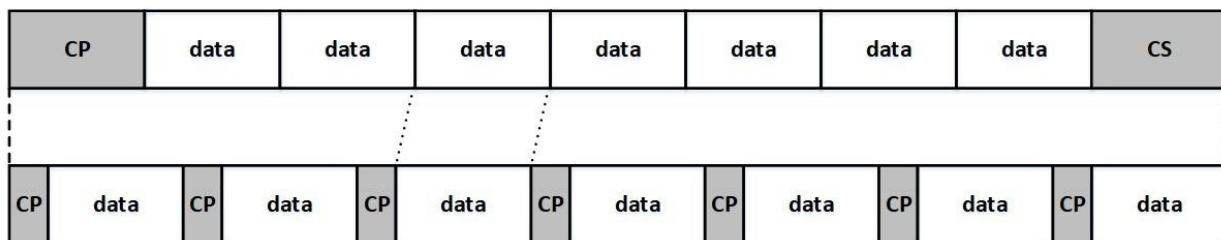


Figure 3-11: Cyclic prefix insertion in OFMD vs. GFDM.

To avoid long filter time-domain length and consequently long CP, a technique called tail biting is deployed. Tail biting means that the operation of GFDM resembles circular convolution in the filtering process instead of the linear convolution used by FBMC [110]. The additional samples that arise from the linear convolution are removed and added at the beginning of the data frame, resembling circular convolution. The OOB emissions are limited through the design

of pulse shapes. However, the lower the required OOB emissions, the longer the impulse response length in the time domain.

The main concerns about GFDM lie in the increased complexity of the receiver due to the use of successive interference cancellation (SIC) methods. In addition, the decoding latency is another challenge since all the block symbols must be received before decoding [115], therefore, shorter block lengths are considered when dealing with burst communication [114].

3.2.5 Non-orthogonal Multiple Access (NOMA)

All the previously addressed schemes are considered orthogonal multiple access (OMA), in which each resource block is orthogonally divided in time or frequency. NOMA means multiplexing different users at the same time/frequency/space resource of OMA thus it can be considered as an add-on which can be integrated with existing systems [94]. The idea of NOMA is utilizing the power and/or code domains to multiplex more users in the same resource block. Although this enhances the ability to utilize the available spectrum and decreases the blockage probability, this comes at the expense of additional interference which needs interference mitigation techniques at the receiver. SIC at the receiver is a fundamental principle for the detection of NOMA signals [119].

Superposition techniques enable the transmitter in NOMA to send two independent signals to two different UE. There are several superposition techniques for users to share the same resource present in literature. The first technique uses power allocation (power-domain NOMA), the second uses different codes (code-domain NOMA) and others consider multiplexing in more than one domain including the spatial domain [95], [120], [121], [122]. Figure 3-12 is an illustration of how power-domain NOMA works. The signals for two users in NOMA are superimposed and each user is allocated a certain power level using the same time-frequency resource.

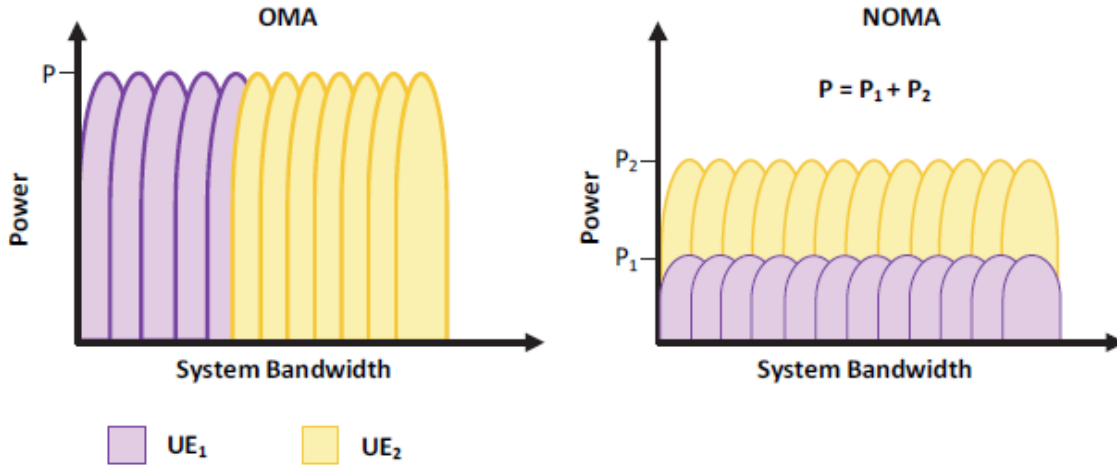


Figure 3-12: OMA vs. power-domain NOMA for two UEs [123].

For 2 users with signals x_1 and x_2 , and power levels P_1 and P_2 respectively, where P_1 plus P_2 equal the total transmission power, the downlink signal could be expressed as:

$$x = x_1\sqrt{P_1} + x_2\sqrt{P_2} \tag{3-3}$$

Different users are allocated different power levels according to their channel conditions [120], [122]. The power is allocated such that the user with the worst channel conditions is assigned the highest power and vice versa, this process is demonstrated in Figure 3-13.

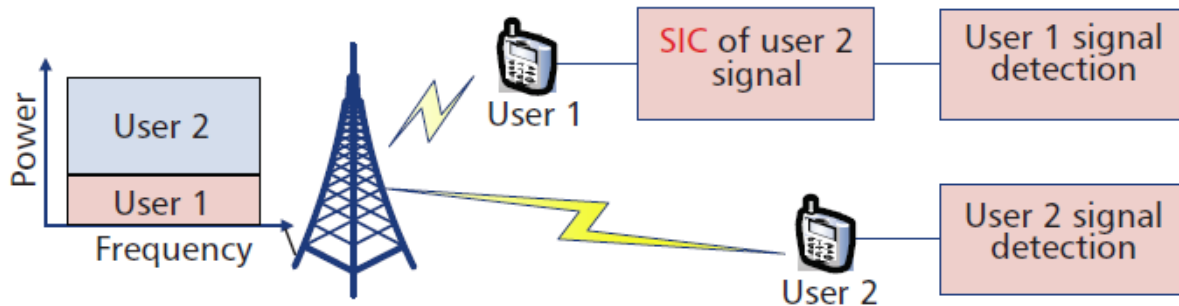


Figure 3-13: NOMA Downlink for two users [122].

In this case P_2 is greater than P_1 since UE₂ is further from the BS and is expected to have worse channel conditions. For the detection process, at UE₁, the signal of UE₂ (x_2) is detected first since it has the larger power and then it is removed using SIC from the total signal x , then x_1 is detected. At UE₂, the signal x_2 is directly detected and x_1 (which has a much lower power level) is treated as interference [122]. Despite the increased complexity of the receiver due to the increased controlled interference, the system capacity and SE are enhanced due to exploiting

another multiplexing domain (power domain). Furthermore, it is easy to integrate with MIMO and backwards compatible with OFDM [120], hence it can be used as an add-on in certain scenarios. Hybrid systems in which both OMA and NOMA co-exist are suggested to acquire the benefits of both approaches [121] and maintain compatibility.

3.3 Multi-carrier Waveforms Comparison

A general overview of all 5G candidate waveforms, motivation, and comparisons with each other and with CP-OFDM can be found in [4], [94], [98], [114], [115], [124] and [125]. In [94], the OMA techniques are classified into those based on subcarrier filtering (FBMC and UFMC) and others based on sub-band filtering (GFDM and f-OFDM). A study of the candidate 5G waveforms under timing and carrier frequency offset is conducted in [19], it is shown that the prototype filter must have smooth edges to reduce sensitivity to time or frequency offsets, and FBMC and UFMC were found to have the best performance. On the other hand, the effects of hardware impairments on MC waveforms, including non-linearity of HPA and phase noise (PN), are presented in [126], [127] and [128]. The energy efficiency of candidate waveforms has been examined in [129] using measures like aggregate energy efficiency and the Complementary Cumulative Distribution Function (CCDF) of the PAPR, to measure the greenness of 5G candidate waveforms, taking into consideration the power consumed at the HPA.

The OFDM-based MC waveforms whose system structure depend on filtering are simulated and compared in this section. These include FBMC, UFMC, f-OFDM in addition to CP-OFDM. The parameters for each MC modulation type are listed in Table 3-1.

Table 3-1 Multi-carrier Waveforms Simulation parameters

	Prototype Filter	Modulation	Prefix
FBMC	PHYDYAS	4QAM - OQAM	None
OFDM	None	4 QAM	CP
UFMC	Chebyshev	4 QAM	ZP
f-OFDM	RC	4 QAM	CP

The simulations are performed for 128 subcarriers for all modulation types, including 16 guard null subcarriers on each side, to illustrate the OOB emissions for each type. The simulations are conducted using the Vienna 5G Link Level simulator [34], which is a MATLAB-based toolbox, with specific link level 5G features and functions. Figure 3-14 displays the PSD of the transmitted signal for the four MC modulation types under investigation. The PSD is plotted to demonstrate the OOB emissions and hence the amount of spectrum localization for each type.

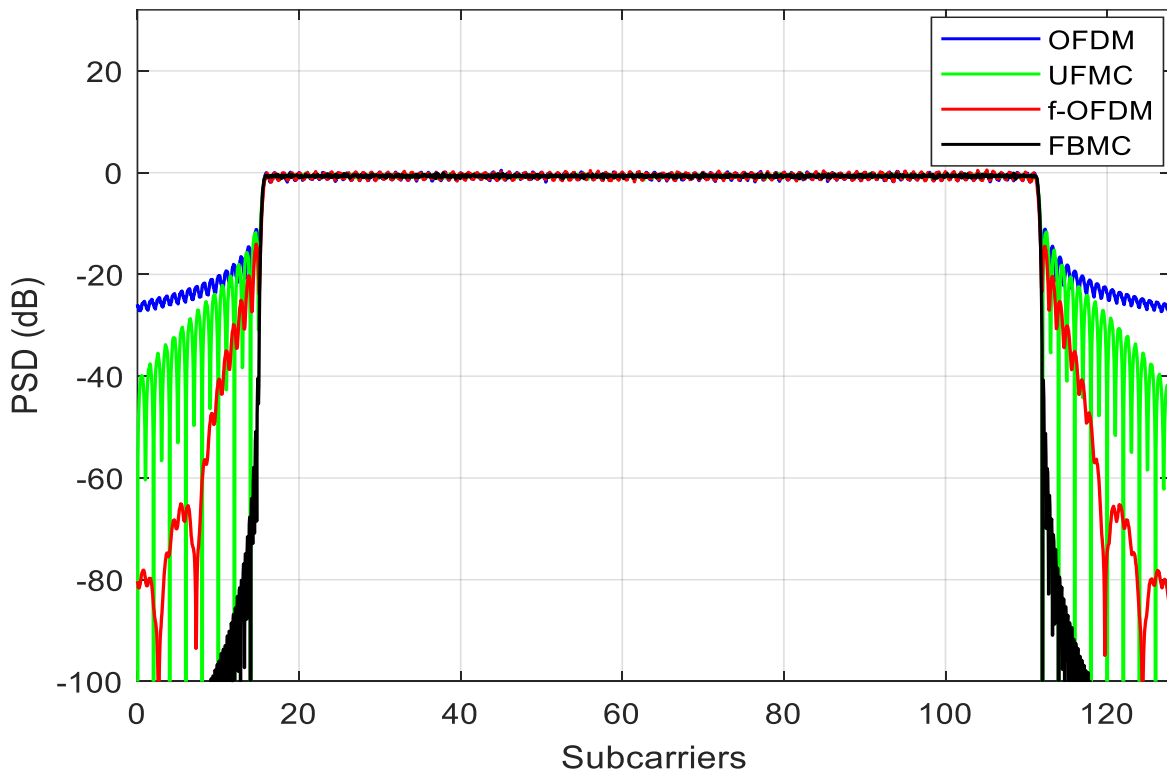


Figure 3-14: PSD of the transmitted signals using different MC techniques.

The figure shows the major advantage of the filtering approaches compared to OFDM, they all have significantly lower OOB emissions. This is the result of the rectangular pulse shape in OFDM which is well-localized in time but has a sinc-shaped spectrum for each subcarrier in frequency, which overlaps producing high OOB emissions as seen in the figure. FBMC has the lowest OOB emissions and thus achieves superior spectral localization, and this is its greatest advantage along with the CP-less transmission. The FBMC's highly localized spectrum allows for reducing the number of required guard subcarriers and thus increasing the SE. This makes it an

ideal option for exploiting fragmented spectrum, and in turn, can boost the data rate of future communication networks.

The CCDF of the PAPR of the transmitted signal of each MC waveform is displayed in Figure 3-15, using the same simulation parameters. All the MC waveforms exhibit similar PAPR performance except UFMC which has slightly higher PAPR. The high PAPR remains a research problem for all MC modulation techniques, and that is why SC-FDMA is used in the uplink of 4G and 5G, to reduce the PAPR of the signal transmitted from the UE, and thus reduce the consumed power at the power amplifier in battery-limited UE. A similar approach is suggested to tackle this problem with the proposed OQAM/FBMC system in chapter 5.

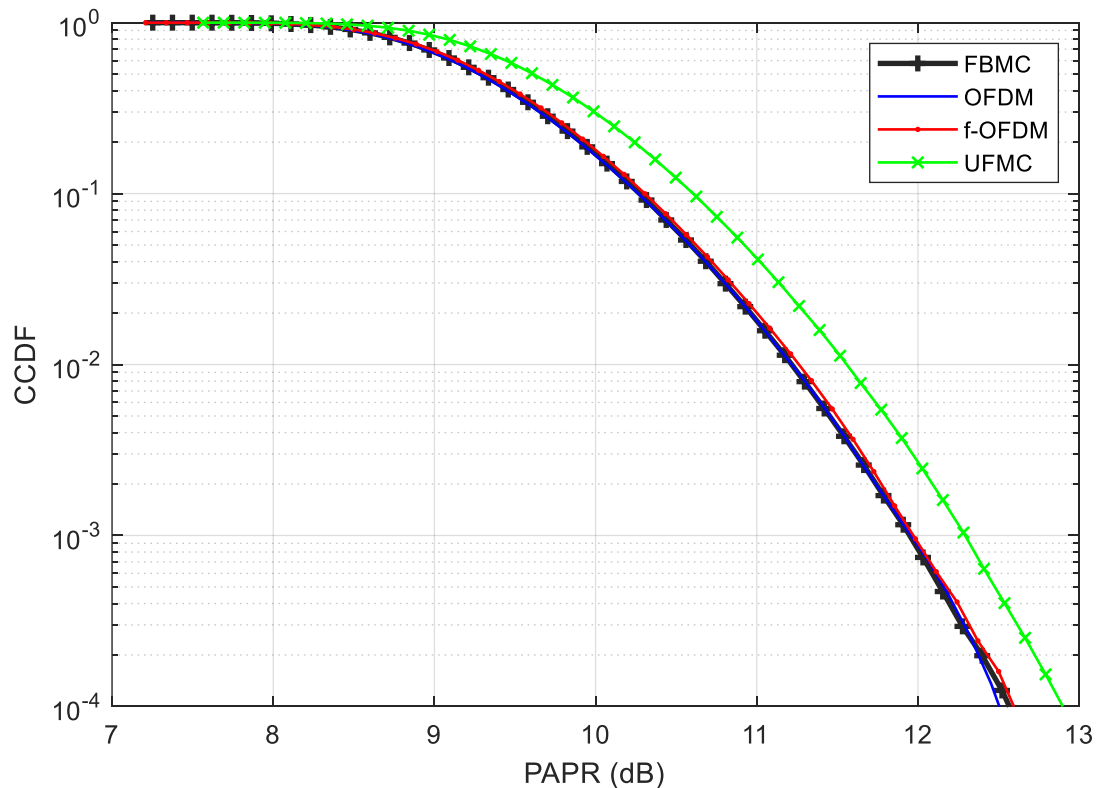


Figure 3-15: CCDF of the PAPR of the transmitted signal of different MC techniques.

To conclude this section, a qualitative comparison of the studied 5G waveforms based on filtering of OFDM is illustrated in Table 3-2. The techniques are compared in terms of system specifications such as the prototype filter type and absence or presence of a CP or a ZP. They are also compared using waveform KPIs like frequency and time localization. The main advantages

and challenges of each waveform are highlighted. It must be noted that there are many variants of each waveform, however, this comparison considers the classical general approach of each.

Table 3-2 Candidate Multi-carrier Waveforms Comparison

	OFDM	FBMC	UFMC	f-OFDM	GFDM
Prefix	CP	None	ZP	CP	CP
Filtering Technique	-	Linear per subcarrier	Linear per sub-band	Linear per sub-band	Circular per subcarrier per time slot
Prototype Filter Type	-	PHYDYAS / Hermite	Dolph-Chebyshev	Soft-truncated sinc / Equiripple	RC / RRC
Average Filter Length	-	3 or 4 times the symbol duration	Less than or equal to ZP length	Half of the symbol duration	Flexible - greater than symbol duration
Modulation	QAM	OQAM / QAM	QAM	QAM	QAM
Frequency Localization	Low	Highest	High	High	High
Complexity	Lowest	Moderate	Highest	Moderate	Moderate
Orthogonality	Complex-Orthogonal	Real-orthogonal	Non-orthogonal	Non-orthogonal	Non-orthogonal
Main Advantage	Low complexity - Compatibility with MIMO	SE - low OOB emission - Relaxed synchronization	Low latency - Spectral confinement	Low latency Flexibility	Flexibility - Low latency
Main Challenge	Strict Synchronization - Poor spectrum localization	Channel Estimation - MIMO integration	Integration with MIMO	Complex receiver - Residual ISI	Complex Receiver

Since FBMC is considered a generalization of the MC concept, with OFDM as a special case with rectangular pulse shapes. Due to its superior spectrum confinement and CP-less transmission, hence its ability to increase the spectrum efficiency and relax the synchronization requirements, FBMC is the strongest competitor amongst the other MC waveforms, to succeed or co-exist with OFDM in future communication networks.

3.4 FBMC in Literature

FBMC was first suggested by the PHYDYAS project [5] as an MC multiple access technique for 5G networks [130]. Due to the intrinsic imaginary interference of the FBMC signal, it is usually paired with OQAM [46]. In FBMC modulation, the subcarriers are filtered so that only neighbouring subcarriers overlap [5]. OQAM is used with FBMC so that the subcarriers one carries a real symbol while its neighbour carries an imaginary one. OQAM/FBMC can achieve the maximum transmission rate and does not need a CP to combat ISI in multipath channels, thus increasing the SE. In addition, the high spectral localization which leads to an extremely low Adjacent Channel Leakage Ratio (ACLR) facilitates the use of fragmented spectrum [8], [16], [43], especially in dynamic spectrum access and cognitive radio scenarios [96], [131], such as exploiting TV white spaces (TVWS) and spectrum holes [10], [11], [132], [133], [134], [135]. The low ACLR also reduces the required guard bands thus increasing the SE [12].

In addition to its ability to increase the SE and exploit fragmented spectrum, OQAM/FBMC is particularly suitable for asynchronous transmission scenarios [14], [15], [16]. Due to its highly localized pulses, OQAM/FBMC has relaxed synchronization requirements compared to OFDM [2], [14], thus enhancing the overall EE of the system. Unlike OFDM with strict synchronization requirements to preserve orthogonality of the overlapping subcarriers, FBMC-filtered subcarriers are strictly band-limited and therefore less sensitive to frequency synchronization errors [16]. Tight synchronization is not EE or cost-effective for a user-centric future system. The use of OQAM/FBMC in IoT scenarios enhances the performance and increases the robustness against timing and frequency offsets [18], [19]. The physical layer of 5G and future networks including IoT, needs to be suitable for a lower degree of synchronization [124], [133]. FBMC is a perfect match in this scenario, allowing simple low-cost low-power IoT devices to operate efficiently.

The suitability of FBMC for mmWave band communication, which is an essential 5G and 6G enabling technology, has been thoroughly examined in literature [136], [137], [21], [22]. Since the PN of an oscillator increases as the frequency increases, therefore PN limitation is inevitable in the mmWave bands [138]. PN is critical in MC schemes since it damages the orthogonality of the subcarriers due to common phase errors causing ICI. Since FBMC has less strict synchronization requirements, it could be efficiently deployed in the mmWave bands, especially when the subcarrier spacing is increased.

3.4.1 OQAM/FBMC Discrete System Model

The detailed system model for OQAM/FBMC is illustrated in Figure 3-16. The real-valued OQAM symbols are denoted $d_{m,n}$ where m is the subcarrier index and n is the time index. The symbols are phase-adjusted by $\theta_{m,n} = \frac{\pi}{2}(m+n)$, such that each symbol has a $\frac{\pi}{2}$ phase shift with the adjacent symbols. The shaping filter for each subcarrier is $h_m(k)$ which is the prototype filter $h(k)$ modulated to the center frequency of the subcarrier m from the total N subcarriers

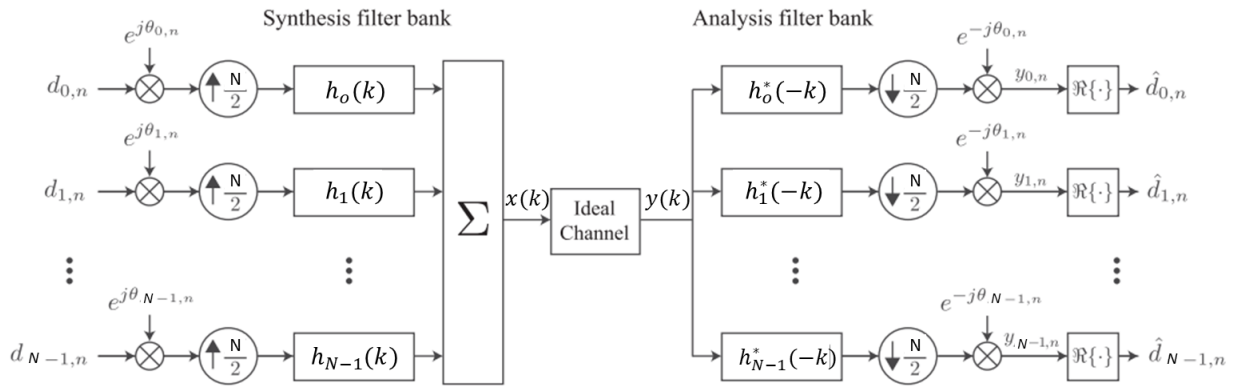


Figure 3-16: OQAM/FBMC system transceiver model [27].

The synthesized time-domain FBMC signal $x(k)$ can be written as:

$$x(k) = \sum_{n=-\infty}^{+\infty} \sum_{m=0}^{N-1} d_{m,n} h_m\left(k - \frac{nN}{2}\right) e^{j\theta_{m,n}} \quad 3-4$$

The time spacing between adjacent symbols is $\frac{N}{2}$ samples, whereas the normalized frequency spacing between successive subcarriers is $\frac{1}{N}$. The received signal can be written as:

$$\mathbf{y}(\mathbf{k}) = \mathbf{c}(\mathbf{k}) * \mathbf{x}(\mathbf{k}) + \boldsymbol{\eta}(\mathbf{k}), \quad 3-5$$

where $c(k)$ is the multipath channel impulse response and $\eta(k)$ represents the additive white gaussian noise (AWGN). The channel is assumed to be time-invariant over the transmitted symbol duration. At the receiver after the signal passes through the analysis bank in Figure 3-16 and before taking the real part the demodulated signal $\mathbf{y}_{m,n}$ can be written as:

$$\mathbf{y}_{m,n} = \sum_{n'=-\infty}^{+\infty} \sum_{m'=0}^{M-1} \mathbf{H}_{mm',nn'} \mathbf{d}_{m',n'} + \boldsymbol{\eta}_{m,n}, \quad 3-6$$

where $\mathbf{H}_{mm',nn'}$ represents both the induced intrinsic interference and the interference due to the channel response and it is a function of the equivalent channel response $h_{mm'}(k)$:

$$\mathbf{h}_{mm'}(\mathbf{k}) = (\mathbf{h}_{m'}(\mathbf{k}) * \mathbf{c}(\mathbf{k}) * \mathbf{h}_m^*(-\mathbf{k})) \downarrow_{\frac{N}{2}} \quad 3-7$$

where $h_{mm'}(k)$ is the equivalent channel response between the transmitted symbols at subcarrier m' and those received at the subcarrier m . This includes the effect of the synthesis filter, the channel response, and the analysis filter. Assuming that the channel is flat over the width of each subcarrier, $\mathbf{y}_{m,n}$ can be written as:

$$\mathbf{y}_{m,n} = \mathbf{H}_m(\mathbf{d}_{m,n} + \mathbf{u}_{m,n}) + \boldsymbol{\eta}_{m,n}, \quad 3-8$$

where $u_{m,n}$ represents the intrinsic interference term, which is the main difference between the analysis of the OFDM received signal and the FBMC received signal. However, since this term is purely imaginary, it will disappear after taking the real part of $\mathbf{y}_{m,n}$ as shown in Figure 3-16. Although the intrinsic interference is eliminated after taking the real part in the previously described system model, the interference terms and their amplitude distribution affect some of the system functions, such as pilot detection, channel estimation and more importantly, the integration with MIMO.

3.4.2 Prototype Filter

The FBMC prototype filter is designed to achieve optimum time-frequency localization. The prototype filter design is based on the Nyquist theory, which implies that the impulse response $p(t)$ of the filter must have zero-crossings at multiples of the symbol duration, which leads to the symmetry condition in the frequency domain [6], [5]. This is realized by splitting the global

Nyquist filter into two half-Nyquist filters at the transmitter and receiver ends, and the symmetry condition is then obtained by the squares of the coefficients. The design of the prototype filter and its optimization to meet desired OOB and BER requirements is discussed in [139], [140], [141], [142], [143], [144], [145] and [146]. The most popular FBMC prototype filter was first presented in the PHYDYAS project [5]. The impulse response of the PHYDYAS prototype filter is given by:

$$h(t) = 1 + 2 \sum_{k=1}^{K-1} H_k \cos\left(\frac{2\pi kt}{KT}\right) \quad 3-9$$

Where K is the overlapping factor, which indicates the number of symbols which overlap in the time domain, it also indicates the oversampling factor in the frequency domain. T_0 is the inverse of the subcarrier spacing, and the symbol time is $T = \frac{T_0}{2}$, due to OQAM transmitting real and imaginary symbols alternatively at half of the symbol duration.

The prototype filter length is $2K - 1$, which is equal to the number of its non-zero frequency coefficients. Its symmetric frequency coefficients H_k are obtained from the interpolation formula of sampled signals as in [5] which uses the frequency sampling method [147], [28]. The coefficients satisfy the following condition:

$$\frac{1}{K} \sum_{k=-K+1}^{K-1} |H_k|^2 = 1 \quad 3-10$$

Table 3-3, displays the PHYDYAS prototype filter frequency coefficients H_k for different overlapping factors K .

Table 3-3 Coefficients of the PHYDYAS prototype filter for different overlapping factors

	H_0	H_1	H_2	H_3
$K = 2$	1	$\sqrt{2}/2$	-	-
$K = 3$	1	0.911438	0.411438	-
$K = 4$	1	0.971960	$\sqrt{2}/2$	0.235147

Another popular prototype filter which satisfies the time-frequency localization, and the Nyquist criterion is the Hermite filter[104], [148], which was first proposed in [149]. It is based on Gaussian pulse and Hermite polynomials, and its impulse response is given by:

$$h(t) = \frac{1}{\sqrt{T_0}} e^{-2\pi\left(\frac{t}{T_0}\right)^2} \sum_i a_i H_i\left(2\sqrt{\pi}\frac{t}{T_0}\right), \quad 3-11$$

where $H_i(x)$ is the Hermite function. The coefficients are calculated as in [149] and [150] for K multiples of 4 ie. (4,8,12,16,20). Figure 3-17 shows the impulse response $h(t)$ and the frequency response $H(f)$ of the PHYDYAS and Hermite prototype filters for $K = 4$.

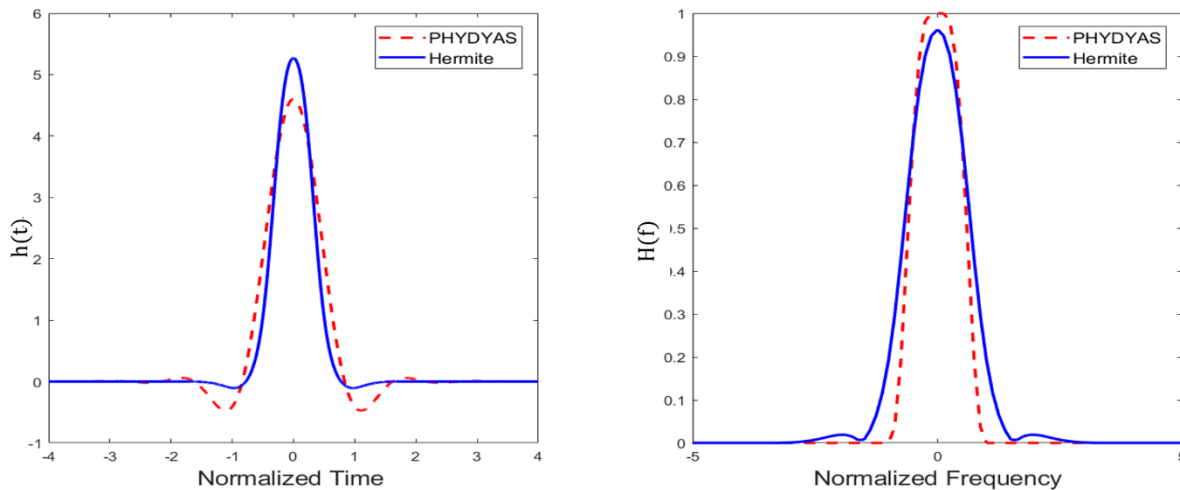


Figure 3-17: Normalized time and frequency response of PHYDYAS and Hermite filters

For the same overlapping factor, the PHYDYAS filter has better frequency localization with the side lobes of $H(f)$ decaying faster than Hermite. While the Hermite filter has better time localization with $h(t)$ decaying faster. However, both filters satisfy the Nyquist criteria and maintain a good time-frequency localization.

To test the effect of the prototype filter on the OOB emissions of the FBMC signal, the normalized PSD of the transmitted signal is plotted against the subcarrier index in Figure 3-18. The PSD is calculated in dB and the frequency axis is divided by the subcarrier frequency. The number of data subcarriers is 24. The PHYDYAS and Hermite are both compared to the RRC filter, for an overlapping factor of $K = 4$.

Figure 3-18 shows why the RRC filter is not considered for OQAM/FBMC, since it gives high OOB side lobes compared to the signals transmitted using PHYDYAS and Hermite filters. On the other hand, the signal transmitted using the PHYDYAS prototype filter has lower OOB emissions compared to the Hermite filter. This verifies the previously discussed comparison that the PHYDYAS filter, which was specially devised for FBMC, provides better frequency localization.

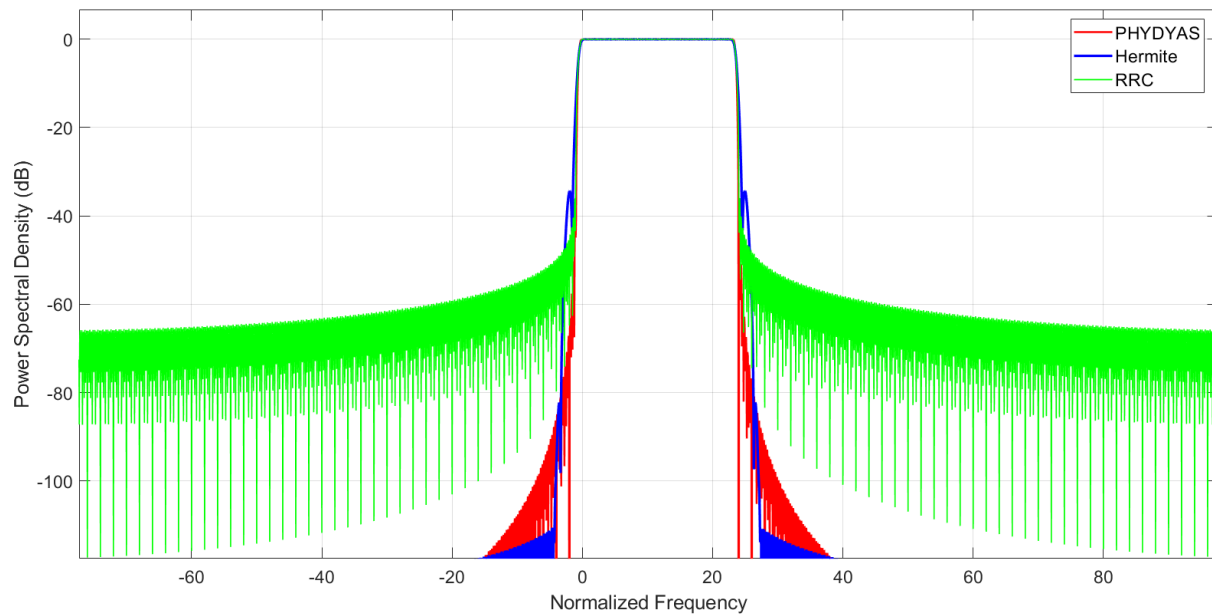


Figure 3-18: PSD of OQAM/FBMC transmitted signal using different prototype filters

Figure 3-19 shows the distributed normalized power over the FBMC symbol duration of $1ms$, for PHYDYAS and Hermite filters OQAM/FBMC transmitted signals. The figure shows that the Hermite filter has slightly better time localization within the symbol duration. However, the difference is not greatly significant.

Figure 3-20 displays the CCDF of the PAPR for both filters. From Figure 3-20, the PAPR of the MC signal transmitted using the Hermite prototype filter is slightly lower than that of PHYDYAS. The previous three figures show that both PHYDYAS and Hermite prototype filters satisfy the time-frequency localization property required for OQAM FBMC with slight differences in performance. Hermite has slightly better time localization and PAPR, while PHYDYAS has better frequency localization, for the same overlapping factor.

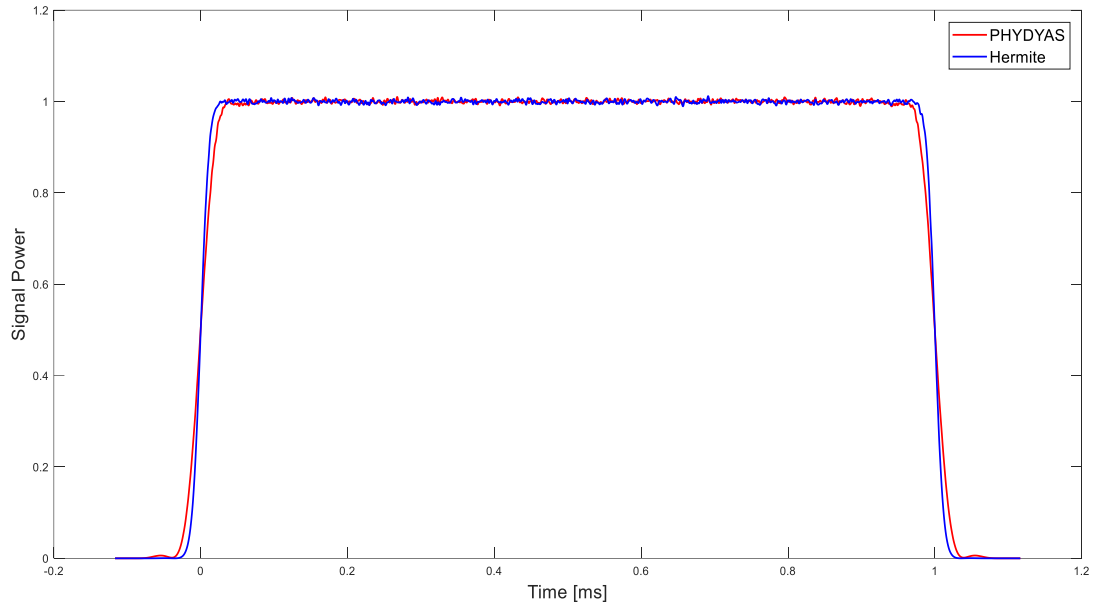


Figure 3-19: Normalized power over symbol duration of OQAM/FBMC with different prototype filters for $K = 4$

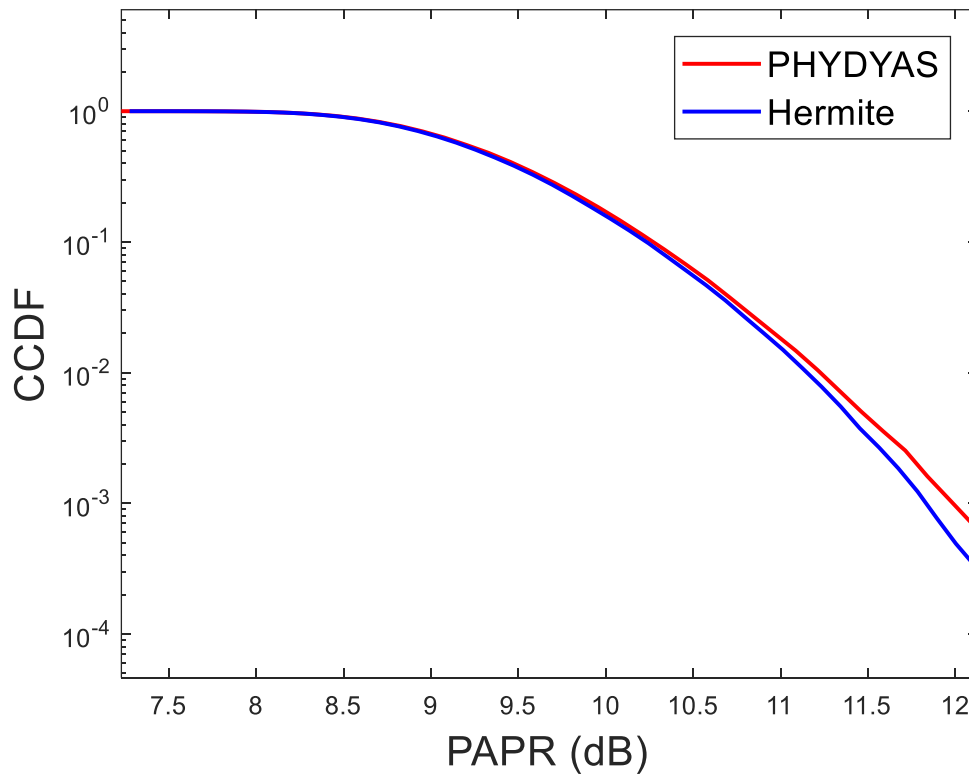


Figure 3-20: CCDF of PAPR of OQAM/FBMC system with different prototype filters with an overlapping factor of 4

3.4.3 Overlapping Factor

Next, the PHYDYAS prototype filter is tested for different overlapping factors. The PSD in dB for OFDM and OQAM/FBMC with different overlapping factors (K) is plotted against the 128 subcarriers in Figure 3-21. Guard subcarriers are inserted on both sides, equal to one-eighth of the total number of subcarriers.

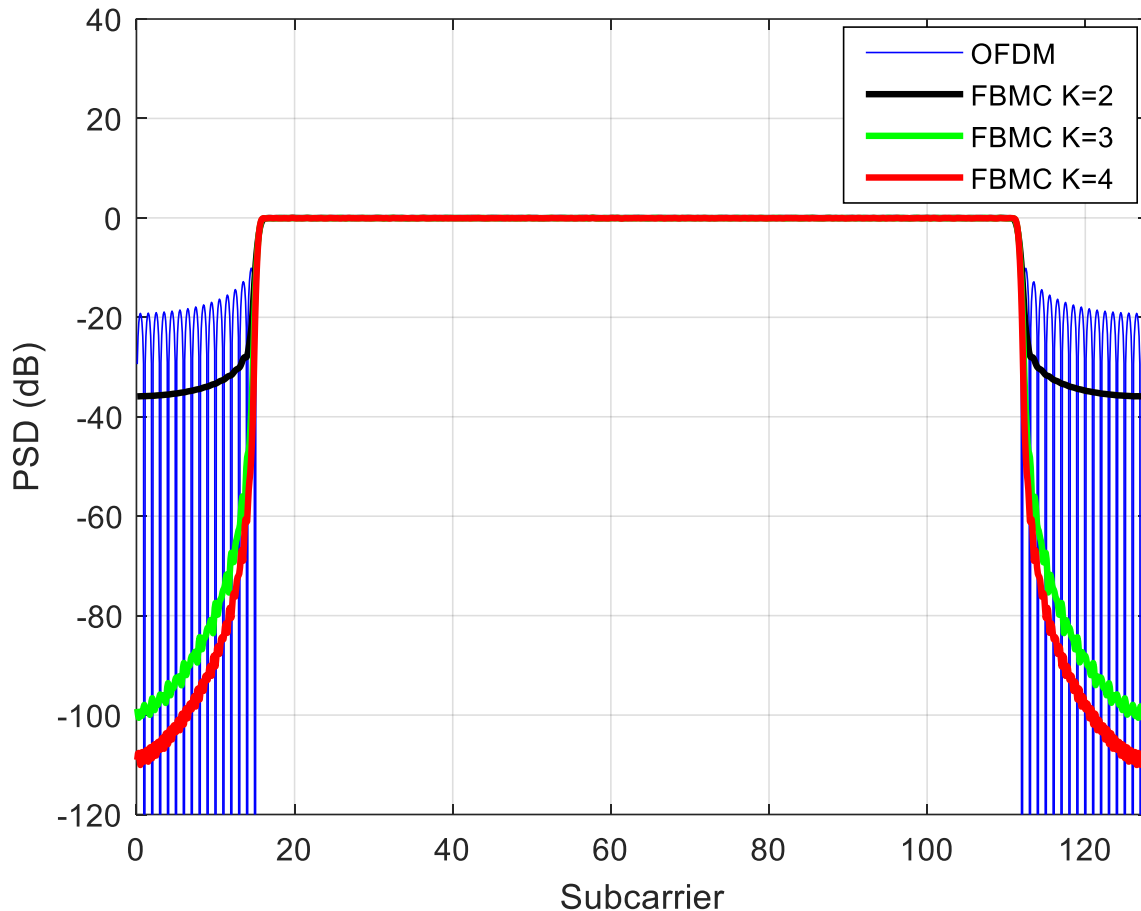


Figure 3-21: PSD of OQAM/FBMC transmitted signal using different K

It is clear from the figure that OQAM/FBMC has a significantly lower OOB spectrum compared to OFDM. The OOB attenuation increases as the overlapping factor increases, therefore, better spectral localization is achieved. For instance, CP-OFDM has an attenuation of 20 dB compared to 100 dB attenuation for OQAM/FBMC with $K = 3$. This illustrates how the FBMC signal spectrum is highly localized compared to OFDM. As the overlapping factor indicates the number of symbols overlapping in time, therefore increasing it increases the intrinsic

interference. There is a trade-off between the frequency and time localization as the overlapping factor is increased, which complies with the Balian-Low rule for waveform design.

The CCDF of the PAPR for different overlapping factors is shown in Figure 3-22.

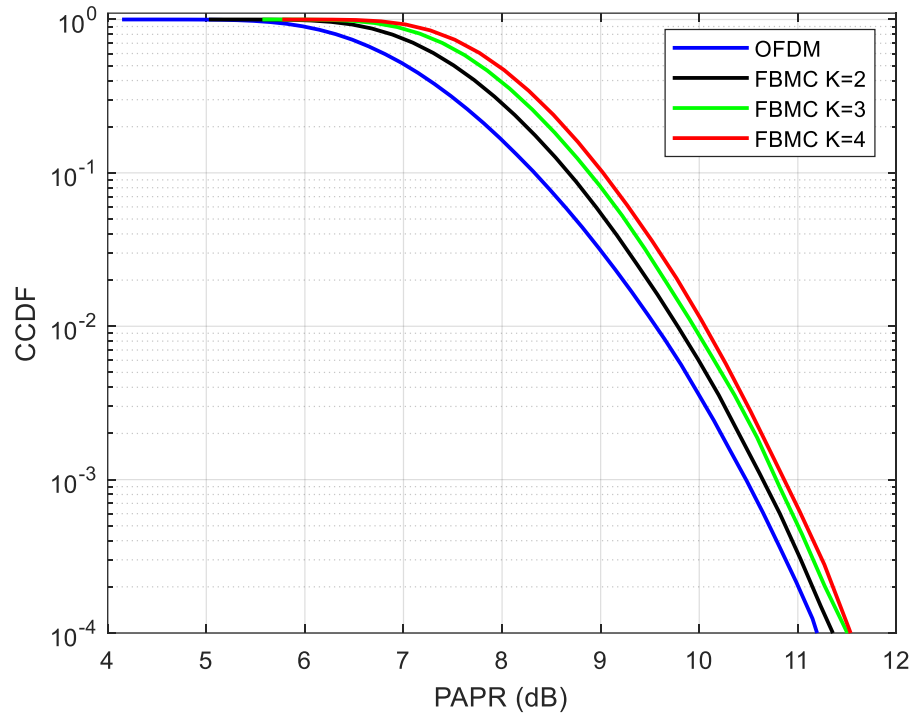


Figure 3-22: PAPR of OQAM/FBMC transmitted signal using PHYDYAS prototype filters with different K

It is noted that increasing the overlapping factor slightly increases the PAPR ratio. However, when the number of subcarriers is increased, the difference becomes small. It is also observed that OFDM has a slightly lower PAPR compared to OQAM/FBMC, this is the result of the overlapping between adjacent symbols. As K increases, the number of overlapping symbols increases, therefore the PAPR increases. However, the increase in PAPR for FBMC over OFDM is insignificant compared to the much lower OOB PSD depicted in Figure 3-21. There is a trade-off between the spectrum localization and the PAPR and system complexity on the other side. When K increases, the OOB attenuation increases but the PAPR increases along with the complexity of the system. However, K can be determined according to the desired OOB attenuation levels according to the application.

4 PROPOSED HYBRID OQAM/FBMC MIMO SYSTEM

This chapter presents the proposed HYBRID OQAM/FBMC MIMO model along with its analysis, simulation, and results. In the first section, the all-FS OQAM/FBMC MIMO system is described. Its performance is tested with SM and Alamouti SFBC, using ZF/MMSE FDE in a frequency-selective Rayleigh fading channel. The system is described using discrete time domain equations. The novelty in our approach is that the Alamouti SFBC is performed before OQAM processing, since the OQAM processing produces a real-orthogonal signal, while the Alamouti coding requires complex orthogonality. By performing the MIMO coding before OQAM processing, the MIMO operation is not affected by the intrinsic imaginary interference, and enhanced BER performance can be obtained by exploiting SD in SFBC. On the other hand, higher data rates can be obtained using SM.

In the second section, the proposed hybrid-structure OQAM/FBMC MIMO system is presented and analysed. The hybrid system uses the modified PPN approach for the transmitter to reduce complexity, along with the FS approach in the receiver to facilitate equalization in the frequency domain, thus achieving less overall complexity in Rayleigh fading channel. In better multipath fading channel conditions with a LOS component, a simple TDE is deployed to further reduce the complexity. When using TDE, the PPN structure is used in the receiver as well to benefit from its reduced complexity without the need for FFT overhead. A complete matrix-representation mathematical model is provided, and the system is generalized for any $P \times P$ MIMO configuration.

The system description is followed by a BER analysis and then an overall complexity analysis and comparison. The chapter is concluded with the simulation of the proposed hybrid model and the results including the BER in different scenarios compared to conventional CP-OFDM, PSD and the simulated BER compared to the analytical formula obtained.

Throughout this chapter, the following mathematical notations are used: $(\cdot)^{-1}$, $(\cdot)^T$, and $(\cdot)^H$ are the inverse, transpose, and Hermitian transpose of a matrix respectively. In addition, \mathbf{I}_M is an $M \times M$ identity matrix, $\mathbf{0}_{M \times P}$ is an all-zero matrix of dimensions $M \times P$, and \mathcal{F}_M is an

$M \times M$ isometric FFT matrix whose elements are calculated as $[\mathcal{F}_M]_{mn} = \frac{1}{\sqrt{L}} e^{-\frac{j2\pi mn}{M}}$. Moreover, \mathbf{k}_n^M are column vectors of length M , with all-zero elements except the n^{th} element equals to one, for example $\mathbf{k}_2^4 = [0 \ 1 \ 0 \ 0]^T$. Also, $\text{diag}(\mathbf{x})$ is the diagonal matrix whose diagonal elements are equal to the elements of the vector \mathbf{x} , $\text{diag}(\mathbf{x}) = \mathbf{x} \mathbf{I}_{\text{length}(\mathbf{x})}$. The term $E(x)$ symbolizes the expectation of the variable x . The operator $*$ represents the linear discrete convolution operator. All signals are represented by their discrete-time baseband equivalents.

4.1 FS-OQAM/FBMC SM/SFBC MIMO Model

In this section, the FS OQAM/FBMC MIMO system is described for SFBC and SM MIMO systems. The operations are described explicitly in the discrete time-domain, whereas in the next section, the hybrid OQAM/FBMC system is fully represented using matrices. The Alamouti coding as an SD MIMO technique [48], aims at reducing the BER by sending dependent (coded) data streams from multiple transmitting antennas. On the other hand, SM aims at increasing the data rate by sending independent data streams on different transmitting antennas [49]. Since Alamouti coding requires complex orthogonality, and OQAM/FBMC signals are only real-orthogonal, the MIMO coding is performed before the OQAM processing, thus avoiding the intrinsic interference problem which arises when Alamouti coding is performed on the OQAM/FBMC modulated signal [58].

4.1.1 Transmitter

The filtering in the FS approach is performed on the upsampled signal before the IFFT operation. The transmitter of the FS OQAM/FBMC MIMO system is shown in Figure 4-1 for a 2×2 MIMO setting.

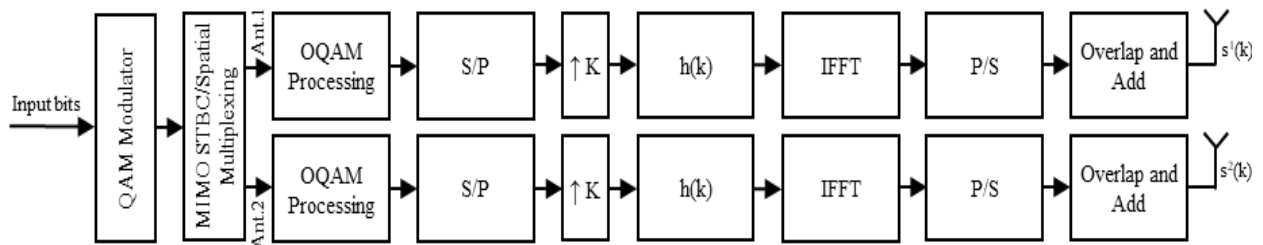


Figure 4-1: The proposed FS-OQAM/FBMC MIMO system transmitter.

First, the input bits are modulated using 4-QAM modulation. Afterwards, the MIMO coding is performed. If x_n is the QAM-modulated symbol at the n^{th} time sample, the output of Alamouti SFBC for the first and second transmitter branches are:

$$\begin{aligned} \mathbf{c}_n^1 &= [x_1, -x_2^*, x_3, -x_4^*, \dots \dots], \\ \mathbf{c}_n^2 &= [x_2, x_1^*, x_4, x_3^*, \dots \dots]. \end{aligned} \quad 4-1$$

As for the SM MIMO system, the odd and even 4-QAM symbols are split across the two branches as follows:

$$\begin{aligned} \mathbf{c}_n^1 &= [x_1, x_3, \dots \dots], \\ \mathbf{c}_n^2 &= [x_2, x_4, \dots \dots]. \end{aligned} \quad 4-2$$

It can be noted that in the SM the rate is double that of the Alamouti SD scheme, while in the Alamouti system the BER performance is enhanced as will be shown in the results section.

After the QAM symbols are split onto the two branches using either Alamouti coding or SM, the coded symbols are input to OQAM processing. The OQAM/FBMC signal preserves real orthogonality since only a real or an imaginary symbol is transmitted per subcarrier, and only neighbouring subcarriers overlap in FBMC in the frequency domain. OQAM processing involves taking the real (\Re) and imaginary (\Im) parts of the complex coded symbols c_n^1 and c_n^2 , and placing them respectively with half of the original symbol duration ($\frac{T}{2}$) as follows:

$$\mathbf{d}_n^i = [\Re(c_1^i), \Im(c_1^i), \Re(c_2^i), \Im(c_2^i), \dots \dots], \quad for \ i = 1, 2. \quad 4-3$$

After the complex to real conversion, each symbol is multiplied by a phase factor $\theta_{m,n} = e^{j\frac{\pi}{2}(m+n)}$, where m is the subcarrier index. The phase factor introduces phase mapping between the real and imaginary parts, according to the symbol order and the subcarrier order being even or odd. These operations are represented using matrices in the following section.

After OQAM processing, FS-FBMC modulation is performed. The signal is upsampled by the overlapping factor K . Then, the signal is filtered using the prototype filter with discrete impulse response $h(k)$. The filter used is the PHYDYAS prototype filter which was previously described in section 3.4.2. It is the most popular for use with FBMC since it provides good time-frequency localization with a shorter filter length. The overlapping factor K indicates the number of symbols

which overlap in time, and it also determines the prototype filter impulse response $h(k)$ length, which is given by $L_F = 2K - 1$.

After filtering in the frequency domain, the signal is converted to the time domain using an IFFT of size $K \times N$. The output frames are overlapped and added to give the output KN -point FBMC signal. The baseband OQAM/FBMC signal with N subcarriers and N_c symbols is given by:

$$s^i(k) = \sum_{m=0}^{N-1} \sum_{n=0}^{N_c-1} d_{m,n}^i h(k - nM) e^{j\frac{2\pi mk}{N}} e^{j\frac{\pi}{2}(m+n)}, \quad \text{for } i = 1, 2, \quad 4-4$$

where $d_{m,n}^i$ is the real-valued n^{th} symbol described by (4-3) for the m^{th} subcarrier and the i^{th} antenna.

4.1.2 Receiver

The transmitted signals are sent over a Rayleigh fading L_H -path frequency-selective channel, with each path coefficient an independent identically distributed (IID) complex Gaussian random variable with zero mean and variance of $1/L_H$. Assuming perfect channel state information (CSI), the received noisy signal vectors thus become:

$$\begin{aligned} \mathbf{r}_1 &= \mathbf{s}_1 * \mathbf{g}_{11} + \mathbf{s}_2 * \mathbf{g}_{12} + \boldsymbol{\eta}_1, \\ \mathbf{r}_2 &= \mathbf{s}_1 * \mathbf{g}_{21} + \mathbf{s}_2 * \mathbf{g}_{22} + \boldsymbol{\eta}_2. \end{aligned} \quad 4-5$$

where $\boldsymbol{\eta}_1$ and $\boldsymbol{\eta}_2$ are the complex Gaussian noise vectors $\boldsymbol{\eta}_j \sim \mathbb{CN}(0; \sigma_j^2 \mathbf{I})$ at the receive antennas 1 and 2 respectively, and \mathbf{s}_1 and \mathbf{s}_2 are the vector representations of $s^1(k)$ and $s^2(k)$ in (4-4) respectively, and \mathbf{g}_{ij} is a vector of the coefficients of the channel's impulse response between the i^{th} transmit antenna and the j^{th} receive antenna. The length of \mathbf{g}_{ij} is equal to the number of channel multipath taps L_H .

The FS-FDE OQAM/FBMC MIMO receiver is depicted in Figure 4-2. At the receiver end, equalization is performed in the frequency domain after converting the received signal to the frequency domain using an NK -point FFT. Equalization is performed in the frequency domain to counteract the effects of multipath fading on the transmitted signal, using ZF or MMSE equalizers. Compare to the corresponding OFDM receiver, there is a processing delay time of length $K - 1$ samples, associated with the FS FBMC demodulation method.

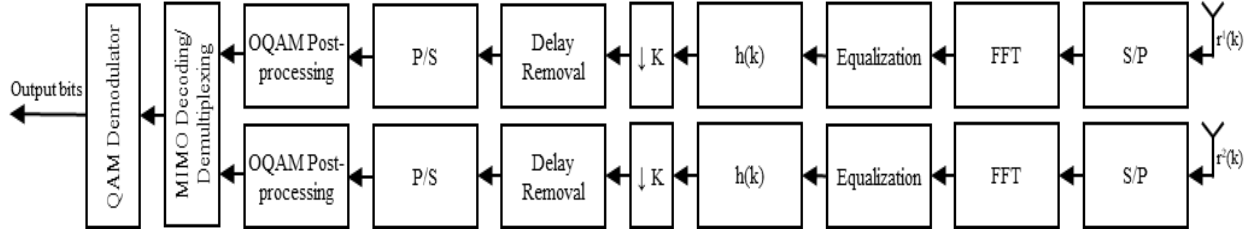


Figure 4-2: The proposed FS-OQAM/FBMC MIMO system receiver.

The channel matrix in the discrete frequency domain is given by:

$$\mathbf{G} = \begin{bmatrix} \mathbf{G}_{11} & \mathbf{G}_{12} \\ \mathbf{G}_{21} & \mathbf{G}_{22} \end{bmatrix}, \quad 4-6$$

where \mathbf{G}_{ij} is a diagonal matrix of the NK -point FFT of g_{ij} . The equalization matrices $\boldsymbol{\beta}$ of the ZF and MMSE FDE equalizers are obtained respectively as follows:

$$\boldsymbol{\beta}_{ZF} = (\mathbf{G}^H \mathbf{G})^{-1} \mathbf{G}^H, \quad 4-7$$

$$\boldsymbol{\beta}_{MMSE} = \left(\mathbf{G}^H \mathbf{G} + \frac{1}{SNR} \mathbf{I}_{2KN} \right)^{-1} \mathbf{G}^H, \quad 4-8$$

where \mathbf{G}^H is the Hermitian matrix of \mathbf{G} , \mathbf{I}_{2KN} is an identity matrix of dimensions $2KN \times 2KN$, and the SNR is the signal-to-noise ratio. The ZF equalizer is designed to cancel the effects of the multipath channel regardless of the AWGN, while the MMSE equalizer is designed to minimize the variance of the difference between transmitted data and the signal at the equalizer output, taking the AWGN into consideration [151].

After FDE, the signal is input to the FBMC frequency de-spreading demodulator as shown in Figure 4-2. First the signal is filtered using the half-Nyquist prototype filter $h(k)$. Next, the signal is downsampled (de-spread) by a factor of K . Afterwards, the delay caused by the prototype filter tails is removed. The signal is then converted back to serial, recovering the estimated OQAM symbols \hat{d}_n^1 and \hat{d}_n^2 for antennas 1 and 2 respectively.

The OQAM post-processing at the receiver performs the inverse operations of the OQAM processing. The real parts of each two consecutive symbols of duration $\frac{T}{2}$, are used to form a complex symbol of duration T as follows:

$$\hat{\mathbf{c}}_n^i = \left[\Re(\hat{d}_1^i) + j\Re(\hat{d}_2^i), \Re(\hat{d}_3^i) + j\Re(\hat{d}_4^i), \dots \dots \right], \quad \text{for } i = 1, 2. \quad 4-9$$

After the coded symbols for each antenna \hat{c}_n^i are recovered, the MIMO decoding is performed. For the Alamouti SFBC system, the symbols on each antenna are decoded as follows:

$$\begin{aligned}\hat{\mathbf{x}}_n^1 &= [\hat{c}_1^1, -\hat{c}_2^{1*}, \hat{c}_3^1, -\hat{c}_4^{1*}, \dots \dots], \\ \hat{\mathbf{x}}_n^2 &= [\hat{c}_2^{2*}, \hat{c}_1^2, \hat{c}_4^{2*}, \hat{c}_3^2, \dots \dots].\end{aligned}\quad 4-10$$

Afterwards, the estimated symbols from each branch are averaged as follows:

$$\hat{\mathbf{x}}_n = \frac{\hat{\mathbf{d}}_n^1 + \hat{\mathbf{d}}_n^2}{2}.\quad 4-11$$

As for the SM system, the estimated symbols are demultiplexed as follows:

$$\hat{\mathbf{x}}_n = [\hat{c}_1^1, \hat{c}_1^2, \hat{c}_2^1, \hat{c}_2^2, \dots \dots].\quad 4-12$$

Finally, the decoded symbols \hat{d}_n are QAM demodulated to recover the input bits.

4.2 Hybrid OQAM/FBMC SFBC MIMO Model

The proposed OQAM/FBMC MIMO model consists of a transmitter implemented using the PPN approach, and a receiver implemented using FS in conjunction with FDE (ZF and MMSE) for Rayleigh fading channel. Another alternative less-complex TDE receiver is suggested for better multipath channel conditions, which have a LOS path. In both systems, the MIMO Alamouti SFBC is performed on the complex-orthogonal signal before the OQAM processing [152], to avoid the intrinsic interference problem of OQAM/FBMC when Alamouti SFBC is performed on the OQAM/FBMC modulated signal. The 2×2 MIMO setting in the previous section is generalized to any $P \times P$ MIMO setting, and any M -ary QAM modulation order. In this section, a mathematical model is developed using matrix representation, which gives a detailed description of the system operations which facilitates the BER analysis, and the complexity analysis is provided in the following sections.

The FBMC prototype filter used is the PHYDYAS prototype filter, whose coefficients H_k are described in Table 3-2 for different overlapping factors K . Its impulse response is described by (3-9). The filter coefficients are symmetric to maintain the half-Nyquist prototype filter condition. An overlapping factor of $K = 4$ is chosen for the system description. For $K = 4$ and thus filter length of $L_F = 7$, the filter vector \mathbf{H}_k is obtained as:

$$\mathbf{H}_k = [H_3 H_2 H_1 H_0 H_1 H_2 H_3]. \quad 4-13$$

4.2.1 PPN Transmitter

The proposed $P \times P$ MIMO PPN-OQAM/FBMC transmitter is displayed in Figure 4-3. The PPN-FBMC modulation in the transmitter is implemented using the modified PPN technique [38], [39], [40], in which filtering is performed after the N -IFFT as explained in section 2.1.2.1.

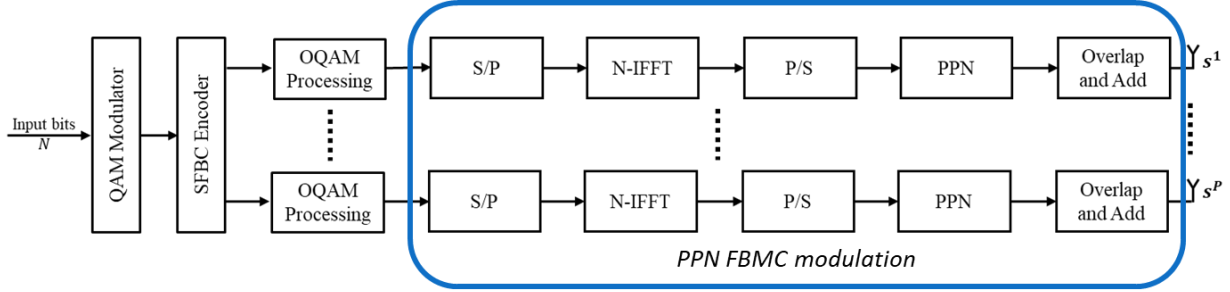


Figure 4-3: The proposed hybrid OQAM/FBMC $P \times P$ MIMO system transmitter

First, the input data bits of length N are M -ary QAM modulated to $N_c = N/M$ complex symbols represented by:

$$\mathbf{X} = [X_1, X_2, \dots, X_{N_c-1}, X_{N_c}]. \quad 4-14$$

Next, the complex-valued symbols \mathbf{X} are MIMO coded using Alamouti SFBC. The MIMO-coded signal for the i^{th} transmit antenna \mathbf{X}^i for the 2×2 MIMO setting is given by:

$$\begin{aligned} \mathbf{X}^1 &= \mathbf{D}\mathbf{X} - \mathbf{E}\mathbf{X}^* = [X_1 \quad -X_2^* \quad \dots \quad X_{N_c-1} \quad -X_{N_c}^*]^T, \\ \mathbf{X}^2 &= \mathbf{F}\mathbf{X} + \mathbf{G}\mathbf{X}^* = [X_2 \quad X_1^* \quad \dots \quad X_{N_c} \quad X_{N_c-1}^*]^T, \end{aligned} \quad 4-15$$

where the matrices \mathbf{D} , \mathbf{E} , \mathbf{F} and \mathbf{G} are $N_c \times N_c$ square matrices defined as:

$$\begin{aligned} \mathbf{D} &= [k_1^{N_c} \quad \mathbf{0}_{N_c \times 1} \quad k_3^{N_c} \quad \mathbf{0}_{N_c \times 1} \quad \dots \quad k_{N_c-1}^{N_c} \quad \mathbf{0}_{N_c \times 1}], \\ \mathbf{E} &= [\mathbf{0}_{N_c \times 1} \quad k_2^{N_c} \quad \mathbf{0}_{N_c \times 1} \quad k_4^{N_c} \quad \dots \quad \mathbf{0}_{N_c \times 1} \quad k_{N_c}^{N_c}], \\ \mathbf{F} &= [k_2^{N_c} \quad \mathbf{0}_{N_c \times 1} \quad k_4^{N_c} \quad \mathbf{0}_{N_c \times 1} \quad \dots \quad k_{N_c}^{N_c} \quad \mathbf{0}_{N_c \times 1}], \\ \mathbf{G} &= [\mathbf{0}_{N_c \times 1} \quad k_1^{N_c} \quad \mathbf{0}_{N_c \times 1} \quad k_3^{N_c} \quad \dots \quad \mathbf{0}_{N_c \times 1} \quad k_{N_c-1}^{N_c}]. \end{aligned} \quad 4-16$$

For a 4×4 MIMO setting, the extended orthogonal Alamouti coding scheme is used [153], [154]. The higher order MIMO aims at further enhancing the BER performance through increasing

the spatial diversity at the expense of the increased complexity. The extended 4×4 MIMO SFBC matrix for a block of four complex symbols $X_n = [X_1, X_2, X_3, X_4]$ is described via the following matrix, where each row represents the n^{th} sample and each column represents the i^{th} transmit antenna.

$$\mathbf{C} = \begin{bmatrix} X_1 & X_2 & X_3 & X_4 \\ X_2^* & -X_1^* & X_4^* & -X_3^* \\ X_3^* & X_4^* & -X_1^* & -X_2^* \\ X_4 & -X_3 & -X_2 & X_1 \end{bmatrix}. \quad 4-17$$

Thus, the transmitted symbols over the i^{th} branch \mathbf{X}^i is given for $i = 1, 2, 3$ and 4, as follows:

$$\begin{aligned} \mathbf{X}^1 &= [X_1 \quad X_2^* \quad X_3^* \quad X_4 \quad \cdots \cdots X_{N_c-3} \quad X_{N_c-2}^* \quad X_{N_c-1}^* \quad X_{N_c}]^T, \\ \mathbf{X}^2 &= [X_2 \quad -X_1^* \quad X_4^* \quad -X_3 \quad \cdots \cdots X_{N_c-2} \quad -X_{N_c-3}^* \quad X_{N_c}^* \quad -X_{N_c-1}]^T, \\ \mathbf{X}^3 &= [X_3 \quad X_4^* \quad -X_1^* \quad -X_2 \quad \cdots \cdots X_{N_c-1} \quad X_{N_c}^* \quad -X_{N_c-3}^* \quad -X_{N_c-2}]^T, \\ \mathbf{X}^4 &= [X_4 \quad -X_3^* \quad -X_2^* \quad X_1 \quad \cdots \cdots X_{N_c} \quad -X_{N_c-1}^* \quad -X_{N_c-2}^* \quad X_{N_c-3}]^T. \end{aligned} \quad 4-18$$

The OQAM processing is next performed on the MIMO-coded symbols \mathbf{X}^i . The OQAM/FBMC signal produces a real-orthogonal signal. OQAM processing involves extracting the real and imaginary parts of the N_c complex coded symbols \mathbf{X}^i , with duration T and placing them separately each at half of the original symbol duration, after multiplication with a phase factor $e^{j\frac{\pi}{2}(m+n)}$, where m is the subcarrier index and n the symbol order. The simplest phase pattern is to keep the extracted real part with zero-phase and multiply the extracted imaginary part by j for even numbered frames, and vice versa for odd-numbered frames.

The OQAM processing with such phase mapping can be alternatively expressed using matrices. The complex signal \mathbf{X}^i is first upsampled by a factor of 2 as follows:

$$\mathbf{X}_u^i = [\mathbf{k}_1^{N_c} \mathbf{k}_1^{N_c} \mathbf{k}_2^{N_c} \mathbf{k}_2^{N_c} \mathbf{k}_3^{N_c} \mathbf{k}_3^{N_c} \cdots \cdots \cdots \mathbf{k}_N^{N_c} \mathbf{k}_N^{N_c}]^T \mathbf{X}^i. \quad 4-19$$

Then, the complex to real and imaginary conversion, and the multiplication by the phase factor are combined in (4-20) and (4-21) for even and odd numbered frames respectively, to produce the OQAM signal \mathbf{X}_o^i as follows:

$$X_o^i = \frac{X_u^i + \rho X_u^{i*}}{2}, \quad 4-20$$

$$X_o^i = \frac{X_u^i - \rho X_u^{i*}}{2}, \quad 4-21$$

where ρ is an N by N matrix which is equal to $[k_1^N - k_2^N \quad k_3^N - k_4^N \quad \dots \dots \dots k_{N-1}^N - k_N^N]$.

The FBMC modulation is next performed using the overlap-and-add PPN approach [38], [39], [40]. After serial to parallel conversion, the OQAM symbols are converted to the time domain using the isometric N -point IFFT matrix \mathcal{F}_N^{-1} as follows:

$$\mathbf{x}^i = \mathcal{F}_N^{-1} X_o^i \quad 4-22$$

Afterwards, the symbols \mathbf{x}^i are duplicated and repeated K -times as:

$$\mathbf{x}_d^i = [J_1 \ J_2 \ \dots \dots \dots J_{N-1} \ J_N]^T \mathbf{x}^i, \quad 4-23$$

where J_k is an L by K matrix and is equal to $[k_k^L \ k_k^L \ k_k^L \ k_k^L]$ for $K = 4$, where $L = NK$.

The duplicated signal \mathbf{x}_d^i is next multiplied (element-by-element) by the NK -sampled impulse response \mathbf{h}_{NK} of the prototype filter $h(t)$ previously defined in (3-9), as follows:

$$\mathbf{x}_F^i = \mathbf{x}_{dup}^i \text{diag}(\mathbf{h}_{NK}) \quad 4-24$$

Lastly, the transmitted symbol vector at the i^{th} transmit antenna \mathbf{s}^i is obtained by the overlap-and-add technique as follows:

$$\mathbf{s}^i = \mathbf{x}_F^i + \begin{bmatrix} \mathbf{0}_{(K-1)N \times N} & \mathbf{I}_{(K-1)N} \\ \mathbf{0}_{N \times N} & \mathbf{0}_{N \times (K-1)N} \end{bmatrix} \mathbf{s}^{i'}, \quad 4-25$$

where $\mathbf{s}^{i'}$ is the previously transmitted symbol shifted by NK samples and i takes the values from 1 to P , where P is the number of transmitting antennas.

4.2.2 FS-FDE Receiver

The block diagram of the hybrid system receiver is presented in Figure 4-4, in which the FBMC demodulation is performed using the frequency de-spreading technique. In the FS receiver, the first operation is performing FFT converting the signal to the frequency domain, hence enabling the direct implementation of FDE after it. When the PPN FBMC receiver where

filtering is performed in the time domain is used with FDE, there is an overhead of converting the received signal to frequency to perform FDE using NK -FFT, and then back to time using another NK -IFFT, and then PPN-FBMC demodulation is performed.

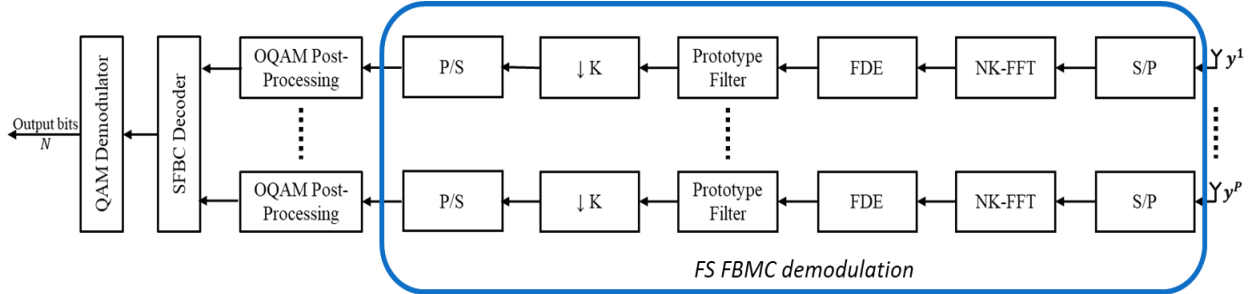


Figure 4-4: The proposed FS-OQAM/FBMC $P \times P$ SFBC MIMO FDE receiver.

After transmission in a multipath fading channel with a number of multipath taps equal to L_h , the received signal vector at the j^{th} antenna \mathbf{y}^j is the sum of the received signals from the P transmit antennas obtained as follows:

$$\mathbf{y}^j = \sum_{i=1}^P \mathbf{s}^i * \mathbf{c}_{ji} + \boldsymbol{\eta}^j, \quad 4-26$$

where $\mathbf{c}_{ji} = [c_{ji}(0) \ c_{ji}(1) \ \dots \ c_{ji}(L_h - 1)]^T$ is the channel impulse response vector, which defines the multipath channel between the i^{th} transmit antenna and the j^{th} receive antenna, while $\boldsymbol{\eta}^j \sim \mathcal{CN}(0, \sigma_{\eta}^2 \mathbf{I})$ represents the complex zero-mean Gaussian noise vector at the j^{th} receive antenna. The channel coefficients are randomly distributed where $\mathbf{c}_{ji} \sim \mathcal{CN}(0, \frac{1}{L_h} \mathbf{I})$.

To perform FDE, the signal is first converted to the discrete frequency domain as in (4-27), where \mathcal{F}_L is the isometric FFT matrix of dimensions $L \times L$.

$$\mathbf{Y}^j = \mathcal{F}_L \mathbf{y}^j. \quad 4-27$$

Afterwards, FDE is applied to the signal as follows:

$$\begin{bmatrix} \hat{\mathbf{Y}}^1 \\ \hat{\mathbf{Y}}^2 \end{bmatrix} = \boldsymbol{\beta} \begin{bmatrix} \mathbf{Y}^1 \\ \mathbf{Y}^2 \end{bmatrix}, \quad \text{for } 2 \times 2 \text{ MIMO} \quad 4-28$$

$$\begin{bmatrix} \hat{\mathbf{Y}}^1 \\ \hat{\mathbf{Y}}^2 \\ \hat{\mathbf{Y}}^3 \\ \hat{\mathbf{Y}}^4 \end{bmatrix} = \boldsymbol{\beta} \begin{bmatrix} \mathbf{Y}^1 \\ \mathbf{Y}^2 \\ \mathbf{Y}^3 \\ \mathbf{Y}^4 \end{bmatrix}, \quad \text{for } 4 \times 4 \text{ MIMO} \quad 4-29$$

where β is the FDE square matrix, which can be expressed as:

$$\beta = \begin{bmatrix} \beta_{11} & \beta_{12} \\ \beta_{21} & \beta_{22} \end{bmatrix}, \quad \text{for } 2 \times 2 \text{ MIMO} \quad 4-30$$

$$\beta = \begin{bmatrix} \beta_{11} & \beta_{12} & \beta_{13} & \beta_{14} \\ \beta_{21} & \beta_{22} & \beta_{23} & \beta_{24} \\ \beta_{31} & \beta_{32} & \beta_{33} & \beta_{34} \\ \beta_{41} & \beta_{42} & \beta_{43} & \beta_{44} \end{bmatrix}, \quad \text{for } 4 \times 4 \text{ MIMO} \quad 4-31$$

where β_{ji} is a diagonal matrix of the channel equalizer coefficients for the i^{th} transmit and j^{th} receive antennas.

For ZF and MMSE, β can be obtained as in (4-7) and (4-8) respectively, where \mathbf{G} is the MIMO channel frequency response matrix previously given by (4-6) for the 2×2 MIMO case, and given by (4-32) for the 4×4 MIMO case.

$$\mathbf{G} = \begin{bmatrix} \mathbf{G}_{11} & \mathbf{G}_{12} & \mathbf{G}_{13} & \mathbf{G}_{14} \\ \mathbf{G}_{21} & \mathbf{G}_{22} & \mathbf{G}_{23} & \mathbf{G}_{24} \\ \mathbf{G}_{31} & \mathbf{G}_{32} & \mathbf{G}_{33} & \mathbf{G}_{34} \\ \mathbf{G}_{41} & \mathbf{G}_{42} & \mathbf{G}_{43} & \mathbf{G}_{44} \end{bmatrix} \quad 4-32$$

where \mathbf{G}_{ji} is a diagonal matrix of the L -point FFT of \mathbf{c}_{ji} given by:

$$\mathbf{G}_{ji} = \text{diag}(\mathcal{F}_{L \times L_h} \mathbf{c}_{ji}), \quad 4-33$$

where $\mathcal{F}_{L \times L_h}$ is a DFT submatrix that contains the first L_h columns of \mathcal{F}_L .

After FDE, FBMC demodulation is performed using the frequency de-spreading method. Since the signal after FDE is already in the frequency domain, then the signal is directly filtered using the prototype filter \mathbf{H}_k as follows:

$$\hat{\mathbf{Y}}_F^j = \mathcal{H} \hat{\mathbf{Y}}^j, \quad 4-34$$

where \mathcal{H} is the convolution matrix of the L_F -point prototype filter coefficients vector \mathbf{H}_k previously described in (4-13), and is formulated as:

$$\mathcal{H} = [\mathbf{H}_k \mathbf{0}_{1 \times Q}; \mathbf{0} \mathbf{H}_k \mathbf{0}_{1 \times (Q-1)}; \mathbf{0} \mathbf{0} \mathbf{H}_k \mathbf{0}_{1 \times (Q-2)}; \dots \dots; \mathbf{0}_{1 \times (Q-1)} \mathbf{H}_k \mathbf{0}; \mathbf{0}_{1 \times Q} \mathbf{H}_k]^T, \quad 4-35$$

where $Q = NK - L_F$.

Afterwards, the signal is downsampled by K as follows:

$$\mathbf{Y}_o^j = [\mathbf{k}_1^N \mathbf{0}_{(K-1) \times N} \mathbf{k}_2^N \mathbf{0}_{(K-1) \times N} \dots \dots \mathbf{k}_{N-1}^N \mathbf{0}_{(K-1) \times N} \mathbf{k}_N^N \mathbf{0}_{(K-1) \times N}]^T \hat{\mathbf{Y}}_F^j. \quad 4-36$$

OQAM post-processing is next performed. First, the real part of the downsampled symbols \mathbf{Y}_R^j is extracted as in (4-37), thus eliminating the imaginary interference.

$$\mathbf{Y}_R^j = \frac{\mathbf{Y}_o^j + \mathbf{Y}_o^{j*}}{2}. \quad 4-37$$

Then, the same phase pattern deployed in the transmitter is used to alternately combine the odd and even symbols of \mathbf{Y}_R^j , to form the complex symbols $\check{\mathbf{Y}}^j$ of length N_c . The combining is performed using (4-38) and (4-39) for even and odd frames respectively.

$$\check{\mathbf{Y}}^j = \boldsymbol{\varepsilon}_1 \mathbf{Y}_R^j + j \boldsymbol{\varepsilon}_2 \mathbf{Y}_R^j, \quad 4-38$$

$$\check{\mathbf{Y}}^j = \boldsymbol{\varepsilon}_2 \mathbf{Y}_R^j + j \boldsymbol{\varepsilon}_1 \mathbf{Y}_R^j, \quad 4-39$$

where $\boldsymbol{\varepsilon}_1 = [\mathbf{k}_1^N \mathbf{k}_3^N \dots \dots \mathbf{k}_{N-3}^N -\mathbf{k}_{N-1}^N]^T$ and $\boldsymbol{\varepsilon}_2 = [\mathbf{k}_2^N \mathbf{k}_4^N \dots \dots \mathbf{k}_{N-2}^N \mathbf{k}_N^N]^T$.

Afterwards, the Alamouti decoding is performed. For the 2×2 MIMO setting, SFBC decoding is achieved as in (4-40) to obtain the MIMO decoded symbol vectors for the j^{th} receive branch $\tilde{\mathbf{Y}}^j$, using the matrices \mathbf{D} , \mathbf{E} , \mathbf{F} and \mathbf{G} previously described by (4-16).

$$\begin{aligned} \tilde{\mathbf{Y}}^1 &= \mathbf{D}\check{\mathbf{Y}}^1 - \mathbf{E}\check{\mathbf{Y}}^{1*} = [\check{Y}_1^1 - \check{Y}_2^{1*} \dots \dots \check{Y}_{N_c-1}^1 - \check{Y}_{N_c}^{1*}]^T \\ \tilde{\mathbf{Y}}^2 &= \mathbf{F}\check{\mathbf{Y}}^{2*} + \mathbf{G}\check{\mathbf{Y}}^2 = [\check{Y}_2^{2*} \check{Y}_1^2 \dots \dots \check{Y}_{N_c}^{2*} \check{Y}_{N_c-1}^2]^T. \end{aligned} \quad 4-40$$

As for the 4×4 MIMO setting, $\tilde{\mathbf{Y}}^j$ is calculated as:

$$\begin{aligned} \tilde{\mathbf{Y}}^1 &= [X_1 \quad X_2^* \quad X_3^* \quad X_4 \dots \dots X_{N_c-3} \quad X_{N_c-2}^* \quad X_{N_c-1}^* \quad X_{N_c}]^T, \\ \tilde{\mathbf{Y}}^2 &= [X_2 - X_1^* \quad X_4^* - X_3 \dots \dots X_{N_c-2} - X_{N_c-3}^* \quad X_{N_c}^* - X_{N_c-1}]^T, \\ \tilde{\mathbf{Y}}^3 &= [X_3 \quad X_4^* \quad -X_1^* - X_2 \dots \dots X_{N_c-1} \quad X_{N_c}^* \quad -X_{N_c-3}^* - X_{N_c-2}]^T, \\ \tilde{\mathbf{Y}}^4 &= [X_4 - X_3^* \quad -X_2^* \quad X_1 \dots \dots X_{N_c} - X_{N_c-1}^* \quad -X_{N_c-2}^* \quad X_{N_c-3}]^T. \end{aligned} \quad 4-41$$

The estimated QAM symbols $\tilde{\mathbf{Y}}$ are next obtained by averaging $\tilde{\mathbf{Y}}^j$ for $j = 1:P$ as follows:

$$\tilde{\mathbf{Y}} = \frac{1}{P} \sum_{j=1}^P \tilde{\mathbf{Y}}^j. \quad 4-42$$

Finally, the symbols are M -ary QAM demodulated to recover the received N bits.

4.2.3 PPN-TDE Receiver

In mild multipath fading channels with a LOS path [31], a less complex TDE is proposed. Since equalization is performed in the time domain, there is no need for using Frequency de-spreading in the FBMC demodulator. Instead, the receiver is implemented using the same less complex PPN approach used in the transmitter. Figure 4-5 shows the block diagram of the proposed TDE PPN-OQAM/FBMC receiver.

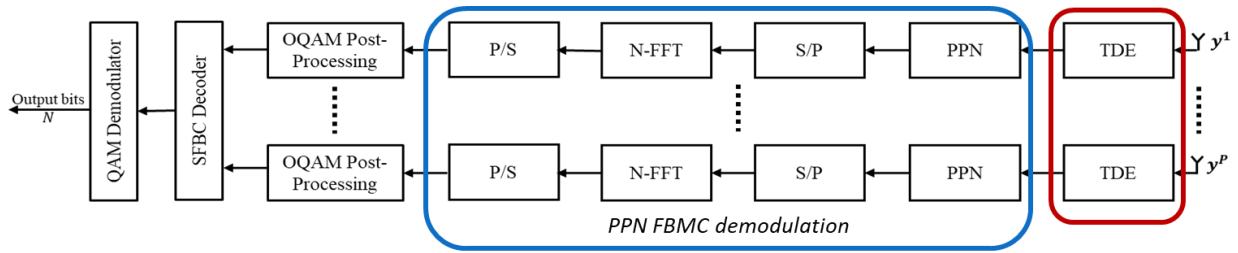


Figure 4-5: The proposed PPN OQAM/FBMC $P \times P$ SFBC MIMO TDE receiver.

The deployed TDE is a ZF equalizer based on a finite impulse response (FIR) transversal filter, which cancels the multipath channel effects, depending on the presence of a LOS path [155], [156]. The length of the equalizer filter can be chosen according to the number of multipath channel taps L_h . The equalizer filter coefficients \mathbf{a}_{ji} are calculated using the inverse of the upper triangular circulant matrix of the channel impulse response vector $\mathbf{c}_{ji} = [c_{ji}(0) \ c_{ji}(1) \ \dots \ c_{ji}(L_h - 1)]^T$ as:

$$\mathbf{a}_{ji} = \mathbf{k}_1^{L_h} * \begin{bmatrix} c_{ji}(0) & c_{ji}(1) & \dots & c_{ji}(L_h - 2) & c_{ji}(L_h - 1) \\ 0 & c_{ji}(0) & \dots & c_{ji}(L_h - 3) & c_{ji}(L_h - 2) \\ \vdots & \vdots & \ddots & \vdots & \vdots \\ 0 & 0 & \dots & c_{ji}(0) & c_{ji}(1) \\ 0 & 0 & \dots & 0 & c_{ji}(0) \end{bmatrix}^{-1}. \quad 4-43$$

The received signal at the j^{th} receiver antenna y^j described by (4-26), is then equalized in the time domain using the equalizer coefficients \mathbf{a}_{ji} as follows:

$$\hat{\mathbf{y}}^j = \sum_{i=1}^P \mathbf{y}^i * \mathbf{a}_{ji}. \quad 4-44$$

After channel equalization, the FBMC PPN demodulation is performed using the PPN approach. First, the signal is multiplied (element-by-element) by the sampled impulse response of the prototype filter \mathbf{h}_{NK} . This is translated to multiplication by the diagonal matrix of \mathbf{h}_{NK} as follows:

$$\mathbf{y}_F^j = \hat{\mathbf{y}}^j \text{diag}(\mathbf{h}_{NK}). \quad 4-45$$

The N -spaced K -parts of the filtered signal are then overlapped and added to extract the symbol \mathbf{y}_o^j of length N , as in (4-46), for $K = 4$.

$$\mathbf{y}_o^j = \begin{bmatrix} \mathbf{I}_N \\ \mathbf{I}_N \\ \mathbf{I}_N \\ \mathbf{I}_N \end{bmatrix}_{NK \times N} \mathbf{y}_F^j. \quad 4-46$$

The signal is next converted back to the frequency domain as follows:

$$\mathbf{Y}_o^j = \mathcal{F}_N \mathbf{y}_o^j. \quad 4-47$$

Afterwards, the signal undergoes OQAM post-processing and MIMO decoding previously described in (4-36)-(4-42), before the complex symbols are M -ary QAM demodulated to recover the bits.

4.3 BER Analysis

The BER analysis of the proposed OQAM/FBMC hybrid MIMO system with ZF-FDE is presented in this section. The ZF equalization reverses the effects of the multipath channel assuming perfect channel state information (CSI), while the imaginary interference of the FBMC received signal is eliminated by taking the real part as in (4-37). The variance σ_η^2 of the zero-mean noise vector at the j^{th} receive antenna $\boldsymbol{\eta}^j$ in (4-26) is traced along the receiver operations, to derive an expression for the resulting noise power at the receiver output.

At the receiver, FFT is first applied to the received signal as in (4-27), followed by FDE using the equalizer matrix $\boldsymbol{\beta}_{ji}$ as in (4-28) and (4-29), and then filtering using the circulant filter matrix \mathcal{H} as in (4-34). By defining $\boldsymbol{\phi}_{ji} = \mathcal{H}\boldsymbol{\beta}_{ji}$, for a $P \times P$ MIMO setting, the noise vector $\tilde{\boldsymbol{\eta}}^j$ becomes:

$$\tilde{\boldsymbol{\eta}}^j = \sum_{i=1}^P \boldsymbol{\phi}_{ji} \mathcal{F}_L \boldsymbol{\eta}^j. \quad 4-48$$

By defining $\boldsymbol{v}_{ji} = \boldsymbol{\phi}_{ji} \mathcal{F}_L \boldsymbol{\eta}^j$, its variance $\sigma_{v_{ji}}^2$ is equal to its second moment since it has zero mean. It can thus be calculated as:

$$\sigma_{v_{ji}}^2 = E[\boldsymbol{\phi}_{ji} \mathcal{F}_L \boldsymbol{\eta}^j \boldsymbol{\eta}^{j*} \mathcal{F}_L^H \boldsymbol{\phi}_{ji}^H]. \quad 4-49$$

where $E[\cdot]$ is the statistical expectation operator. Since $E[\boldsymbol{\eta}^j \boldsymbol{\eta}^{j*}] = \sigma_{\eta}^2 \mathbf{I}$, and \mathcal{F}_L is the isometric FFT matrix and hence $\mathcal{F}_L \mathcal{F}_L^H = \mathbf{I}$, therefore $\sigma_{v_{ji}}^2$ reduces to:

$$\begin{aligned} \sigma_{v_{ji}}^2 &= \sigma_{\eta}^2 E[\boldsymbol{\phi}_{ji} \boldsymbol{\phi}_{ji}^H] \\ &= \sigma_{\eta}^2 \kappa_{ji}, \end{aligned} \quad 4-50$$

where κ_{ji} is the average power of $\boldsymbol{\phi}_{ji}$. Since $\boldsymbol{\phi}_{ji}$ is a diagonal matrix, therefore its power can be approximated as the average of its squared diagonal elements $\boldsymbol{\phi}_{ji}(l, l)$ defined as:

$$\kappa_{ji} = \frac{1}{L} \sum_{l=1}^L E[\boldsymbol{\phi}_{ji}(l, l)]^2. \quad 4-51$$

After equalization and FBMC demodulation, the signal is OQAM post-processed. This involves taking the real part of the signal as in (4-37), which halves the noise power, then combining consecutive symbols, with the phase pattern as in (4-38) and (4-39), which doubles the power. Therefore, the OQAM post-processing doesn't affect the noise variance overall.

Afterwards, the Alamouti SFBC decoding is performed as in (4-40) and (4-41), and then the outputs are averaged as in (4-42). The resulting averaged noise vector $\bar{\boldsymbol{\eta}}$ using (4-48) thus becomes:

$$\bar{\boldsymbol{\eta}} = \frac{\sum_{j=1}^P \tilde{\boldsymbol{\eta}}^j}{P} = \frac{\sum_{j=1}^P \sum_{i=1}^P \boldsymbol{v}_{ji}}{P}. \quad 4-52$$

Averaging the noise vectors $\tilde{\boldsymbol{\eta}}^j$ which are uncorrelated, reduces the output noise variance according to the MIMO order P . As the number of antennas increases, the averaged noise

variance decreases leading to an enhanced BER performance. The averaged noise variance becomes:

$$\sigma_{\bar{\eta}}^2 = \frac{\sum_{j=1}^P \sum_{i=1}^P \sigma_{v_{ji}}^2}{P^2}. \quad 4-53$$

Using (4-51), (4-52) and (4-53) $\sigma_{\bar{\eta}}^2$ becomes:

$$\sigma_{\bar{\eta}}^2 = \frac{\sigma_{\eta}^2 \sum_{j=1}^P \sum_{i=1}^P \kappa_{ji}}{P^2}, \quad 4-54$$

where σ_{η}^2 is the AWGN variance equal to $N_o/2$. In the case of 2×2 MIMO (4-44) reduces to:

$$\sigma_{\bar{\eta}}^2_{2 \times 2} = \frac{\sigma_{\eta}^2 (\kappa_{11} + \kappa_{12} + \kappa_{21} + \kappa_{22})}{4}. \quad 4-55$$

For M -ary QAM modulation, the theoretical probability of bit-error P_b can be obtained according to [157] and [158] as:

$$P_b = \frac{1}{\log_2 \sqrt{M}} \sum_{k=1}^{\log_2 \sqrt{M}} P_b(k) \quad 4-56$$

where $P_b(k)$ is calculated as in [157] as follows:

$$P_b(k) = \frac{1}{\sqrt{M}} \sum_{i=0}^{(1-2^{-k})\sqrt{M}-1} \left\{ (-1)^{\lfloor \frac{i \cdot 2^{k-1}}{\sqrt{M}} \rfloor} \times \left(2^{k-1} - \left\lfloor \frac{i \cdot 2^{k-1}}{\sqrt{M}} + \frac{1}{2} \right\rfloor \right) \cdot 2Q \left((2i+1) \sqrt{\frac{3 \log_2 M \cdot E_b}{2(M-1)\sigma_{\bar{\eta}}^2}} \right) \right\}, \quad 4-57$$

where $E_b = E_s / \log_2(M)$ where E_s and E_b are the average energy per symbol and per bit respectively, and $Q(\cdot)$ is the Q-function defined as:

$$Q(a) = \frac{1}{2\pi} \int_a^{\infty} e^{-\frac{w^2}{2}} dw. \quad 4-58$$

By substituting the noise power from (4-50) in (4-56) and (4-57), the expression for the BER of the proposed OQAM/FBMC MIMO system is obtained for any M -ary QAM modulation and $P \times P$ MIMO setting.

For the case of 4-QAM the expression in (4-56) and (4-57) reduces to the well-known formula of the theoretical BER of 4-QAM [159] given by:

$$P_b = Q\left(\sqrt{\frac{E_b}{\sigma_{\eta}^2}}\right) = Q\left(\sqrt{\frac{E_s}{2\sigma_{\eta}^2}}\right). \quad 4-59$$

For the case of 4-QAM and 2×2 MIMO, by substituting by (4-55) in (4-59), the expression for the thus BER becomes:

$$P_b = Q\left(\sqrt{\frac{2E_s}{\sigma_{\eta}^2 (\kappa_{11} + \kappa_{12} + \kappa_{21} + \kappa_{22})}}\right). \quad 4-60$$

4.4 Computational Complexity Comparison

This section illustrates the difference in the overall computational complexities of different OQAM/FBMC structures, including the proposed hybrid structure and the PPN-TDE systems. The considered overall complexity includes the complexity of the transmitter (FBMC modulation) and that of the receiver (Equalization + FBMC demodulation) for one transmitter/receiver branch. The complexity of other operations in the systems is not considered since it is constant for all the investigated systems. The computational complexity is measured in terms of the number of real multiplication operations, as a function of the oversampling factor K and the number of subcarriers N . It must be noted that one complex multiplication is equivalent to 4 real multiplications [160].

For the FS transmitter described in section 4.14.1.1, the complexity is that of filtering the NK -point signal by the prototype filter of length $2K - 1$, in addition to that of the NK -point IFFT [41]. The total is $2NK \log_2(NK) + 2(2K - 1)NK$ real multiplications. Since the FS receiver performs the same operations in a reversed manner, it also has the same computational complexity. As for the PPN transmitter, described in section 4.2.1, the complexity is that of the N -point FFT in (4-22), in addition to the NK element-by-element multiplication in (4-24), and it is given by $2N \log_2(N) + 2NK$, and same for the PPN OQAM/FBMC receiver described in section 4.2.3.

As for the TDE used, its computational complexity is that of the $L_H \times L_H$ matrix inversion in (4-43) and the convolution operation in (4-44). Complex matrix inversion generally needs $4L_H^3$ real multiplications. However, taking into consideration that the inverted matrix is an upper triangular matrix, the required number of real multiplications is halved, so it becomes $2L_H^3$. The complexity of the convolution process is $4NKL_H$, and hence the total TDE complexity for the summation in (4-44) is $4L_H^3 + 8NKL_H$.

As for FDE, its complexity is that of calculating the equalization matrix in (4-7) and (4-8), in addition to the multiplication in (4-28). This involves a total of three complex matrix multiplications and one complex matrix inversion all on matrices of the size of $2NK \times 2NK$. Since the matrix \mathbf{G} consists of 4 diagonal matrices, therefore its multiplication by \mathbf{G}^H requires $4NK$ complex multiplications, while its inversion involves $8NK$ complex multiplications instead of $(2NK)^3$ [161]. Therefore, the total number of real multiplications required for FDE on each receiver branch is $40NK$. In the case where FDE is used in the all PPN-based system, an additional complexity of $4NK \log_2(NK)$ is required due to the necessity of converting the signal to the frequency domain using FFT before FDE, and then back to time after FDE using IFFT, to be able to perform the PPN OQAM/FBMC demodulation in which the signal is filtered in the time domain. This overhead overshadows the advantage of the reduced complexity of the all-PPN OQAM/FBMC structure when using FDE.

A comparison of the overall computational complexity expressed in the number of real multiplications per branch of the different OQAM/FBMC system settings is presented in Table 4-1.

To further illustrate the comparison, the overall number of real multiplications of the 4 main different OQAM/FBMC transceiver structures listed in Table 4-1, is plotted against the number of subcarriers for an overlapping factor of $K = 2$ and $K = 4$ in Figure 4-6 and Figure 4-7 respectively. The two cases are considered to illustrate the effect of increasing the overlapping factor K on the computational complexity of the different structures. The complexity is plotted using logarithmic scale, while the number of subcarriers is on a linear scale from 2 to 2048 subcarriers. For the TDE equalizer, channel lengths L_H of 3 and 5 taps are considered.

Table 4-1 Total number of real multiplications of different OQAM/FBMC system structures

	Transmitter	Receiver	Equalization	Total
FS with FDE	$2NK(\log_2(NK) + 2K - 1)$	$2NK(\log_2(NK) + 2K - 1)$	$40NK$	$4NK(\log_2(NK) + 2K + 9)$
PPN with FDE	$2N(\log_2 N + K)$	$2N(\log_2 N + K)$	$4NK(10 + \log_2(NK))$	$4N(\log_2 N + 11K + K\log_2(NK))$
Hybrid with FDE	$2N(\log_2 N + K)$	$2NK(\log_2(NK) + 2K - 1)$	$40NK$	$2N(\log_2 N + K(\log_2(NK) + 20 + 2K))$
PPN with TDE	$2N(\log_2 N + K)$	$2N(\log_2 N + K)$	$4L_H^3 + 8NKL_H$	$4N(\log_2 N + K + 2KL_H) + 4L_H^3$

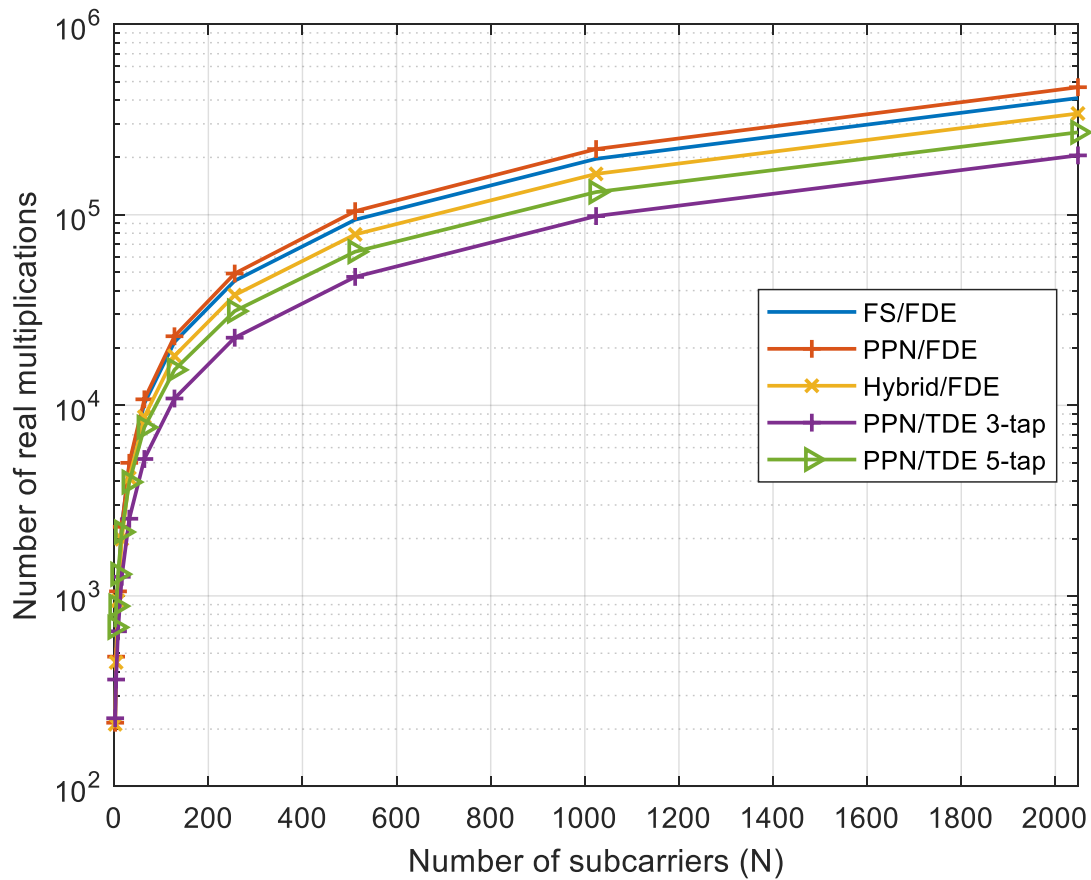


Figure 4-6: Order of computational complexity for different OQAM/FBMC systems for $K = 2$.

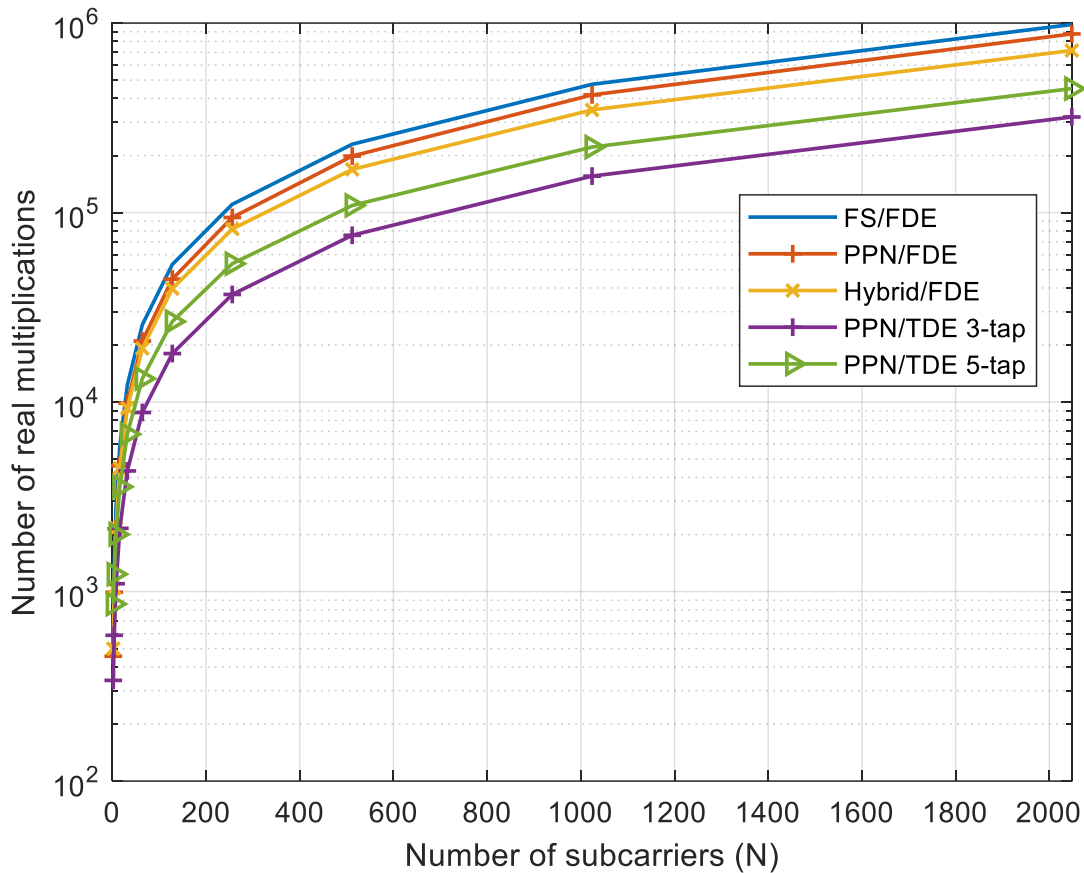


Figure 4-7: Number of real multiplications for different OQAM/FBMC systems for $K = 4$.

Although the PPN technique is generally less complex than the FS technique, in conjunction with FDE necessary to equalize the channel effects, they both have almost the same complexity for $K = 4$, and the all-FS system has even lower complexity at $K = 2$, due to the FFT/IFFT overhead previously explained. The figures also show that the proposed hybrid system has the lowest overall complexity in Rayleigh fading channels. On the other hand, the PPN-TDE system has significantly lower overall complexity, however, it is only suitable for multipath channels with a LOS path, unlike the systems with FDE which are more robust and suitable for highly frequency-selective channels. It can also be noted that the complexity of the TDE equalizer slightly increases as the channel length and the required number of equalizer taps increase. For example, for $K = 4$ and $N = 512$ subcarriers, the FS/FDE, the PPN/FDE and the proposed hybrid/FDE involve 229400, 198700, 169000 real multiplications respectively, while the TDE PPN system involves 109000 and 75880 for L_H equal to 3 and 5 taps respectively.

Table 4-2 shows the number of real multiplications for a different number of subcarriers N and the percentage of complexity reduction compared to the original FS OQAM/FBMC system.

Table 4-2 Number of real multiplications for different number of subcarriers.

	$N = 256$	$N = 512$	$N = 1024$
FS/FDE	110600	229400	475100
PPN/FDE	94210 16%	198700 13%	417800 12%
Hybrid/FDE	81920 25.9%	169000 26.3%	348200 26.7%
PPN/TDE 5-tap	53750 51%	109000 52.5%	221700 53.3%
PPN/TDE 3-tap	36970 66.6%	75880 66.9%	155800 67.2%

4.5 Simulation and Results

In this section, the simulation results of the proposed hybrid OQAM/FBMC MIMO system are presented. The simulation is performed using MATLAB scripts and a sample of the developed codes is presented in the appendix. The simulation measures the performance through different KPIs including the BER and the PSD of the transmitted signal. First, the analytical BER is compared to the simulated BER of the hybrid system using ZF-FDE. Then the proposed system is simulated over Rayleigh multipath fading channel using FDE; ZF and MMSE and compared to CP-OFDM for reference. On the other hand, the less complex PPN-FBMC system with TDE is simulated over a multipath fading channel with a LOS component. The plotted results are obtained by averaging the results for Monte Carlo simulations with 10^5 iterations. The simulation parameters are listed in Table 4-3.

The range of SNR thresholds considered in the simulations is between 0 and 25 dB, which includes the desirable SNR ranges for different applications. For example, in LTE, an SNR above 20 dB is considered a strong signal with maximum data speed, while between 13 to 20 dB is

considered a good signal with good data speed [162]. As the SNR goes lower closer to 0 dB, the performance drops drastically and when it reaches 0 dB there is no signal (disconnection).

Table 4-3 OQAM/FBMC Simulation Parameters.

Number of Monte Carlo Simulations	10 ⁵
Modulation Order	4-QAM, 16-QAM
Number of Subcarriers (N)	256
Overlapping Factor (K)	4
Prototype Filter Type	PHYDYAS
Equalization Type	FDE (ZF/MMSE) / TDE (ZF)
MIMO Coding	Alamouti SFBC / Spatial Multiplexing
Simulation Scenarios	SISO – 2 × 2 MIMO – 4 × 4 MIMO
OFDM CP-length	$N/8$
Transmission Channel	Frequency-selective Rayleigh fading / Multipath fading with LOS path (Pedestrian A)

4.5.1 Channel Model

The channel model used for simulation of the hybrid OQAM/FBMC FDE system is a Rayleigh fading L_H -path frequency-selective quasi-static independent channels with each path coefficient an IID complex Gaussian random variable with variance $1/L_H$. It is generated by adding two normally distributed, zero-mean random vectors of length L_H , one real and one imaginary, hence producing a complex random multipath channel for each symbol. Increasing the number of multipath channel taps increases the channel delay spread and hence the frequency selectivity increases. Channel lengths of 3 and 7 multipath taps have been chosen to simulate the behaviour of the system in different channel conditions. To illustrate the nature of the channel model, a random sample of the normalized power delay profiles (PDP) of a 7-tap Rayleigh channel is plotted in Figure 4-8 (a), and a random sample of the frequency response of the same channel is plotted in Figure 4-8 (b) against normalized frequency.

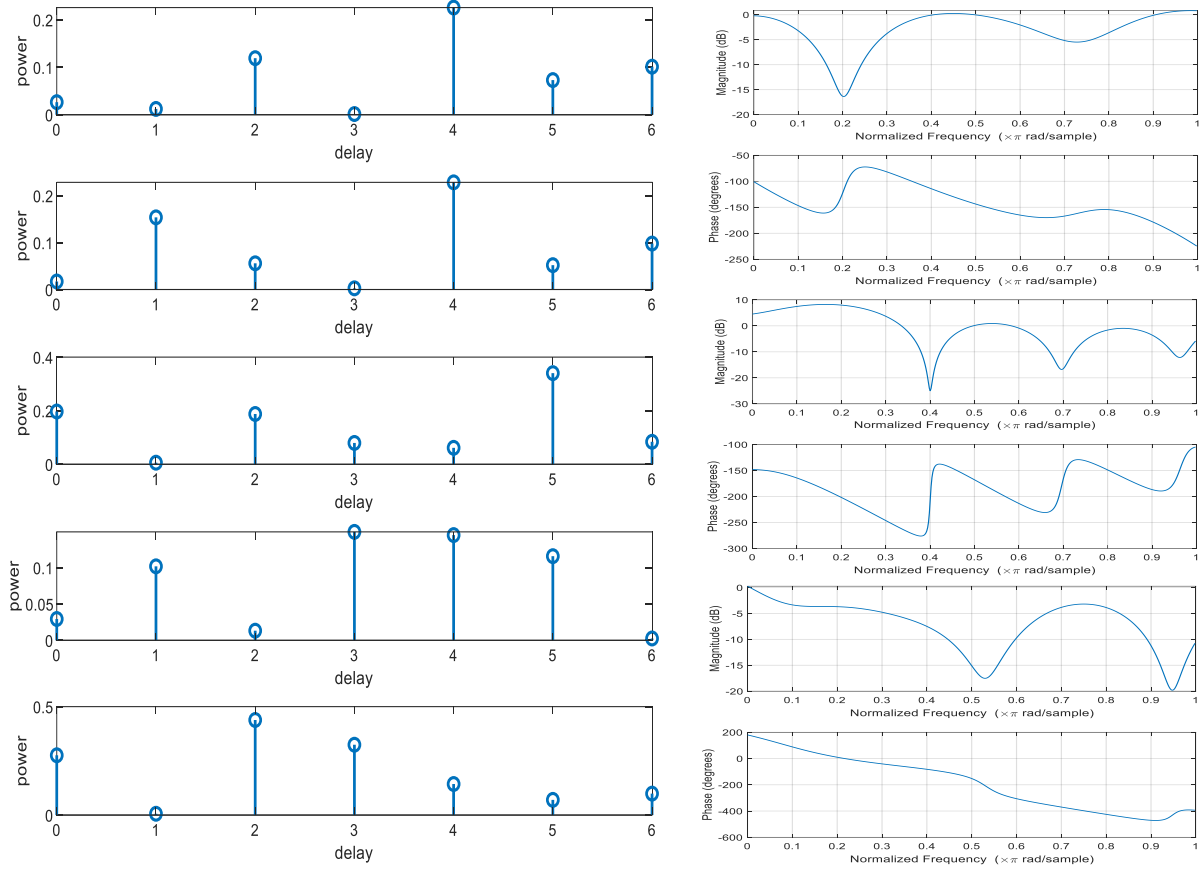


Figure 4-8: (a) Random sample of the PDP of 7-tap Rayleigh fading channel
 (b) Random sample of the normalized frequency response of 7-tap Rayleigh fading channel

4.5.2 Analytical vs. Simulated BER performance

The BER is calculated as the ratio of the bits received in error to the total number of bits per frame. It is used to measure the performance of the system over different signal-to-noise ratio (SNR) thresholds. The BER measures the EE of the modulation technique, since a system which achieves lower BER in a certain channel, requires less transmitted signal power to deliver a signal at a specific SNR threshold.

For the proposed hybrid OQAM/FBMC MIMO system, the analytical P_b derived in section 4.3 for the 2×2 MIMO scenario for 4-QAM in (4-60) and the same one obtained for 16-QAM constellation obtained by substituting by 4-55 in (4-56) and (4-57), are plotted with the corresponding simulated BER against different values of SNR in Figure 4-9. The figure also shows the corresponding results for the 4×4 MIMO scenario. The simulation is performed over a 7-

tap Rayleigh multipath fading channel and the simulated system uses ZF-FDE, as was assumed in the BER analysis.

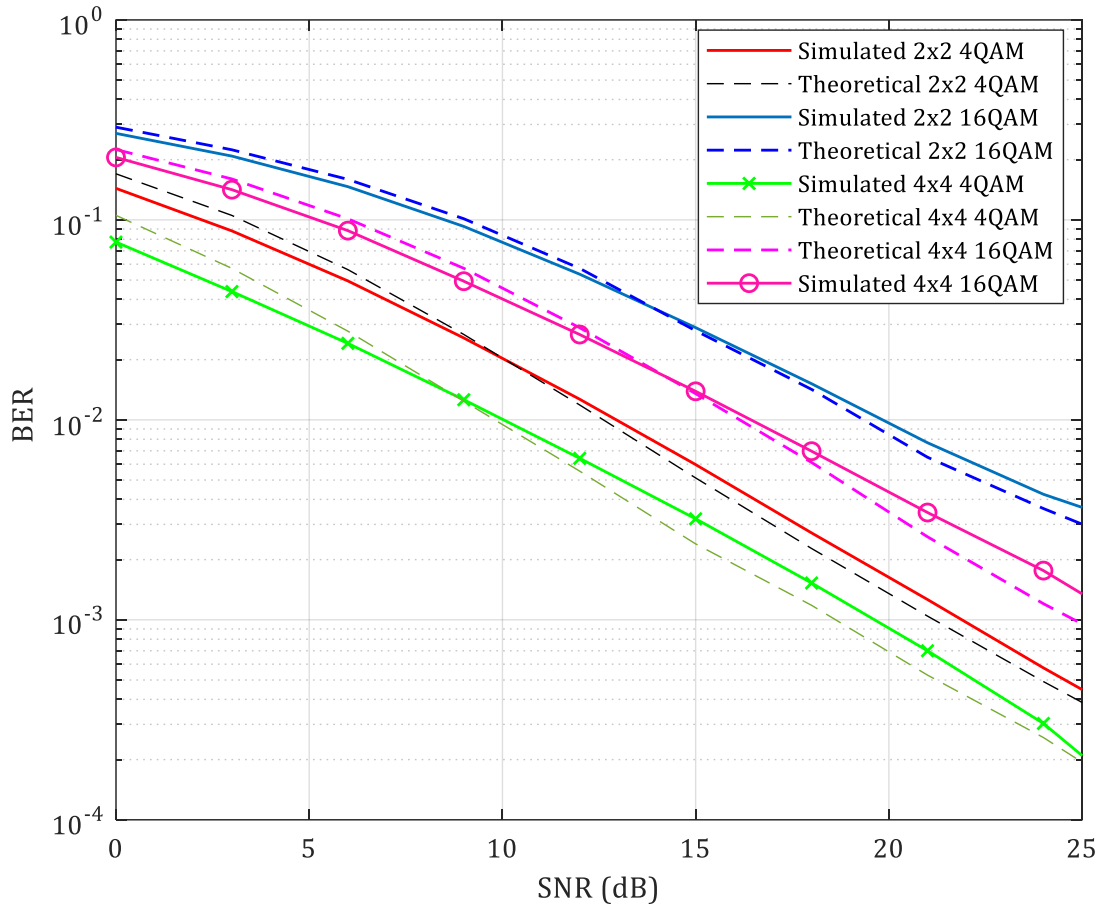


Figure 4-9: Analytical vs. simulated BER for hybrid OQAM/FBMC MIMO system using ZF-FDE in 7-tap Rayleigh fading channel.

The results show that the simulated curves highly match the theoretical curves for both MIMO settings and both 4 and 16 QAM constellations, which indicate the high accuracy of the simulation results. The same results are obtained for a different number of taps.

4.5.3 Power Spectral Density & Spectral Efficiency

The PSD is used to measure the spectrum localization of the transmitted signal over the transmission bandwidth. The frequency axis can be normalized by dividing by the subcarrier spacing, and the PSD axis can be normalized by dividing by the average signal power. The PSD

shows the signal power distributed over the normalized bandwidth or the subcarriers. The PSD is calculated in dB for a signal with spectrum $S(f)$ as:

$$PSD = 10 \log (|S(f)|^2) \quad 4-61$$

The normalized PSD of the hybrid OQAM/FBMC and the CP-OFDM systems are both plotted against the normalized frequency in Figure 4-10. A number of guard subcarriers equal to one-eighth of the total number of subcarriers are inserted on both sides of the data-carrying subcarriers to illustrate the OOB emission.

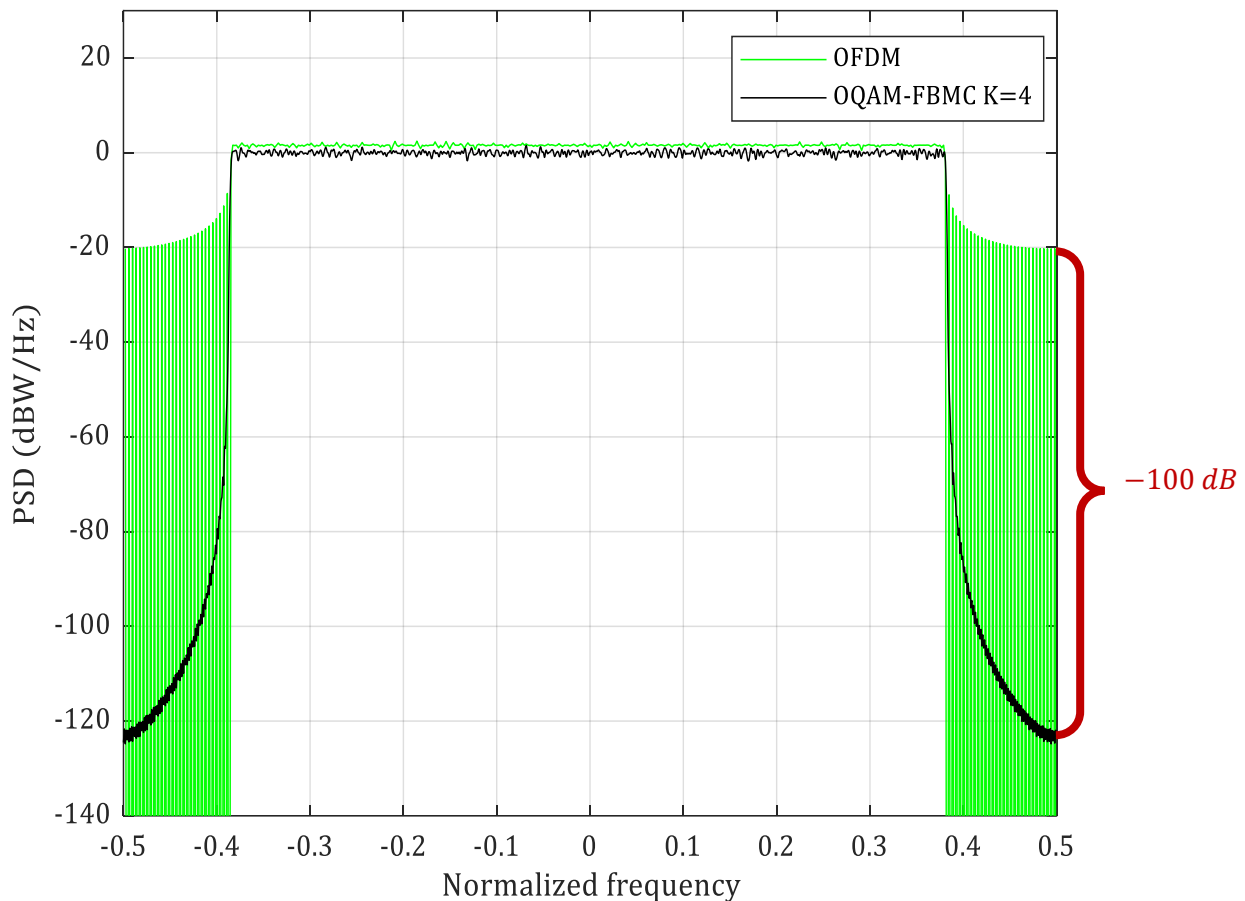


Figure 4-10: Normalized PSD of the proposed hybrid OQAM/FBMC system vs. CP-OFDM.

Figure 4-10 shows that the hybrid OQAM/FBMC system with $K = 4$ has dramatically lower OOB emission as previously mentioned, having a 100 dBW/Hz lower sidelobes compared to that of OFDM. It is worth noting that changing the overlapping factor K does not significantly impact the BER performance of the proposed system in Rayleigh fading channel, although it affects other aspects of the system. For instance, increasing K decreases the OOB emission and thus increases

the spectral localization, at the expense of increasing the complexity and the PAPR as was previously illustrated in section 3.4.3. More spectrally confined signal means smaller required guard bands and thus increased SE, in addition to the ability to utilize fragmented spectrum.

The enhancement in the throughput efficiency due to the absence of CP in the proposed hybrid OQAM/FBMC can be calculated as a ratio of the number of data symbols in the FBMC frame (N), to the number of data symbols of the OFDM frame of the same length ($N - N_{cp}$). For example, for a CP length of $1/8$ of the symbol length N , the enhancement in the throughput efficiency is 12.5%. In severe multipath fading conditions, where longer CP-length is needed, the enhancement in throughput efficiency increases. Figure 4-11 shows the enhancement in throughput efficiency in per cent of FBMC over OFDM with variable CP-lengths relative to the number of subcarriers N .

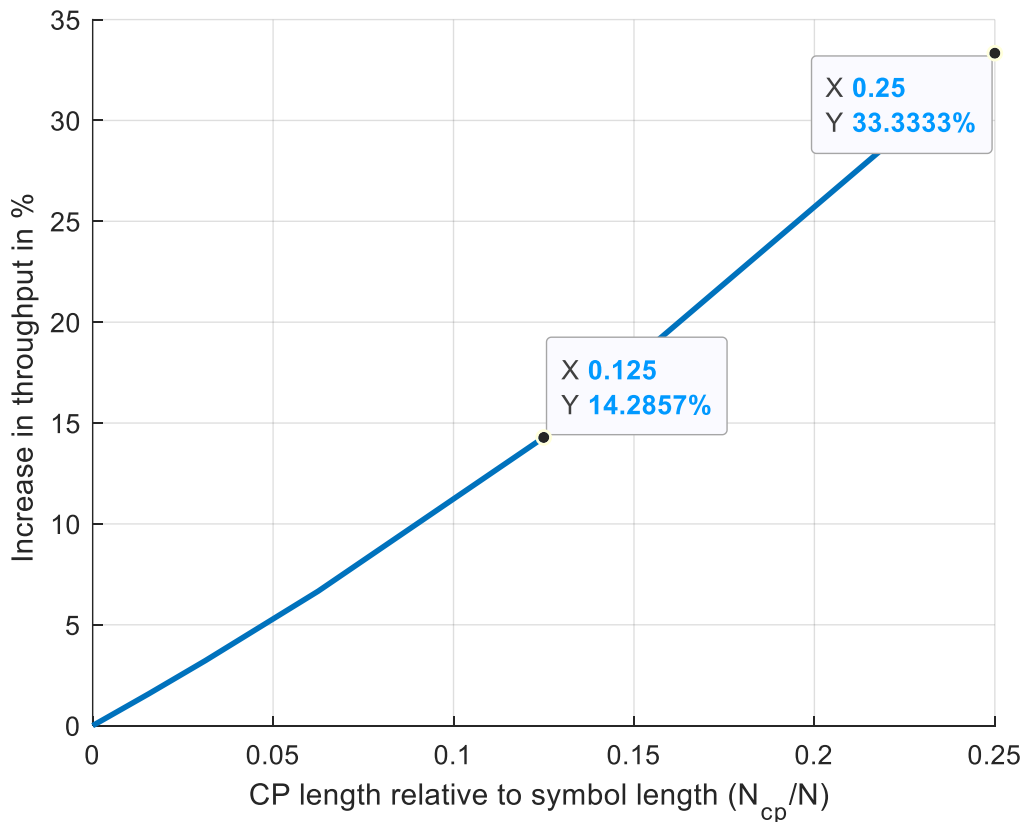


Figure 4-11: Percentage of enhancement in throughput efficiency FBMC over OFDM with variable $\frac{N_{cp}}{N}$.

4.5.4 BER performance of the proposed hybrid OQAM/FBMC MIMO System

In this section, the BER performance of the proposed hybrid OQAM/FBMC MIMO system in Rayleigh fading channel is examined and compared to OFDM. Figure 4-12 and Figure 4-13 show the BER performance of the proposed system versus OFDM over 3 and 7 tap Rayleigh fading channels respectively, using 4-QAM modulation for all systems. The OFDM system in comparison uses a CP of $N/8$ which is longer than the channel's maximum delay spread, whereas the proposed OQAM/FBMC system does not use a CP.

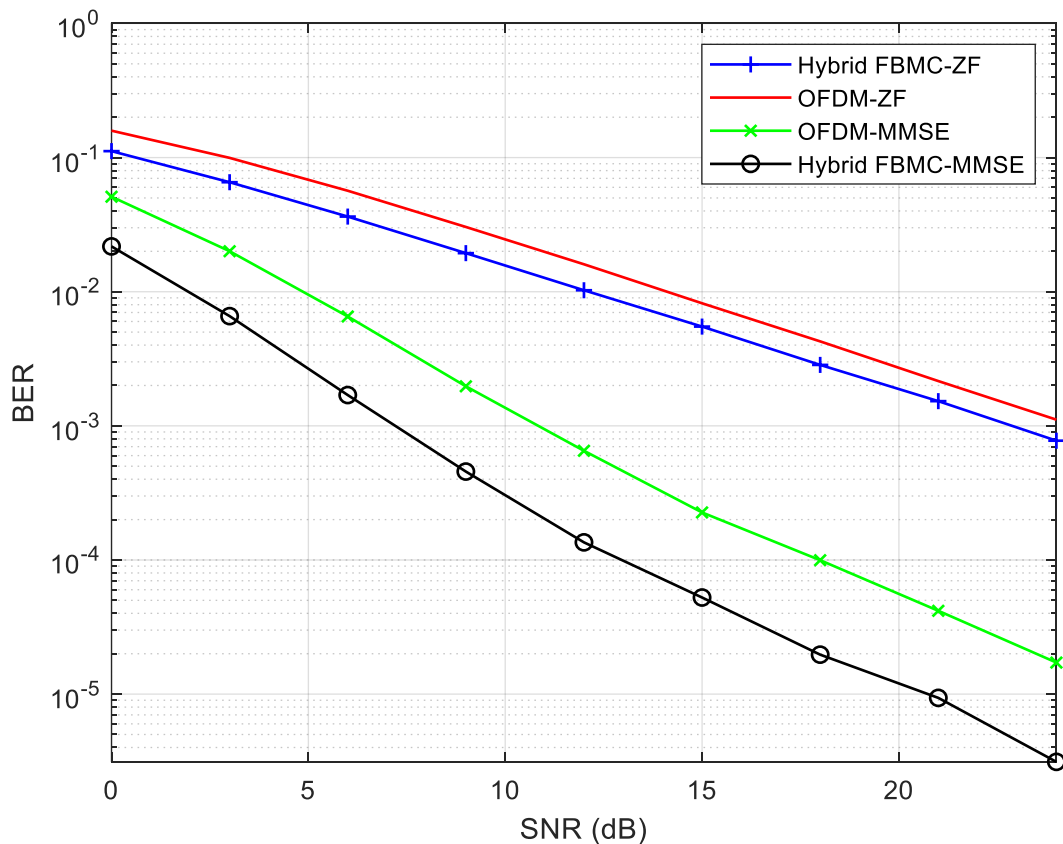


Figure 4-12: BER of 4-QAM hybrid OQAM/FBMC 2×2 MIMO system vs. OFDM in 3-tap Rayleigh fading channel.

Both figures show that the proposed hybrid OQAM/FBMC MIMO that uses MMSE FDE gives the lowest BER hence the best performance. In Figure 4-12, at a BER of 10^{-4} , there is a 5 dB gain for the hybrid OQAM/FBMC MMSE system over the CP-OFDM MMSE system.

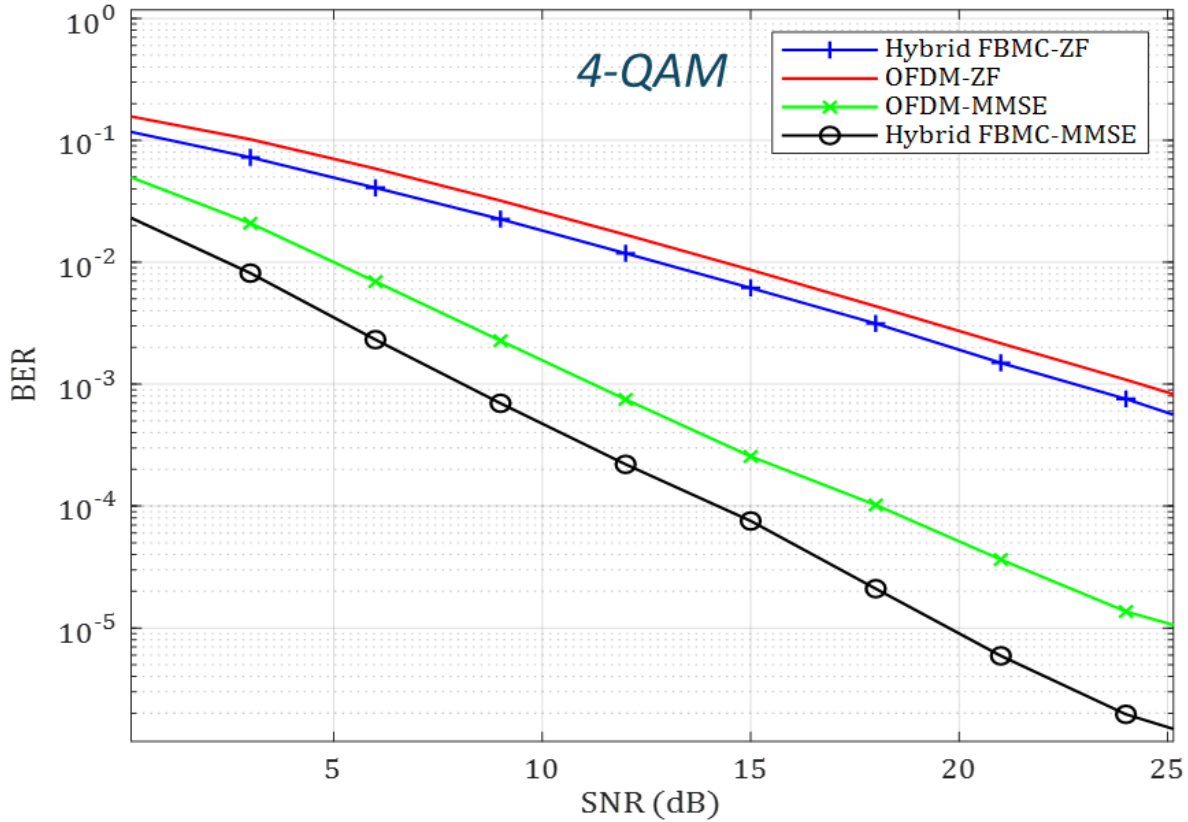


Figure 4-13: BER of 4-QAM hybrid OQAM/FBMC 2×2 MIMO system vs. OFDM in 7-tap Rayleigh fading channel.

Figure 4-13 shows the effect of longer multipath channel length and therefore accounts for the effect of worse multipath channel conditions and higher frequency selectivity. The hybrid OQAM/FBMC with the MMSE system still gives the best performance. At a BER of 10^{-4} , there is a 3 dB gain for the Hybrid OQAM/FBMC MMSE system over the corresponding CP-OFDM MMSE system. However, the OQAM/FBMC and the CP-OFDM systems which use ZF-FDE have close performances, with only a gain of 2 dB in favor of OQAM/FBMC in both figures.

4.5.4.1 Effect of increasing the modulation order

To investigate the effect of increasing the modulation order M , for cases where a higher bit rate is needed, the BER performance of the proposed system in a 2×2 MIMO setting using 16-QAM is simulated in a 3-tap Rayleigh fading channel. The results are compared to the corresponding CP-OFDM system and are depicted in Figure 4-14.

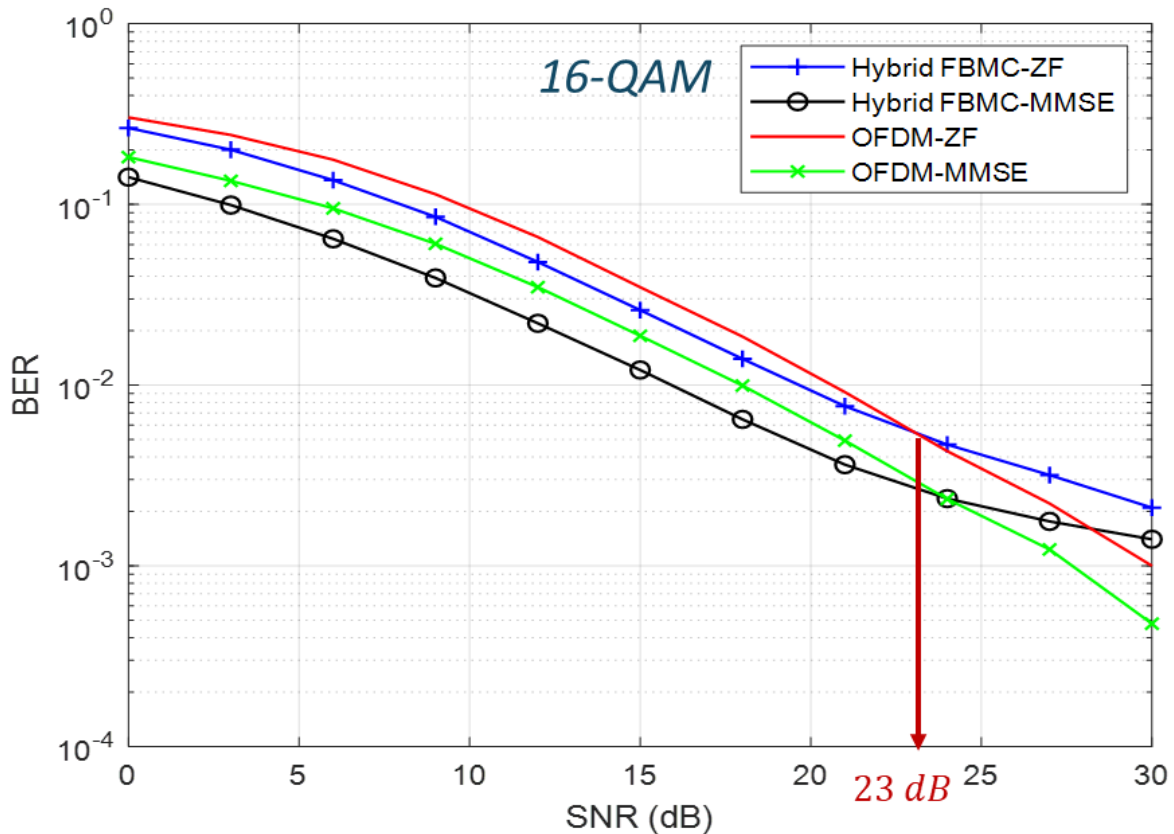


Figure 4-14: BER of 16-QAM hybrid OQAM/FBMC 2×2 MIMO system vs. OFDM in 3-tap Rayleigh fading channel

The figure shows that for 16-QAM at low values of SNR, the OQAM/FBMC system still performs better than its OFDM counterpart. At high values of SNR, specifically higher than 23 dB in this simulation scenario, the corresponding CP-OFDM system in comparison begins to have a better BER performance than the OQAM/FBMC system. In other words, at high SNR thresholds, the BER performance of the OQAM/FBMC system begins to saturate despite increasing the SNR. This complies with the saturation theory for systems at higher order modulation, due to the inherent intrinsic interference. In conclusion, the results show that the hybrid OQAM/FBMC system is better suited for lower order modulation, however, it still performs when increasing the modulation order to achieve higher bitrates in certain application scenarios.

4.5.4.2 Effect of increasing the MIMO order

To test the suitability of the proposed hybrid OQAM/FBMC system for higher order MIMO scenarios, it is simulated for a 4×4 MIMO settings with $P = 4$ transmit/receive antennas in

Rayleigh fading channel. The extended Alamouti coding/decoding is used for the SFBC in the 4×4 setting as previously explained in section 4.2.1. Figure 4-15 displays the simulation results of the proposed system in the 4×4 vs. the 2×2 MIMO settings, using 4-QAM modulation for both MMSE and ZF FDE in a 7-tap fading channel.

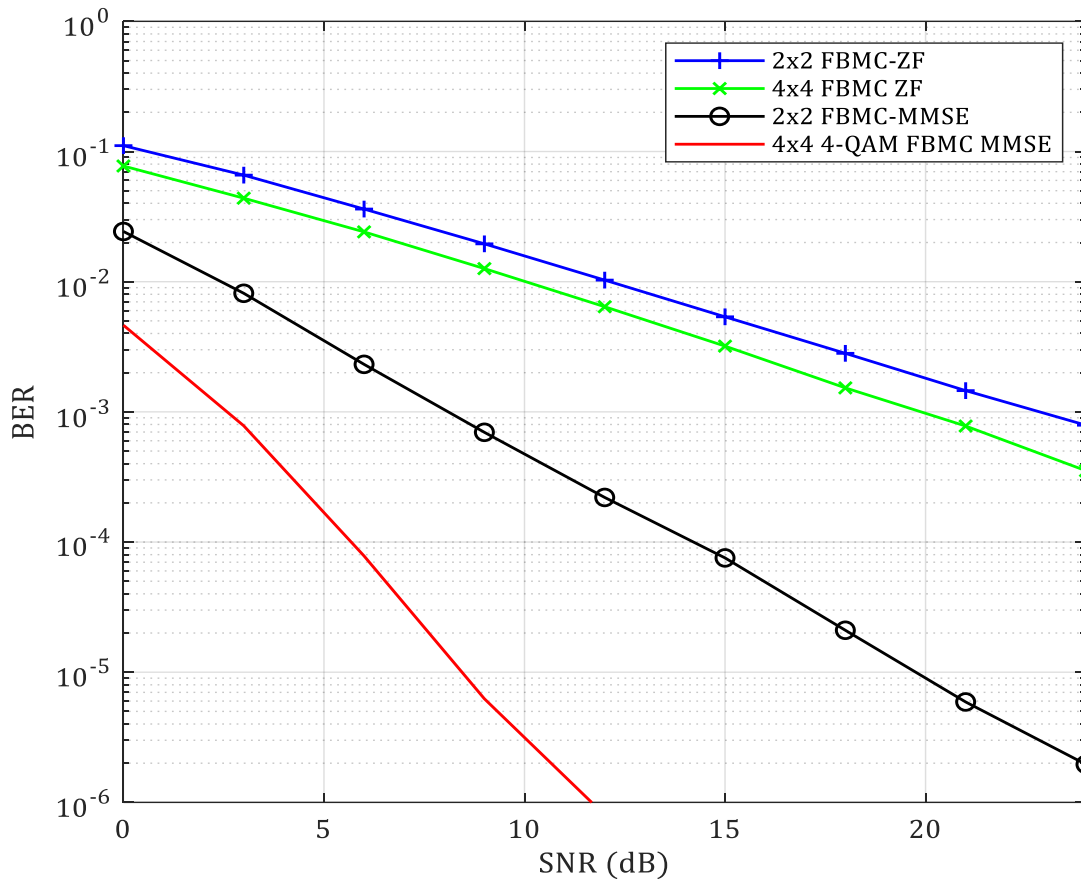


Figure 4-15: BER of 4-QAM hybrid OQAM/FBMC 2×2 vs. 4×4 MIMO systems in 7-tap Rayleigh fading channel.

The figure shows that by increasing the MIMO order, the BER performance is enhanced for both types of equalizers. However, for MMSE equalization, the enhancement in performance is more significant. For example, at a BER of 10^{-5} , there is a 12 dB gain for the 4×4 system over the 2×2 system. The results show that upon increasing the MIMO order, the system performs much better with MMSE equalizers compared to ZF equalizers.

To examine the effect of increasing the MIMO order with higher order QAM modulation for the proposed system, Figure 4-16 shows the BER performance of the 2×2 vs. 4×4 MIMO settings, for both 4-QAM and 16-QAM using MMSE, in 7-tap Rayleigh fading channel using MMSE equalization. The figure shows that the performance of the hybrid system with MMSE for the 4×4 MIMO setting is enhanced for the 16-QAM modulation system as well. For the 16-QAM case at a BER of 10^{-2} there is a 6 dB gain for the 4×4 system over the 2×2 system.

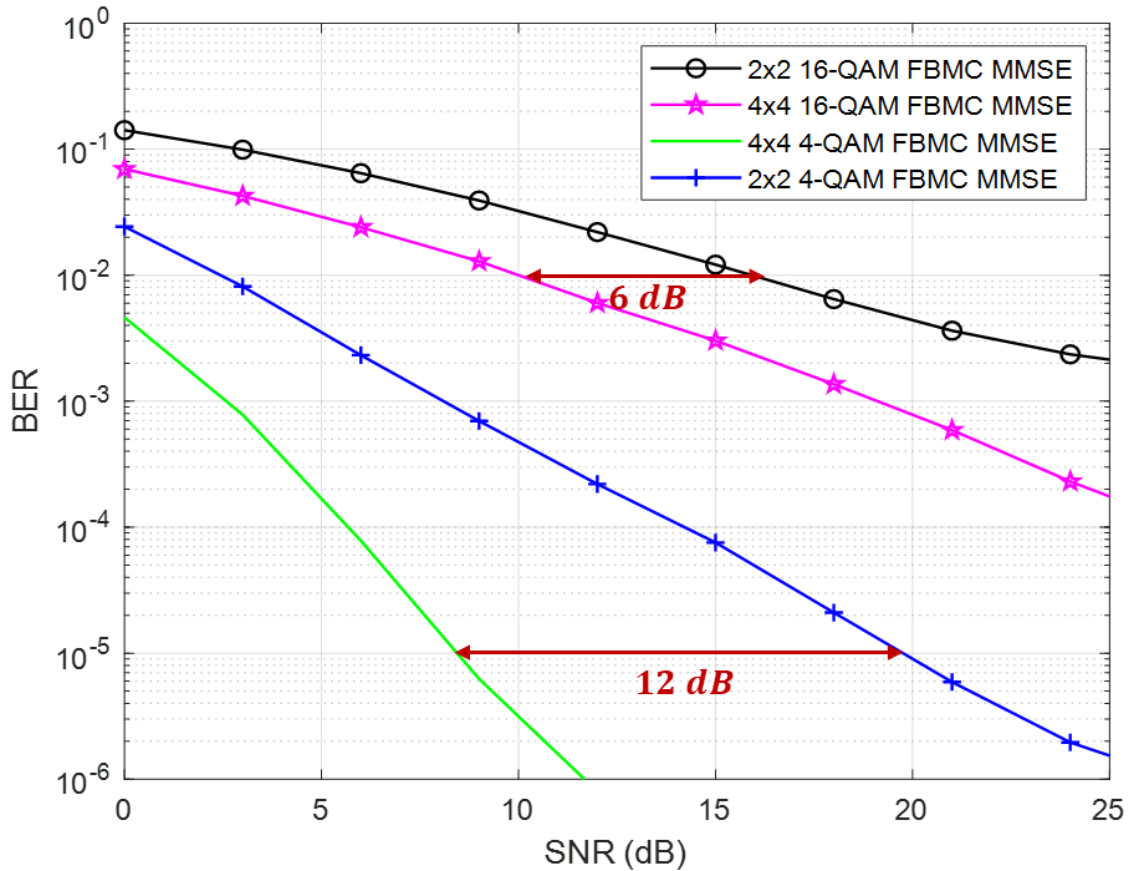


Figure 4-16: BER of M -ary QAM hybrid OQAM/FBMC 2×2 vs. 4×4 MIMO systems with MMSE in 7-tap Rayleigh fading channel.

In conclusion, the results show that our proposed system is suitable for deployment in scenarios with an increased number of antennas, which exploit spatial diversity to combat the channel's frequency selectivity. However, this comes at the expense of increased complexity. This makes our system suitable in different operation scenarios in which either higher order MIMO is needed to reach a specific BER in highly frequency-selective channels for example in 5G downlink, or in other systems where lower complexity is desirable and hence lower order MIMO, or SISO

like some IoT scenarios, which require operation in a narrow bandwidth benefitting from the superior spectral localization of the FBMC signal [10][11].

4.5.5 BER performance of the proposed PPN-TDE OQAM/FBMC System

The BER performance of the TDE-PPN MIMO system in a multipath fading channel with a LOS path is examined and compared to the Hybrid FDE system in this sub-section. The TDE equalizer has much lower complexity as was shown in section 4.4, while it depends on the presence of a LOS path, which is the case in many D2D and IoT applications. The channel used for simulation is a 4-tap Pedestrian channel A model with relative average power in dB [0 – 9.7 – 19.2 – 22.8] [163]. The channel taps are assumed to be uniformly spaced. Figure 4-17 shows the BER performance of the TDE equalizer vs. FDE ZF and MMSE equalizers for a SISO setting.

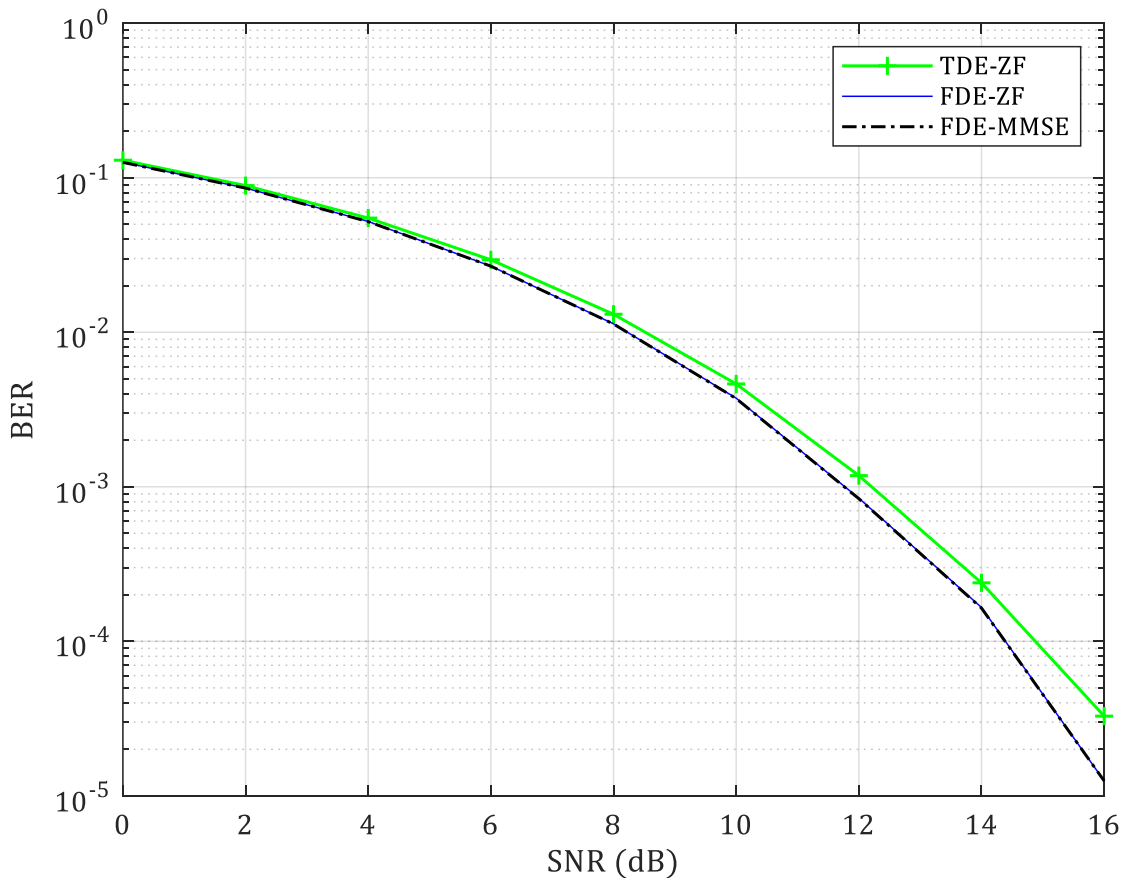


Figure 4-17: BER of OQAM/FBMC using hybrid-FDE vs. PPN-TDE structures in pedestrian channel A.

It is noticed from Figure 4-17 that the three systems under investigation have identical performances with a slight difference at high SNR, in mild frequency-selective channels. At 10^{-4} BER, a slight gain of 0.5 dB comes in favour of the hybrid FDE system over the PPN-TDE OQAM/FBMC system. At the same time, the PPN-TDE equalizer has significantly the least computational complexity as was shown in section 4.4. For example, in the case of 256 subcarriers, the PPN-TDE system reduces the computational complexity by 25% less than that of the hybrid FDE system, using a 5-tap equalizer. However, the performance of the TDE system deteriorates in highly frequency-selective multipath channels with no LOS path.

This makes the PPN-TDE OQAM/FBMC suitable for applications with mild channel fading conditions and low complexity requirements, like some narrow-band IoT applications [2], [10], [97], [133], [164], [165] in which the superior spectral localization, the CP-less transmission and robustness against CFO of FBMC signals are required.

4.5.6 BER performance of the proposed SM OQAM/FBMC vs. SFBC MIMO systems

This sub-section presents the simulation results of the SM/SFBC OQAM/FBMC system described in section 4.1. The simulation results of the SM-OQAM/FBMC 2×2 system are displayed in Figure 4-18 and compared to the corresponding 2×2 SM CP-OFDM system in a 3-tap Rayleigh fading channel for 4-QAM modulation order.

The figure shows that the SM OQAM/FBMC system yields a better BER performance than the corresponding SM CP-OFDM system for both types of MMSE and ZF equalizers. For MMSE equalization, at a BER of 10^{-3} , there is a 5 dB for the FBMC system over the OFDM system. As for the ZF equalization, at a BER of 10^{-2} , there is a 1 dB for the FBMC system over the OFDM system, which is almost constant over all the range of SNR values. The enhancement in performance for the SM OQAM/FBMC system is clearly greater when using MMSE equalization.

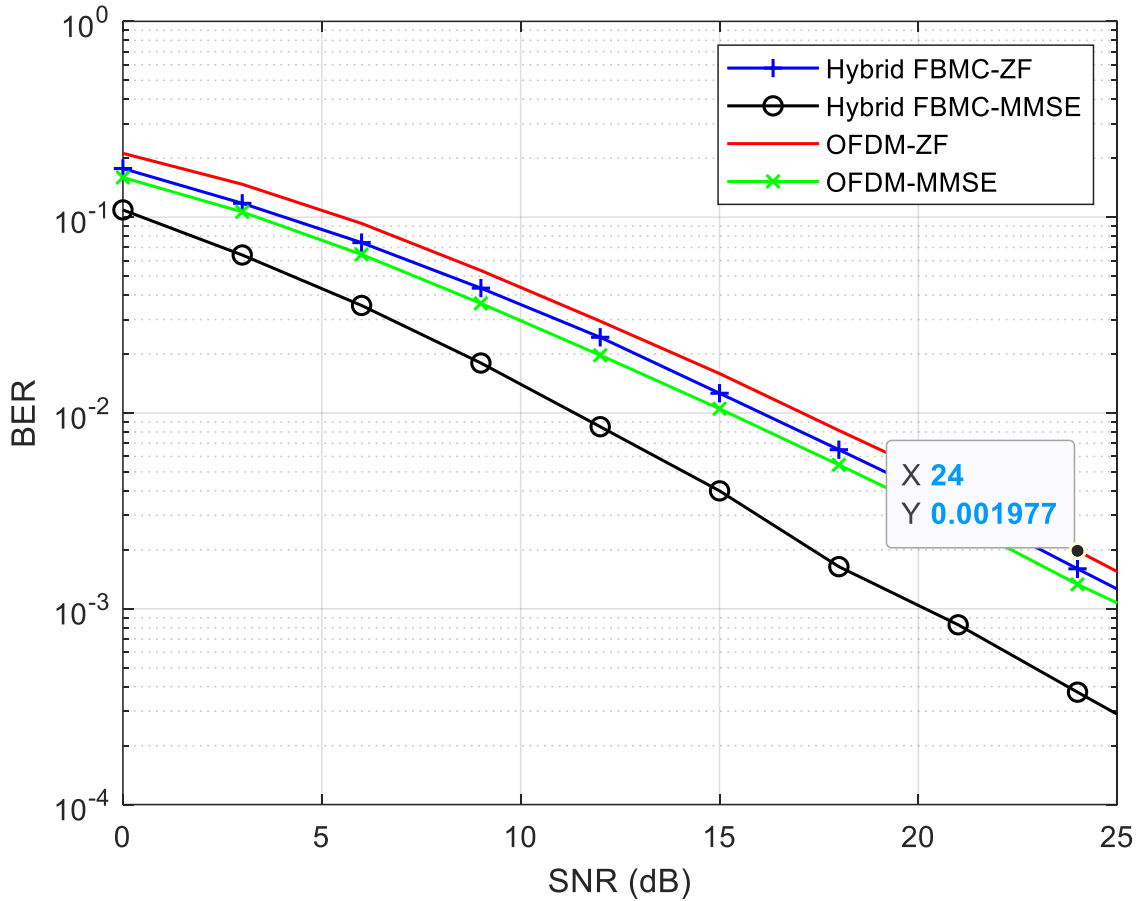


Figure 4-18: BER of 4-QAM OQAM/FBMC SM MIMO vs SM CP-OFDM in 3-tap Rayleigh fading channel.

When comparing the STBC and SM OQAM/FBMC systems, the first yields a better BER performance as shown in Figure 4-19. However, the SM system provides double the bitrate in the case of a 2×2 MIMO scenario. The OQAM/FBMC system performs better with SFBC than with SM and yields the best performance with MMSE FDE as could be seen from the figure. However, spatial multiplexing is used to increase the bitrate by sending independent data streams from the MIMO antennas, while Alamouti SFBC is used as an SD scheme to enhance the BER performance.

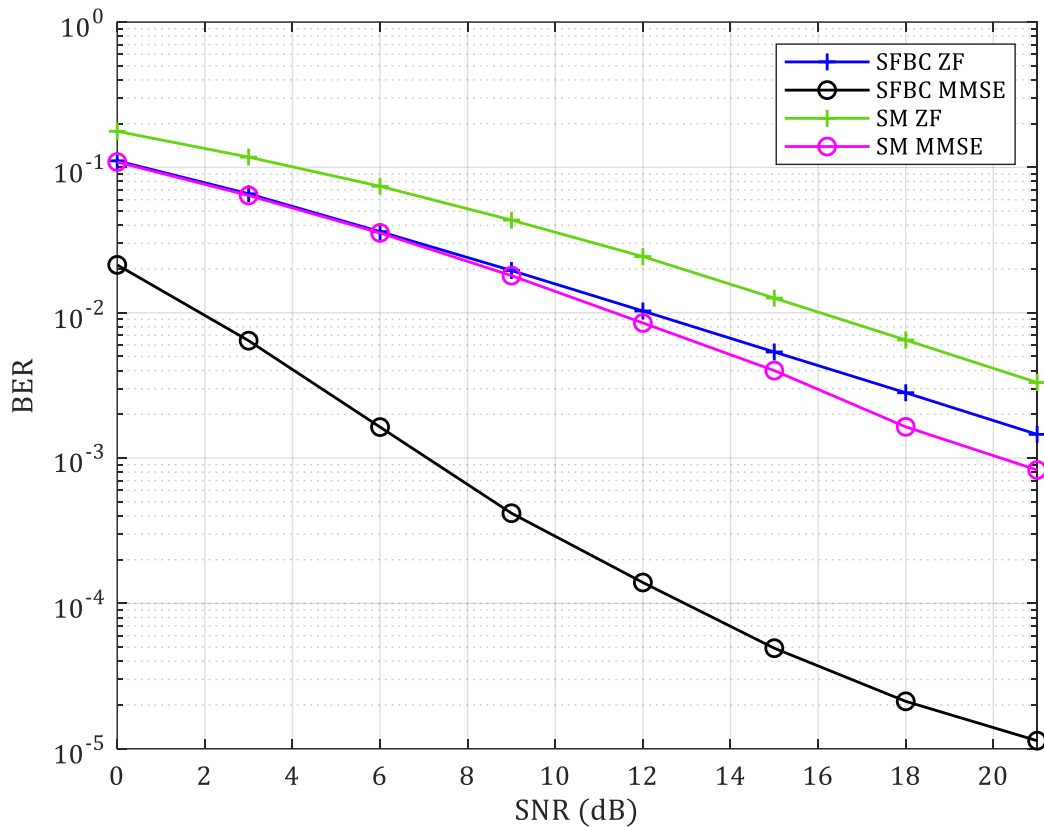


Figure 4-19: BER of 4-QAM OQAM/FBMC SM MIMO vs SFBC MIMO in 3-tap Rayleigh fading channel.

4.5.6.1 Effect of available bandwidth

The proposed SM OQAM/FBMC system is suitable for high data rate applications where a higher bit rate and high spectral efficiency are required in a given bandwidth [166], such as OQAM/FBMC applications in industrial big-data communications [20]. If the available bandwidth is increased, SISO or lower MIMO orders can be selected to achieve the desired bitrate with lower complexity. If the available bandwidth is decreased, higher MIMO orders can be selected to achieve the desired bit rate, but this comes at the expense of the additional complexity.

4.5.7 BER performance of the proposed OQAM/FBMC SFBC system in Rician channel

In this sub-section, the BER performance of the proposed hybrid OQAM/FBMC MIMO system is examined and compared to OFDM in Rician multipath fading channel. Figure 4-20 shows the BER performance of the proposed system versus OFDM over a 5-tap Rician fading channel with

a K -factor equals to 2, and a PDP of the Vehicular Channel model but with constant delays assumed between the channel paths. The receiver uses MMSE equalization, and the figure shows the results for the 2×2 MIMO setting for both 4 and 16 QAM modulation.

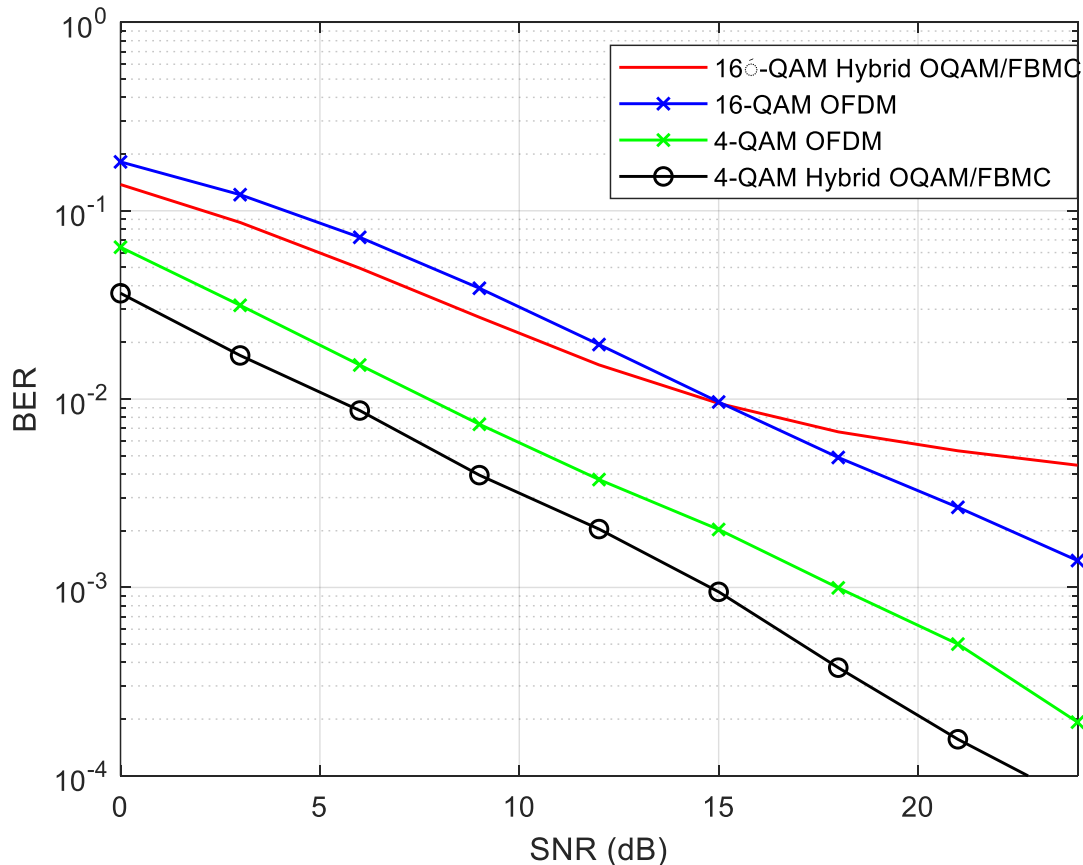


Figure 4-20: BER of hybrid OQAM/FBMC 2×2 MIMO vs CP-OFDM in 5-tap Rician fading Channel.

The figure shows that the proposed OQAM/FBMC SFBC system exhibits enhanced performance compared to CP-OFDM, just like the results in Rayleigh fading channels. However, for 16-QAM at high values of SNR, specifically higher than 15 dB in this simulation scenario, the corresponding CP-OFDM system in comparison has better performance, since the BER performance of the OQAM/FBMC system begins to saturate despite increasing the SNR when using higher M -ary modulation orders. The results also are affected by the correlation between the Rician channel multipath taps, while in the Rayleigh fading channel the multipath tap gains are completely uncorrelated. It can be thus concluded that, in both Rician and Rayleigh fading

channels, our proposed SFBC OQAM/FBMC system provides better BER performance than OFDM specifically when using lower order M -ary QAM modulation.

5 PROPOSED SC-OQAM/FBMC SYSTEM

As OQAM/FBMC aims at increasing the spectral and energy efficiency, the high PAPR problem hinders it from achieving the desired goals, especially in the uplink scenario. In battery-operated UE, the high PAPR transmitted signal is energy inefficient due to the high power required by the HPA to operate in the linear region, and the high power required by the DAC to increase its dynamic range. That is why in the uplink scenario, the SC-OQAM/FBMC system is proposed. The proposed system uses DFT-precoding and interleaved subcarrier mapping to significantly reduce the PAPR of the OQAM/FBMC signal, using MMSE FDE. SC-OQAM/FBMC can be considered as precoded OQAM/FBMC, that is why in addition to the enhanced PAPR, it offers enhanced BER performance due to its frequency diversity, just like SC-FDMA compared to OFDM [167].

What distinguishes the proposed SC-OQAM/FBMC MIMO model is that the precoding is performed after the OQAM processing, which has shown a significant reduction in PAPR in addition to an enhanced BER performance using MMSE equalization in Rayleigh fading channel. The additional computational complexity is significantly lower than all other PAPR reduction techniques while the reduction in the PAPR is superior. In the presence of a non-linear HPA, the SC-OQAM/FBMC signal shows no degradation in the BER performance, unlike the OQAM/FBMC system which suffers from the non-linearity of the HPA due to the high PAPR. On the other hand, the proposed SC-OQAM/FBMC model retains the advantages of OQAM/FBMC regarding the CP-less transmission, and superior spectral localization, as shown later in the results section.

5.1 SC-OQAM/FBMC MIMO System Model

5.1.1 Transmitter

The proposed SC-OQAM/FBMC MIMO transmitter model is presented in Figure 5-1. The system follows the same steps presented in Section 4.2 in addition to the DFT-spreading and subcarrier mapping after OQAM processing and before the PPN-FBMC modulation. The DFT-spreading added block consists of an $N \times N$ FFT matrix \mathcal{F}_N .

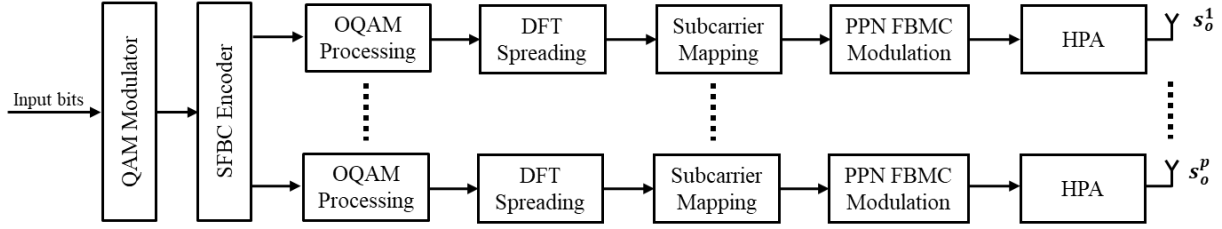


Figure 5-1: Proposed SC-OQAM/FBMC MIMO transmitter model

Following the analysis presented in Section 4.2, after OQAM processing and serial to parallel conversion in (4-19), the OQAM symbols are DFT-spread as in (**Error! Reference source not found.**5-1) using \mathcal{F}_N .

$$\mathbf{X}^i = \mathcal{F}_N \mathbf{X}_o^i \quad 5-1$$

The subcarrier mapping is next applied to the DFT-spread symbols of length N , to map them onto N_s subcarriers, where $Q = N_s/N$ is greater than or equal to one. The mapping is performed using the matrix \mathbf{M}^u of dimensions $N_s \times N$ for the u^{th} user. The mapped symbols become

$${}^u\mathbf{X}^i = \mathbf{M}^u \mathbf{X}^i. \quad 5-2$$

The subcarrier mapping matrix \mathbf{M}^u is constructed according to the desired mapping strategy, either localized or interleaved. Interleaved mapping (IM) offers additional frequency-diversity gain as will be seen in the results section, while localized mapping (LM) reduces inter-user interference. In LM, N_s consecutive subcarriers are assigned for the user, hence \mathbf{M}^u is equal to:

$$\mathbf{M}^u = [\mathbf{0}_{(u-1)N \times N}; \mathbf{I}_N; \mathbf{0}_{(N_s - uN) \times N}], \quad 5-3$$

where u is the user number. In IM, the symbols are interleaved on N_s subcarriers with a factor of Q , ie. they are placed on Q -spaced subcarriers. This way \mathbf{M}^u is equal to:

$$\mathbf{M}^u = [\mathbf{0}_{(u-1) \times N}; \mathbf{k}_1^{N^T}; \mathbf{0}_{(Q-1) \times N}; \mathbf{k}_2^{N^T}; \dots; \mathbf{k}_N^{N^T}; \mathbf{0}_{(Q-u) \times N}]. \quad 5-4$$

For the case of $Q = 2$ and user $u = 1$, hence $N_s = 2N$, the matrix \mathbf{M}^u reduces to:

$$\mathbf{M}^1 = [\mathbf{I}_N; \mathbf{0}_{N \times N}], \quad \text{for LM} \quad 5-5$$

$$\mathbf{M}^1 = [\mathbf{k}_1^{N^T}; \mathbf{0}_{1 \times N}; \mathbf{k}_2^{N^T}; \dots; \mathbf{k}_N^{N^T}; \mathbf{0}_{1 \times N}]. \quad \text{for IM} \quad 5-6$$

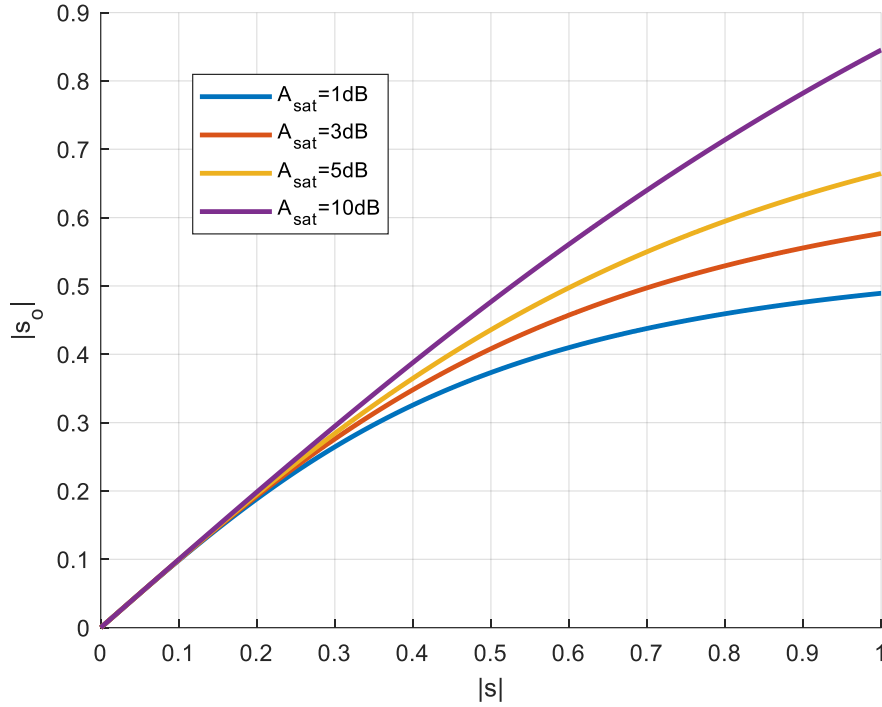
After the subcarrier mapping, the signal \mathbf{X}_{map}^i undergoes the same processes of FBMC PPN-modulation previously described by (4-22) till (4-25), giving the transmitted signal vector on the i^h antenna \mathbf{s}^i .

The last block of the transmitter is the HPA, which is added to illustrate the effect of its non-linearities on the transmitted signal. There are various models used for the HPA. The simplest is a clipping model which is linear over a certain region and clips the values of the signal above the saturation level. A more realistic model is the Rapp model [168], [141], which is chosen for simulation to model the non-linearity of the HPA. It is also used to simulate the effects of different degrees of non-linearity of HPA on MC modulation schemes including OFDM [169]. If the complex input signal \mathbf{s}^i has a magnitude vector $|\mathbf{s}^i|$ and phase vector $\boldsymbol{\theta} = \angle \mathbf{s}^i$, the output signal vector of the HPA \mathbf{s}_o^i is described as follows:

$$\mathbf{s}_o^i = \frac{a|\mathbf{s}^i|}{\sqrt[2p]{\mathbf{1} + \left(\frac{|\mathbf{s}^i|}{E[\mathbf{s}^i]A_{sat}}\right)^{2p}}} e^{j\boldsymbol{\theta}}, \quad 5-7$$

where A_{sat} is the saturation level of the HPA and p is a positive integer which controls the non-linearity of the HPA, and a is the HPA gain. The equation shows that the phase of the input signal $\boldsymbol{\theta}$ remains unchanged and only the amplitude is affected i.e. AM/AM.

The transfer function of the HPA is plotted in Figure 5-2 for $p = 1$, $a = 1$ and different A_{sat} . The figure illustrates the operation of the HPA, which linearly amplifies the signal below a certain level which depends on A_{sat} . As A_{sat} increases, the linear region increases along with the power needed to operate the HPA. As A_{sat} decreases, the non-linear region of the HPA increases thus causing increased distortion to the transmitted signal. The amplified signal \mathbf{s}_o^i is then transmitted into the frequency-selective multipath Rayleigh fading channel previously described in Section 4.5.1.


 Figure 5-2: Transfer function of HPA for different A_{sat}

5.1.2 Receiver

The receiver for the proposed SC-OQAM/FBMC MIMO model is presented in Figure 5-3. The FBMC demodulation is performed using the FS method since the equalization is performed in the frequency domain (FDE) as in the hybrid system in Section 4.2.2.

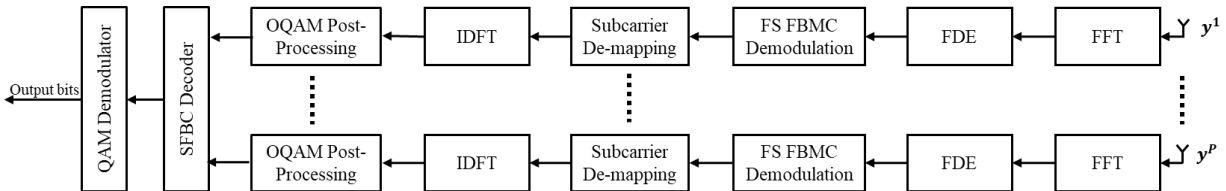


Figure 5-3: Proposed SC-OQAM/FBMC MIMO receiver model

After the FFT and the channel equalization using MMSE or ZF FDE, FBMC FS demodulation is performed as in equations 4-27 till 4-36. Next, the subcarrier de-mapping is performed using the transpose of the mapping matrix \mathbf{M}^u (IM or LM) for the u^{th} user, and then the DFT de-spreading is performed as follows:

$$\mathbf{Y}_d^j = \mathcal{F}_N^{-1} \mathbf{M}^{uT} \mathbf{Y}_o^j, \quad 5-8$$

where \mathbf{Y}_d^j is the de-mapped and de-spread signal vector for the j^{th} receive antenna. Afterwards, the signal undergoes the same operations as that of the hybrid system including OQAM post-processing, MIMO decoding and QAM demodulation as described by equations 4-37 till 4-42.

5.2 Additional Complexity

The complexity of the proposed SC-FBMC hybrid system is the same as that of the original hybrid system calculated in Section 4.4 in addition to the complexity associated with the DFT-spreading and subcarrier mapping in the transmitter, and the inverse operations in the receiver. As for the transmitter, the DFT-spreading operation requires $2N \log_2(N)$ real multiplications. The subcarrier mapping afterwards involves the multiplication of the N -point complex signal by the real-entries mapping matrix \mathbf{M}^u of dimensions $N_s \times N$, giving a complexity of $2N \times N_s$. The total additional complexity of the SC modulation part is $2N(\log_2(N) + N_s)$, and the same for its counterpart for de-spreading and de-mapping at the receiver.

It is worth noting that the additional complexity compared to the overall complexity of the SC-FBMC system is the same as the additional complexity of SC-OFDM compared to that of OFDM. However, since the OQAM/FBMC system is more complex than OFDM, the additional complexity in SC-FBMC is smaller compared to the original complexity. The SC-FBMC MIMO FBMC system is proposed for the uplink to significantly reduce the PAPR for the signal transmitted from UE as will be shown in the results in the following section, this justifies the increase in complexity. On the other hand, the proposed system has the least additional computational complexity, compared to other FBMC PAPR techniques described in chapter 3, as it does not involve candidate selection, like most other techniques.

5.3 Simulation & Results

In this section, the simulation results of the proposed hybrid SC-OQAM/FBMC MIMO system are presented. The simulation is performed using MATLAB scripts, and a sample code is provided in the appendix. The simulation measures and compares the efficiency of the SC-FBMC system to decrease the PAPR and thus achieve better BER performance taking into consideration the non-linearity of the HPA. The proposed system is simulated over Rayleigh multipath fading channel

described in section 4.5.1. The channel equalization is performed using MMSE FDE, which achieves better BER performance as was previously shown in Section 4.5.4. The same simulation parameters listed in Table 4-3 are used, while the additional parameters are listed in Table 5-1.

Table 5-1 SC-OQAM/FBMC Simulation Parameters

Q	2
Subcarrier Mapping	Interleaved, Localized
Number of Subcarriers (N)	64, 128, 256
HPA	Rapp model: $p = 1, a = 1,$ $A_{sat} = 5dB, 10dB$
QAM modulation order	4, 16
Overlapping factor (K)	3, 4

5.3.1 PAPR

As explained before, waveforms with high PAPR require a widely linear HPA, which in turn increases the power consumption of the HPA. The PAPR is measured in dB for the transmitted signal u_s^i as follows:

$$PAPR = 10 \log \left(\frac{\max(|u_s^i|^2)}{E(|u_s^i|^2)} \right) \quad 5-9$$

The complementary cumulative distribution function (CCDF) is used to measure the probability of the PAPR to be greater than or equal to a specific value $PAPR_o$. The CCDF curves show how much of the signal is at or above a given power level. It is calculated as:

$$ccdf(PAPR_o) = P(PAPR \geq PAPR_o) \quad 5-10$$

The SC-OQAM/FBMC system is proposed for the UE in the uplink scenario, where the power consumed in the HPA, which is proportional to the PAPR of the transmitted signal, is a major concern. Figure 5-4 shows the CCDF of the PAPR of OQAM/FBMC vs. proposed SC-OQAM/FBMC for IM and LM for 128 subcarriers using 4-QAM, and using an overlapping factor of $K = 3$ and 4.

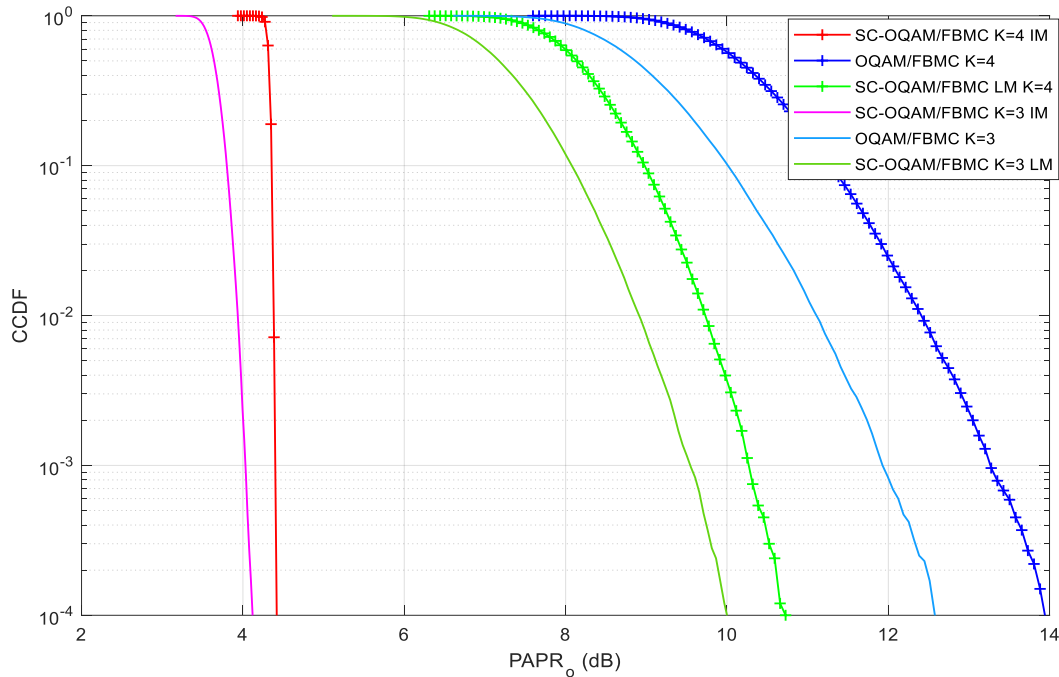


Figure 5-4: PAPR of 4-QAM OQAM/FBMC vs. SC-OQAM/FBMC for IM and LM for $N=128$.

Figure 5-4 shows that the proposed SC-OQAM/FBMC with IM dramatically reduces the PAPR by 9.5 dB compared to the original OQAM/FBMC system, and 6 dB compared to SC-OQAM/FBMC with localized subcarrier mapping. The IM is hence chosen for the proposed SC system due to its major PAPR advantage over the LM system, which makes it suitable for the uplink scenario and makes it worth the additional computational complexity. The reduction in the PAPR is superior to all other DFT-spreading-based PAPR reduction techniques described in Section 2.3, including pruned-FBMC [86] and low PAPR FBMC [39], [92].

The figure also shows that increasing the overlapping factor K , increases the PAPR, since it means that more symbols overlap in time as explained before. However, the SC-OQAM/FBMC IM scheme still reduces the PAPR by 8 dB for $K = 3$. It is worth noting that changing the number of subcarriers doesn't significantly affect the PAPR. On the other hand, increasing the modulation order slightly increases the PAPR as depicted in Figure 5-5 for 16-QAM. The reduction in the PAPR thus becomes 7.5 dB for the IM SC-OQAM/FBMC system as shown in the figure.

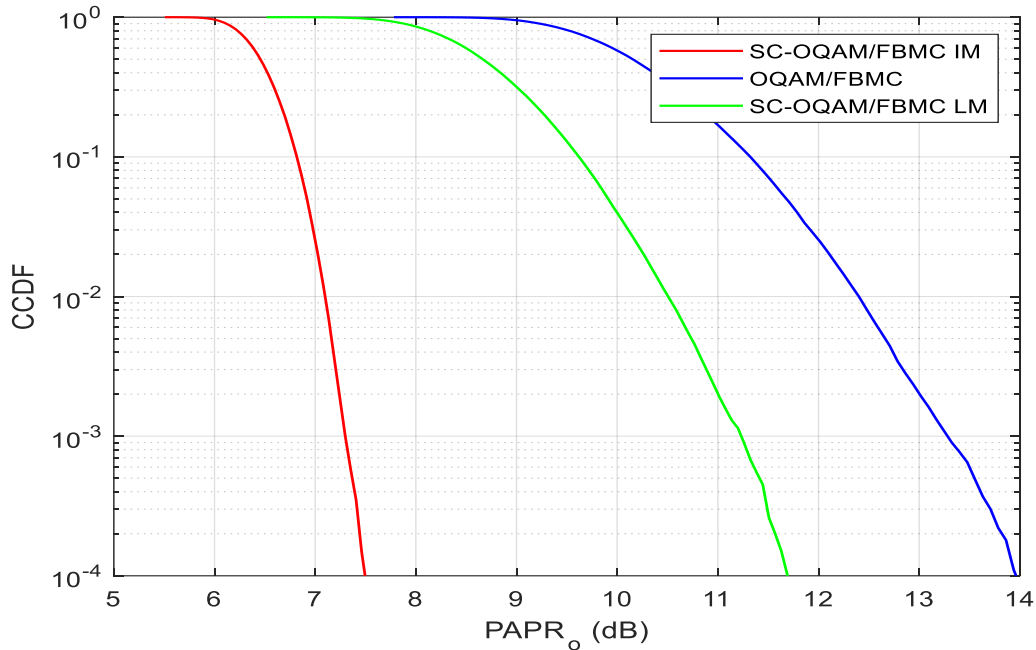


Figure 5-5: PAPR of 16-QAM OQAM/FBMC vs. SC-OQAM/FBMC for IM and LM for $N = 128$.

5.3.2 PSD

The PSD of the proposed SC-OQAM FBMC system is measured to ensure that the additional operations added to the hybrid OQAM/FBMC structure, still maintain FBMC's major advantage of low OOB emissions. A number of guard subcarriers (zero subcarriers) equal to $N/2$ are added on both sides of the data-carrying subcarriers, to illustrate the level of OOB emissions. The PSD curves are obtained using the periodogram MATLAB function, with a flattop window.

Figure 5-6 displays the PSD of the proposed SC-OQAM/FBMC system vs. OQAM/FBMC with $K = 4$ and 128 subcarriers, against normalized frequency, assuming ideal HPA. The figure shows that the OOB emissions of both systems are the same, therefore the SC-OQAM FBMC system retains the advantage of the low OOB emission of all OQAM/FBMC systems.

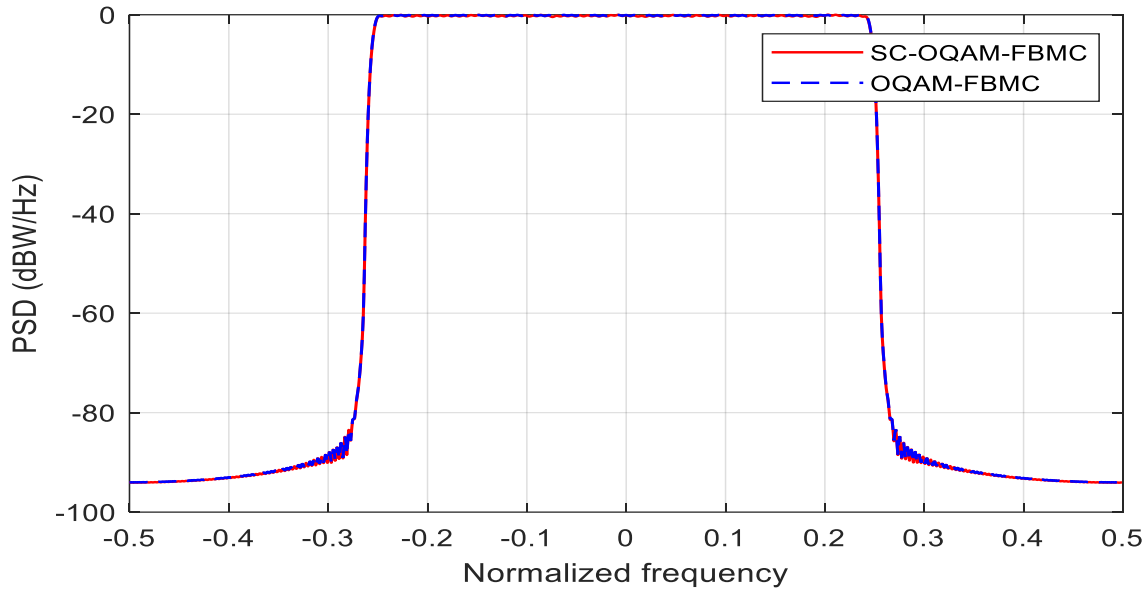


Figure 5-6: PSD of SC-OQAM/FBMC system vs. OQAM/FBMC with $K=4$, $N=128$, no HPA.

To display the effect of the HPA on the PSD, the PSD of both OQAM/FBMC and SC-OQAM/FBMC is plotted in Figure 5-7, using an HPA with $A_{sat} = 5$ dB and 10 dB respectively.

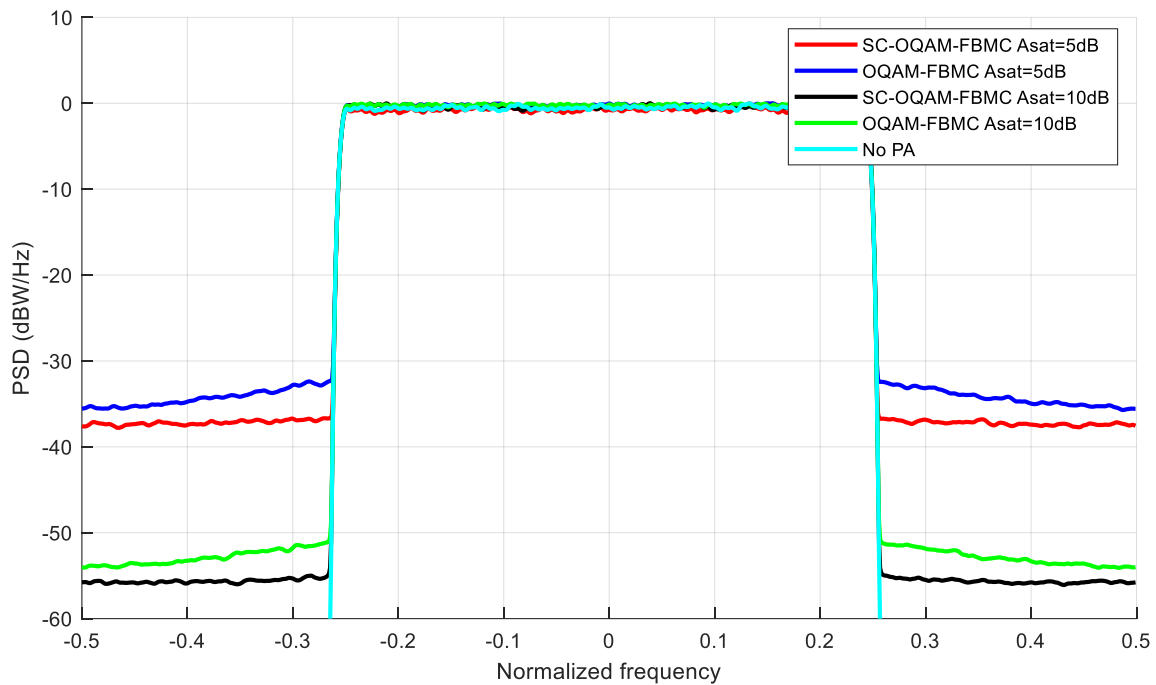


Figure 5-7: PSD of SC-OQAM/FBMC system vs. OQAM/FBMC with $K = 4$, $N = 128$, with HPA.

The figure shows that the SC-OQAM/FBMC system offers slightly lower OOB emission (2 dB) in both cases with the non-linearities of the HPA taken into consideration. As the saturation level A_{sat} of the HPA decreases, the OOB emissions level expectedly becomes higher.

5.3.3 BER

The BER performance of the proposed MIMO SC-OQAM/FBMC MIMO system is measured and compared to OQAM/FBMC in this section in presence of a non-linear HPA, in Rayleigh multipath fading channel. First, the BER performance of both MIMO systems is measured in a 3-tap channel, and the results are depicted in Figure 5-8 for $K = 4$ and $N = 128$ subcarriers, for 4-QAM and 16-QAM respectively.

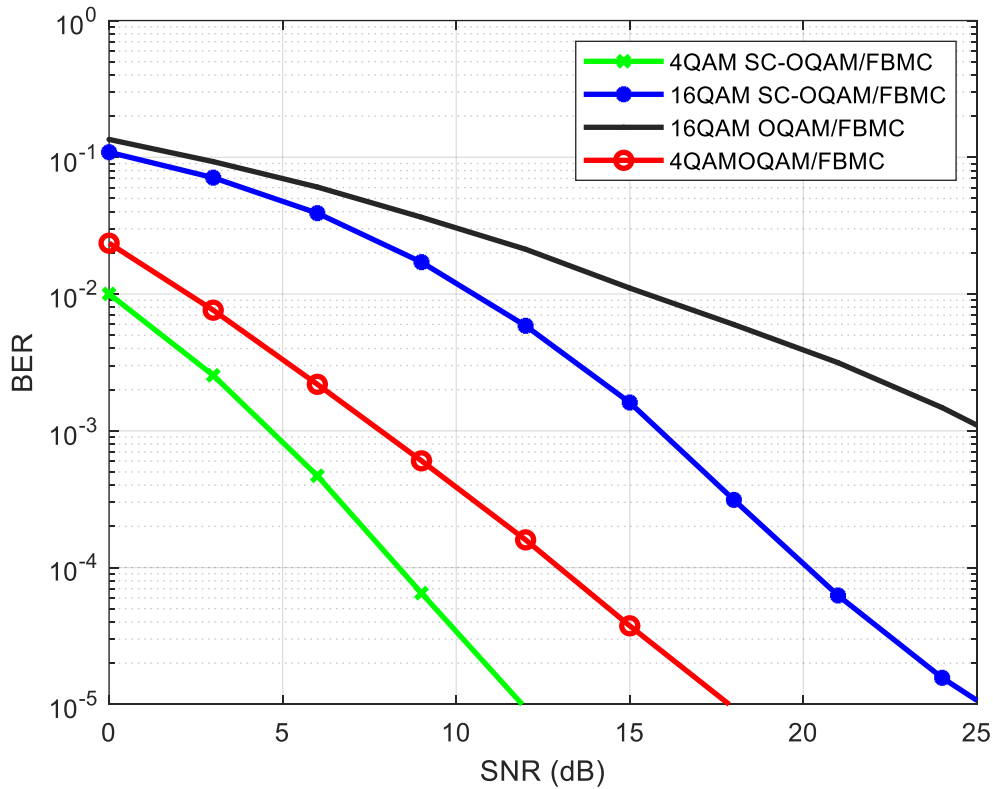


Figure 5-8: BER of 2×2 SFBC SC-OQAM/FBMC vs. OQAM/FBMC with MMSE FDE in 3-tap Rayleigh fading channel.

The figure shows that the proposed SC-OQAM/FBMC system enhances the BER of the OQAM/FBMC system. For the 4-QAM, at a BER of 10^{-5} , the SC system offers a gain of 6 dB. For the 16-QAM, the proposed SC system offers a gain of 9 dB at a BER of 10^{-3} . This enhancement

is due to the fact that the SC-OQAM/FBMC can be considered as precoded OQAM/FBMC. The BER is enhanced due to the gain of frequency diversity in the SC signal with IM.

To test the performance of the system in worse fading conditions, Figure 5-9 shows the BER results in Rayleigh fading channel with 20 multipath taps.

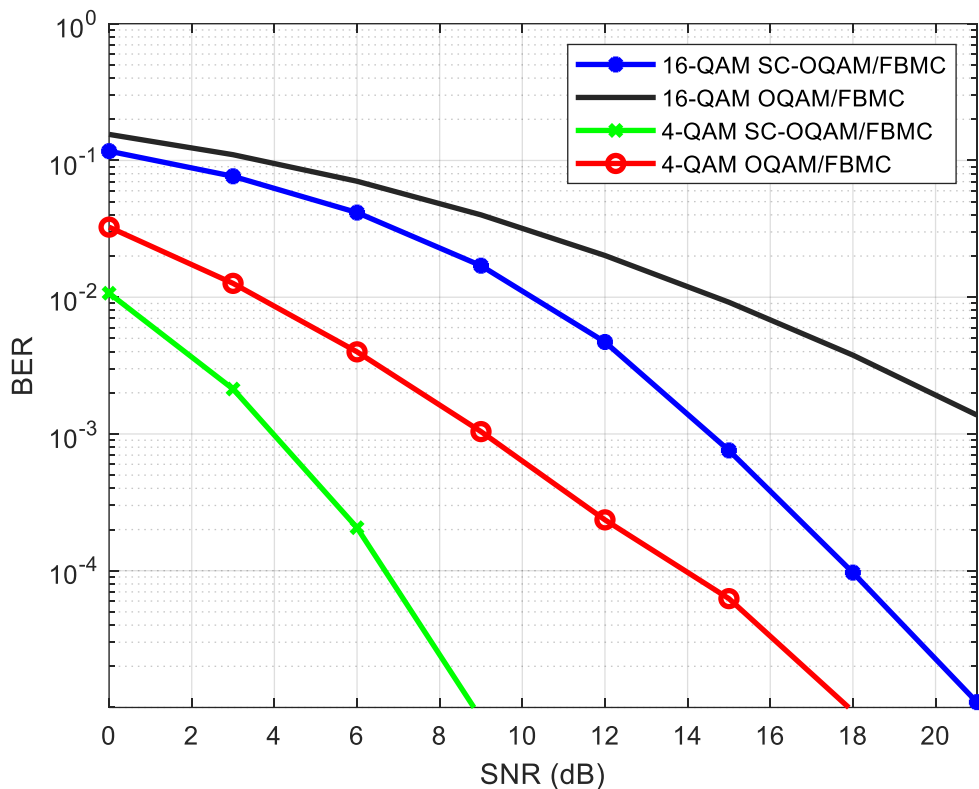


Figure 5-9: BER of 2×2 SFBC SC-OQAM/FBMC vs. OQAM/FBMC with MMSE FDE in 20-tap Rayleigh fading channel.

It can be noted that the gain achieved by the SC-OQAM/FBMC system increases as the channel's frequency selectivity increases. At a channel with 20 multipath taps, the 4-QAM SC system achieves a 9 dB gain over the OQAM/FBMC system at a BER of 10^{-5} , while it achieves a gain of 7 dB for 16-QAM. This shows that the system is suitable for deployment in scenarios with highly frequency-selective channels.

To test the efficiency of the proposed system in scenarios with higher order MIMO, the BER performance is measured and compared for a 4×4 MIMO setting in Figure 5-10, in Rayleigh fading channel.

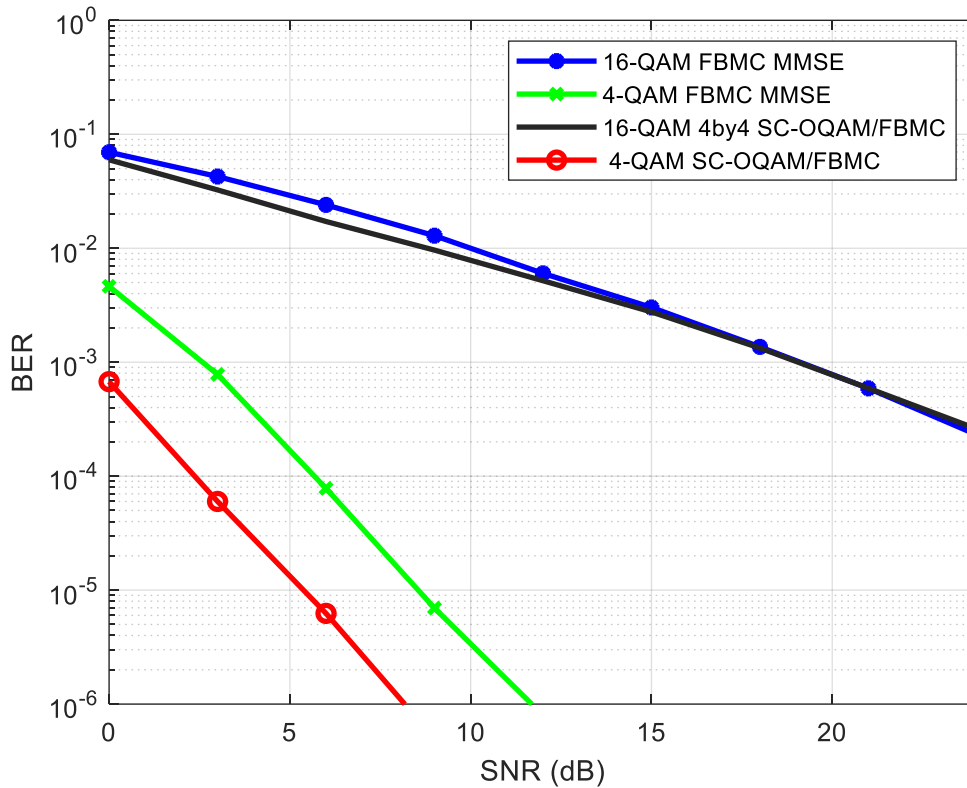


Figure 5-10: BER of 2×2 SFBC SC-OQAM/FBMC vs. OQAM/FBMC with MMSE FDE in 20-tap Rayleigh fading channel.

It can be noticed in the figure that increasing the MIMO order with the SC-OQAM/FBMC SFBC system still has a gain of 3 dB at a BER of 10^{-5} for 4-QAM modulation. However, when increasing the MIMO order with higher modulation order (16-QAM), there is no significant gain for the SC system over the original hybrid OQAM/FBMC.

The BER curves show the ability of the proposed SC-OQAM/FBMC SFBC system to be deployed in various operation scenarios, efficiently reducing the PAPR, retaining the low OOB emissions, and enhancing the BER performance thus increasing the overall spectral and energy efficiency of communication systems. However, when increasing the MIMO order with higher order modulation, the gain in the BER performance is negligible, however, the other benefits of the low PAPR and low OOB emissions are maintained.

6 CONCLUSION

6.1 Summary

OQAM/FBMC is a promising multi-carrier modulation technique, suitable for various scenarios and applications in future communication networks. Its major advantages are that it does not require a CP to combat ISI, and the very low OOB emissions resulting in reduced guard bands, which enhances the overall SE of the communication system. The superior spectral confinement also makes FBMC ideal in scenarios with strict spectral masks or exploiting fragmented spectra. Furthermore, since filtered subcarriers are strictly band-limited, OQAM/FBMC systems are less sensitive to frequency synchronization errors compared to OFDM, which requires strict synchronization requirements to preserve the orthogonality of the overlapping subcarriers and eliminate ICI. All the above-mentioned merits made the OQAM/FBMC waveform a strong candidate to play an important role in future heterogeneous communication networks.

Our work started by highlighting the importance of waveform design in the progression of cellular communications generations, with a focus on the main aspects of waveform design, followed by a review of the main filtering OFDM-based multi-carrier waveforms. These waveforms address some OFDM drawbacks including high OOB emissions, the need for long CP in heavy multipath fading channels and the strict synchronization requirements. The techniques were simulated and compared, showing that OQAM/FBMC is superior in various aspects mainly the spectral confinement, relaxed synchronization requirements and preserving real-orthogonality. Afterwards, the main aspects of the OQAM/FBMC waveform were examined and its main research problems were highlighted.

Our work addresses major research problems in the OQAM/FBMC system including integration with MIMO, multipath channel equalization, complexity reduction and PAPR reduction. The outcome was the proposed hybrid OQAM/FBMC SFBC MIMO system which offers a solution for the implementation of SFBC with OQAM/FBMC, without suffering from intrinsic interference, with the least possible complexity according to the transmission channel and

promising BER performance. In the uplink scenario, where low PAPR is desirable, the SC-OQAM SFBC FBMC system is proposed which effectively reduces the PAPR and gives enhanced BER performance. A mathematical model with matrix representation was presented, followed by BER analysis and complexity analysis. For simulations, MATLAB codes were developed to enable altering different parts of the OQAM/FBMC system at the signal processing level and measuring different KPIs for the systems including BER, PSD and PAPR. Different equalization techniques, MIMO settings, transmission channels and overlapping factors have been tested, to determine the best possible system settings for each usage scenario.

6.2 Conclusions

- In frequency-selective Rayleigh fading multipath channels, the best solution is the hybrid-structure OQAM/FBMC MIMO system with MMSE FDE. The results show that the BER performance is better than that of CP-OFDM, with the advantage of a highly localized spectrum and CP-less transmission, which increases the throughput efficiency by 12.5%, for a CP length of $N/8$.
- The SFBC being performed on the complex signal before the OQAM processing prevents the effects of the intrinsic interference of OQAM/FBMC on MIMO coding.
- The proposed hybrid system offers the least computational complexity and the best performance with FDE.
- In mild multipath fading where there is a LOS path, the PPN OQAM/FBMC system with ZF-TDE is deployed to significantly reduce the computational complexity. In such cases, the PPN-TDE system gives a comparable BER performance, with the least computational complexity, nearly 25% less than that of the hybrid OQAM/FBMC FDE systems. This makes it suitable for deployment in scenarios which involve simple devices in favourable multipath channel conditions, like some D2D and IoT scenarios.
- Any other FBMC complexity reduction techniques can be deployed to further reduce the computational complexity of the hybrid OQAMFBMC.

- In the uplink scenario, where a low PAPR of the transmitted signal is desirable to reduce the power consumed by the HPA at the battery-operated UE, the SC-OQAM/FBMC system is more efficient. The additional complexity of the system is relatively low compared to the original complexity of the OQAM/FBMC systems.
- The proposed SC-OQAM/FBMC MIMO system offers a superior reduction in the PAPR compared to other DFT-spreading FBMC PAPR reduction techniques.
- Any other FBMC PAPR reduction techniques, other than the DFT spreading, can be added to the system to further decrease the PAPR.

6.3 Future Work

Our research can be extended in various aspects. At the signal processing level, different spreading matrices other than DFT can be tried with the SC OQAM/FBMC system, to further reduce the PAPR and enhance different aspects of the SC system performance. Also, discrete wavelet packet transform (DWPT) can be tested in replacement of the FFT at the transmitter and receiver to evaluate its benefits in terms of the system's KPIs. In another direction, the systems can be studied and simulated in the massive MIMO context. The compatibility and co-existence with OFDM is another research direction.

REFERENCES

- [1] W. Saad, M. Bennis, and M. Chen, "A vision of 6G wireless systems: Applications, trends, technologies, and open research problems," *IEEE network*, vol. 34, no. 3, pp. 134–142, 2019.
- [2] S. Mahama, D. Asiedu, Y. Harbi, K. Lee, D. Grace and A. Burr, "Multi-User Wireless Information and Power Transfer in FBMC-Based IoT Networks," *IEEE Open Journal of the Comm. Soc.*, vol. 2, pp. 545-563, 2021.
- [3] B. Farhang-Boroujeny, "Multicarrier Modulation with Blind Detection Capability using Cosine Modulated Filter Banks," *IEEE Trans. on Comm.*, vol. 51, no. 12, pp.2057-2070, 2003.
- [4] A. Hammoodi, L. Audah and M.A. Taher, "Green coexistence for 5G waveform candidates: a review," *IEEE Access*, vol. 7, pp.10103-10126, 2019.
- [5] M. Bellanger, D. Le Ruyet, D. Roviras, M. Terré, J. Nossek, L. Baltar, Q. Bai, D. Waldhauser, M. Renfors and T. Ihalainen, "FBMC Physical Layer: A Primer," *PHYDYAS*, 2010.
- [6] B. Farhang-Boroujeny, "OFDM versus filter bank multicarrier," *IEEE Signal Processing Magazine*, vol. 28, no. 3, pp. 92–112, 2011.
- [7] D. Chen, R. Wang and T. Jiang, "Channel Estimation and Pilot Symbol Optimization Based on Intrinsic Interference Utilization for OQAM/FBMC Systems," *IEEE Trans. on Sig. Proc.*, vol. 69, pp. 4595-4606, 2021.
- [8] J.B. Doré, V. Berg and D. Ktésas, "Channel estimation techniques for 5G cellular networks: FBMC and multiuser asynchronous fragmented spectrum scenario," *Transactions on Emerging Telecommunications Technologies*, vol. 26, no. 1, pp. 15-30, 2014.
- [9] B. Farhang-Boroujeny, "Filter bank multicarrier modulation: A waveform candidate for 5G and beyond" *Advances in Electrical Engineering*, 2014.
- [10] K.W. Barlee, R.W. Stewart and L.H. Crockett, "Secondary User Access for IoT Applications in the FM Radio Band using FS-FBMC," *IEEE 5G World Forum*, Santa Clara, USA, pp. 468-473, 2018.

- [11] K. Barlee, R. Stewart, L. Crockett and N. MacEwen, "Rapid Prototyping and Validation of FS-FBMC Dynamic Spectrum Radio with Simulink and ZynqSDR," *IEEE Open Journal of the Comm. Soc.*, vol. 2, pp. 113-131, 2021.
- [12] R. Arjun, H. Shah, S. Dhua, K. Appaiah and V.M. Gadre, "Low Complexity FBMC for Wireless MIMO Systems," *Physical Communications*, vol. 47, 2021.
- [13] M. Vaezi, Z. Ding and H.V. Poor, "Multiple access techniques for 5G wireless networks and beyond," Berlin, Germany, Springer, 2018.
- [14] S. Mahama, Y. Harbi, D. Grace and A. Burr, "Multi-User Interference Cancellation for Uplink FBMC-Based Multiple Access Channel," *IEEE Communication Letters*, vol. 25, no. 8, pp. 2733-2737, 2021.
- [15] D. Jaswanth, S.K. Sahoo, G. Satapathy and S.P. Dash, "Optimal Coverage Analysis of a CP-OFDM/FBMC based Device-to-Device Communication System," *IEEE 93rd Vehicular Technology Conference*, Finland, pp. 1-6, 2021.
- [16] J. Doré, V. Berg, N. Cassiau and D. Ktésas, "FBMC receiver for multi-user asynchronous transmission on fragmented spectrum," *EURASIP Journal on Adv. in Sig. Proc.*, vol. 2014, no. 1, 2014.
- [17] J. Zhang, S. Hu, Z. Liu, P. Wang, P. Xiao and Y. Gao, "Real-Valued Orthogonal Sequences for Iterative Channel Estimation in MIMO-FBMC Systems," *IEEE Access*, 2019.
- [18] C. Sexton, Q. Bodinier, A. Farhang, N. Marchetti, F. Bader and L.A. DaSilva, "Enabling Asynchronous Machine-Type D2D Communication Using Multiple Waveforms in 5G," *IEEE internet of things journal*, 5(2), pp.1307-1322, 2018.
- [19] A. Aminjavaheri, A. Farhang, A. Rezazadeh Reyhani, and B. Farhang-Boroujeny, "Impact of timing and frequency offsets on multicarrier waveform candidates for 5G," *IEEE Signal Processing and Signal Processing Education Workshop*, pp. 178-183, 2015.
- [20] H. Wang, L. Xu, Z. Yan and T. Gulliver, "Low-Complexity MIMO-FBMC Sparse Channel Parameter Estimation for Industrial Big Data Communications," *IEEE Transactions on Industrial Information*, vol. 17, no. 5, pp. 3422-3430, 2021.

- [21] S. Srivastava, P. Singh, A. Jagannatham, A. Karandikar and L. Hanzo, "Bayesian Learning-Based Doubly-Selective Sparse Channel Estimation for Millimeter Wave Hybrid MIMO-FBMC-OQAM Systems," *IEEE Transactions on Communications*, vol. 69, no. 1, pp. 529-543, 2020.
- [22] A.T. Latunde, A. Papazafeiropoulos, P. Kourtessis, and J.M. Senior, "Co-existence of OFDM and FBMC for resilient photonic millimeter-wave 5G mobile fronthaul. *Photonic Network Communications*," 37(3), pp.335-348, 2019.
- [23] H. Yamada, H. Suganuma and F. Maehara, "System Capacity Analysis of Asynchronous FBMC and OFDM Systems in the Presence of Adjacent Channel Interference and Multipath Fading," *IEEE Radio and Wireless Symposium*, pp. 171-173, 2022.
- [24] P. Singh, H.B. Mishra, A.K. Jagannatham, K. Vasudevan, and L. Hanzo, "Uplink sum-rate and power scaling laws for multi-user massive MIMO-FBMC systems," *IEEE Transactions on Communications*, 68(1), pp.161-176, 2019.
- [25] S. Singh, P. Singh, S. Sahu, K. Vasudevan and H.B. Mishra, "Uplink Transmission in MU Multi-Cell Massive MIMO-FBMC Systems over Ricean Fading," *IEEE 94th Vehicular Technology Conference*, pp. 01-06, 2021.
- [26] H. Hosseiny, A. Farhang and B. Farhang-Boroujeny, "FBMC Receiver Design and Analysis for Medium and Large Scale Antenna Systems," *IEEE Transactions on Vehicular Technology*, 2022..
- [27] A. Aminjavaheri, A. Farhang and B. Farhang-Boroujeny, "Filter bank multicarrier in massive MIMO: Analysis and channel equalization," *IEEE Transactions on Signal Processing*, 66(15), pp.3987-4000, 2018.
- [28] M. Bellanger, "FS-FBMC: An alternative scheme for filter bank based multicarrier transmission," *5th International Symposium on Communications, Control and Signal Processing* pp. 1-4, 2012.
- [29] S. Shaikhah and S. Mustafa, "A robust filter bank multicarrier system as a candidate for 5G," *Physical Communications*, vol. 43, 2020..

- [30] R. Gomes, J. Reis, Z. Al-Daher, A. Hammoudeh and R. Caldeirinha, "5G: Performance and Evaluation of FS-FBMC against OFDM for High Data Rate Applications at 60 GHz," *IET Sig. Proc.*, vol. 12, no. 5, pp. 620-628, 2018.
- [31] X. Cheng, Y. Li, B. Ai, X. Yin and Q. Wang, "Device-to-device channel measurements and models: a survey," *IET Comm.*, vol. 9, no. 3, pp. 312-325, 2015.
- [32] M. Peng, Y. Li, T. Quek and C. Wang, "Device-to-Device Underlaid Cellular Networks under Rician Fading Channels", *IEEE Transactions on Wireless Communication*, vol. 13, no. 8, pp. 4247-4259, 2014.
- [33] V. Savaux and Y. Louët, "PAPR Analysis as a ratio of two random variables: Application to multicarrier systems with low subcarriers number," *IEEE Transactions on Communications*, 66(11), pp.5732-5739, 2018.
- [34] S. Pratschner, B. Tahir, L. Marijanovic, M. Mussbah, K. Kirev, R. Nissel, S. Schwarz, and M. Rupp, "Versatile mobile communications simulation: The Vienna 5G link level simulator," *EURASIP Journal on Wireless Communications and Networking*, p.226, 2018.
- [35] H. Al-amaireh, and Z. Kollár, "Optimization of hopping DFT for FS-FBMC receivers," *Signal Processing*, 2021.
- [36] J. Nadal, C.A. Nour and A. Baghdadi, "Design and evaluation of a novel short prototype filter for FBMC/OQAM modulation," *IEEE access*, 19610-19625, 2018.
- [37] A. Viholainen , M. Bellanger , M. Huchard, "Prototype Filter and Structure Optimization," Project PHYDYAS (Physical Layer for Dynamic Access and Cognitive Radio), Technical Report D5. 1, 2009.
- [38] L. Varga and Z. Kollár, "Low Complexity FBMC Transceiver for FPGA Implementation," in *3rd International Conference Radioelektronika*, Pardubice, Czech Republic, pp.219-223, 2013.
- [39] D. Na and K. Choi, "Low PAPR FBMC," *IEEE Trans. on Wireless Comm.*, vol. 17, no. 1, pp. 182-193, 2018.

- [40] M. Terre, FBMC Modulation / Demodulation. [Online]. Available: <https://www.mathworks.com/matlabcentral/fileexchange/45100-fbmc-modulation-demodulation>.
- [41] Z. Kollar and H. Al-Amaireh, "FBMC Transmitters with Reduced Complexity," *Radioengineering*, vol. 27, no. 4, pp. 1147-1154, 2018.
- [42] A.A. Husam and Z. Kollár, "Complexity Comparison of Filter Bank Multicarrier Transmitter Schemes," in *11th Inter. Symp. on CSNDSP, Hungary*, pp. 1-4, 2018.
- [43] V. Berg, D. Jean-Baptiste Doré and N. Dominique, "A flexible FS-FBMC receiver for dynamic access in the TVWS," *9th International Conference on Cognitive Radio Oriented Wireless Networks and Communications*, pp. 285-290, 2014.
- [44] Y. Dandach and P. Siohan, "FBMC/OQAM Modulators with Half Complexity," in *2011 IEEE GLOBECOM, USA*, pp.1-5, 2011.
- [45] J. Nadal, C. Abdel Nour and A. Baghdadi, "Low-Complexity Pipelined Architecture for FBMC/OQAM Transmitter," *IEEE Trans. on Circuits and Sys. II: Express Briefs*, vol. 63, no. 1, pp. 19-23, 2016.
- [46] M. Chen, A. Deng, L. Zhang, R. Li, J. Yang, H. Zhou, Q. Chen, and Y. Cheng, "Precoding-Enabled FBMC/OQAM for Short-Reach IMDD Transmission," *IEEE Photonics Technology Letters* 33, no. 23, 1305-1308, 2021.
- [47] H. Al-amaireh , Z. Kollar , "Reducing the complexity of FS-FBMC receivers using hopping DFT," *29th International Conference Radioelektronika*, pp. 1–5, 2019.
- [48] S.M. Alamouti, "A simple transmit diversity technique for wireless communications," *IEEE Journal on selected areas in communications*, vol. 16, no. 8, pp.1451-1458, 1998.
- [49] L. Zheng and D.N.C. Tse, "Diversity and multiplexing: A fundamental trade-off in multiple-antenna channels," *IEEE Transactions on Information Theory*, vol. 49, no. 5, pp.1073-1096, 2003.
- [50] D. Na, and K. Choi, "Intrinsic ICI-free Alamouti coded FBMC," *IEEE Communications Letters*, pp.1971-1974, 2016.

- [51] C. Le, S. Moghaddamnia and J. Peissig, "On the performance of alamouti scheme in 2 x 2 mimo-fbmc systems," in 19th International Conference on OFDM and Frequency Domain Techniques ICOF, pp. 1-6, 2016.
- [52] R. Nissel and M. Rupp, "Enabling low-complexity MIMO in FBMC-OQAM," IEEE Globecom Workshops, pp. 1-6, 2016.
- [53] K. Choi, "Alamouti coding for DFT spreading-based low PAPR FBMC," IEEE Transactions on Wireless Communications, vol. 18, no. 2, pp. 926-941, 2019.
- [54] J. Li, D. Chen, D. Qu, Y. Zhang and T. Jiang, "Receiver design for Alamouti coded FBMC system in highly frequency selective channels," IEEE Transactions on Broadcasting, vol. 65, no. 3, pp.601-608, 2018.
- [55] R. Zakaria, D. Le Ruyet and M. Bellanger, "Maximum likelihood detection in spatial multiplexing with FBMC," in European Wireless Conference, pp. 1038-1041, 2010.
- [56] D. Demmer, J.B. Doré, D. Le Ruyet and R. Gerzaguet, "Performance of soft-decision linear receivers for spatial-multiplexing FBMC/OQAM," in International Symposium on Wireless Communication Systems, pp. 404-408, 2016.
- [57] R. Zakaria and D. Le Ruyet, "A novel filter-bank multicarrier scheme to mitigate the intrinsic interference: Application to MIMO systems," IEEE Transactions on Wireless Communications, 11(3), pp.1112-1123, 2012.
- [58] R. Zakaria and D. Le Ruyet, "On interference cancellation in Alamouti coding scheme for filter bank based multicarrier systems," ISWCS The Tenth International Symposium on Wireless Communication Systems, pp. 1-5, 2013.
- [59] S. Kaur, L. Kansal, and G. S. Gaba, "Impact of Hybrid PAPR Reduction Techniques on FBMC for 5G Applications," International Journal on Smart Sensing and Intelligent Systems, 2020.
- [60] T. Ihalainen, A. Ikhlef, J. Louveaux and M. Renfors, "Channel equalization for multi-antenna FBMC/OQAM receivers," IEEE transactions on vehicular technology, 60(5), pp.2070-2085, 2011.

- [61] A. Aminjavaheri, A. Farhang, N. Marchetti, L.E. Doyle and B. Farhang-Boroujeny, "Frequency spreading equalization in multicarrier massive MIMO," in IEEE International Conference on Communication Workshop, pp. 1292-1297, 2015.
- [62] R. Nissel, J. Blumenstein and M. Rupp, "Block frequency spreading: A method for low-complexity MIMO in FBMC-OQAM," IEEE 18th International Workshop on Signal Processing Advances in Wireless Communications, pp. 1-5, 2017.
- [63] D. Wulich, "Definition of efficient PAPR in OFDM," IEEE communications letters , no. 9, pp. 832-834, 2005.
- [64] H. Wang, P.M. Asbeck, and C. Fager, "Millimeter-wave power amplifier integrated circuits for high dynamic range signals," IEEE Journal of Microwaves, no. 1, pp. 299-316, 2021.
- [65] H. Hashemi, "Millimeter-wave power amplifiers & transmitters," in IEEE Custom Integrated Circuits Conference, pp. 1-8., 2017.
- [66] E. Balti and B.K. Johnson, "On the joint effects of hpa nonlinearities and iq imbalance on mixed RF/FSO cooperative systems," IEEE Transactions on Communications 69, no. 11: 7879-7894, 2021.
- [67] C. Vittorio, R. Quaglia, A. Piacibello, D. P. Nguyen, H. Wang, and A. V. Pham, "A review of technologies and design techniques of millimeter-wave power amplifiers," IEEE Transactions on Microwave Theory and Techniques, vol. 68, no. 7: 2957-2983, 2020.
- [68] S. Jang, D. Na, and K. Choi, "Comprehensive performance comparison between OFDM-based and FBMC-based uplink systems," in IEEE 2020 International Conference on Information Networking, pp. 288-292, 2020.
- [69] I.A. Shaheen, A. Zekry, F. Newagy, and R. Ibrahim, "Performance evaluation of PAPR reduction in FBMC system using nonlinear companding transform," ICT Express 5, no. 1, 41-46, 2019.
- [70] S. Ramavath and U.C. Samal, "Theoretical analysis of PAPR companding techniques for FBMC systems," Wireless Personal Communications 118, no. 4: 2965-2981, 2021.

- [71] P. Jirajaracheep, S. Sanpan, P. Boonsrimuang, and P. Boonsrimuang, "PAPR reduction in FBMC-OQAM signals with half complexity of trellis-based SLM," 20th International Conference on Advanced Communication Technology, pp. 1-5, 2018.
- [72] L. Rujiprechanon, P. Boonsrimuang, S. Sanpan, and P. Boonsrimuang, "Proposal of sub-optimum algorithm for trellis-based SLM reducing PAPR of FBMC-OQAM signals," International Workshop on Advanced Image Technology, pp. 1-4, 2018.
- [73] X. Cheng, D. Liu, W. Shi, Y. Zhao, Y. Li, and D. Kong, "A novel conversion vector-based low-complexity SLM scheme for PAPR reduction in FBMC/OQAM systems," IEEE Transactions on Broadcasting vol. 66, no. 3: 656-666, 2020.
- [74] Y. Yan and X. Pingping, "PAPR reduction of FBMC-OQAM signals based on cuckoo search optimization algorithm," IEEE International Conference on Signal Processing, Communications and Computing, pp. 1-5, 2017.
- [75] Z. He, L. Zhou, Y. Chen and X. Ling, "Low-complexity PTS scheme for PAPR reduction in FBMC-OQAM systems," IEEE Communications Letters 22, no. 11 2322-2325, 2018.
- [76] I.A. Shaheen, A. Zekry, F. Newagy and R. Ibrahim, "PAPR Reduction of FBMC/OQAM Systems Based on Combination of DST Precoding and A-law Nonlinear Companding Technique," International Conference on Promising Electronic Technologies, pp. 38-42, 2017.
- [77]] Z. He, L. Zhou, Y. Chen and X. Ling, "A novel algorithm for peak-to-average power ratio reduction in FBMC-OQAM system," in IEEE 17th International Conference on Communication Technology, pp. 64-68, 2017.
- [78] R. Gopal and S.K. Patra, "Combining tone injection and companding techniques for PAPR reduction of FBMC-OQAM system," in Global Conference on Communication Technologies, pp. 709-713, 2015.
- [79] S. Sidiq, J.A. Sheikh, F. Mustafa, B.A. Malik, and I.B. Sofi, "PAPR Minimization of FBMC/OQAM Scheme by Hybrid SLM and PTS Using Artificial: Bee-Colony Phase—Optimization," Arabian Journal for Science and Engineering vol. 46, no. 10, 9925-9934, 2021.

- [80] H.F. Abdalla, E.S. Hassan, M.I. Dessouky, and A.S. Elsafrawy, "Three-layer PAPR reduction technique for FBMC based VLC systems," *IEEE Access*: 102908-102916, 2021.
- [81] K. Ayappasamy, G. Nagarajan and P. Elavarasan, "DFT Spread C-DSLM for Low PAPR FBMC with OQAM Systems," In *Machine Learning, Deep Learning and Computational Intelligence for Wireless Communication*, pp. 281-302. Springer, Singapore, 2021.
- [82] Y. Aimer, B.S. Bouazza, S. Bachir and C. Duvaud, "Shaping code in conjunction with DCT for PAPR reduction in multicarrier system," *EURASIP Journal on Wireless Communications and Networking*, 2021.
- [83] Y.J. Ho, "Peak cancellation for PAPR reduction in filter bank based multicarrier system," in *International Conference on Information and Communication Technology Convergence*, pp. 1029-1031, 2016.
- [84] C. H. Yuen, P. Amini, and B. Farhang-Boroujeny, "Single carrier frequency division multiple access (SC-FDMA) for filter bank multicarrier communication systems," in *Proc. CROWNCOM*, pp. 1–5, Jun. 2010.
- [85] B.S. Chang, C.A. da Rocha, D. Le Ruyet, and D. Roviras, "On the effect of ISI in the error performance of precoded FBMC/OQAM systems," in *18th Asia-Pacific Conference on Communications (APCC)*, pp. 987-991, 2012.
- [86] R. Nissel and M. Rupp, "Pruned DFT-Spread FBMC: Low PAPR, Low Latency, High Spectral Efficiency," *IEEE Transactions on Communications*, 66(10), pp.4811-4825.
- [87] K. Choi, "Alamouti coding for DFT spreading-based low PAPR FBMC," *IEEE Transactions on Wireless Communications*, 2018.
- [88] M.A. Aboul-Dahab, M.M. Fouad, and R.A. Roshdy, "Generalized discrete Fourier transform for FBMC peak to average power ratio reduction," *IEEE access*, 2019.
- [89] K. Ayappasamy, G. Nagarajan, and P. Elavarasan, "Decision feedback equalizers and Alamouti coded DFT spread for low PAPR FBMC-OQAM system," *International Conference on Emerging Trends in Information Technology and Engineering*, pp. 1-7. IEEE, 2020.

- [90] X. Zhang, C. Zhang, M. Zhu, W. Jin, C. Chen, X. Gao and K. Qiu, "SSB pruned DFT-spread FBMC signal with low PAPR in direct-detection PONs," *IEEE Photonics Journal* vol. 12, no. 3: 1-13 2020.
- [91] R. Pereira, C.A. da Rocha, B.S. Chang and D. Le Ruyet, "A Generalized DFT Precoded Filter Bank System," *IEEE Wireless Communications Letters*, 2022.
- [92] D. Na and K. Choi, "DFT spreading-based low PAPR FBMC with embedded side information," *IEEE Transactions on Communications*, vol 68, no. 3: 1731-1745, 2019.
- [93] 3GPP Release 17. Available at: <https://www.3gpp.org/release-17>
- [94] P. Banelli, S. Buzzi, G. Colavolpe, A. Modenini, F. Rusek and A. Ugolini, "Modulation formats and waveforms for 5G networks: Who will be the heir of OFDM?: An overview of alternative modulation schemes for improved spectral efficiency," *IEEE Signal Processing Magazine*, vol. 31, no. 6, pp.80-93, 2014.
- [95] Y. Cai, Z. Qin, F. Cui, G.Y. Li and J.A. McCann, "Modulation and multiple access for 5G networks." *IEEE Communications Surveys & Tutorials*, 2017.
- [96] Y. Xu, G. Gui, H. Gacanin and F. Adachi, "A survey on resource allocation for 5G heterogeneous networks: Current research, future trends and challenges," *IEEE Communications Surveys & Tutorials*, 2021.
- [97] I. B. F. de Almeida, L. L. Mendes, J. J. Rodrigues and M.A. da Cruz, "5G Waveforms for IoT Applications," *IEEE Communications Surveys & Tutorials*, vol. 21, no. 3, pp.2554-2567, 2019.
- [98] F.L. Luo, and C. Zhang, editors, "Signal processing for 5G: algorithms and implementations," John Wiley & Sons, 2016.
- [99] B. Farhang-Boroujeny, "Filter bank multicarrier modulation: A waveform candidate for 5G and beyond" *Advances in Electrical Engineering*, 2014.
- [100] M.A. Jamshed, K. Ali, Q.H. Abbasi, M.A. Imran, and M. Ur-Rehman, "Challenges, applications and future of wireless sensors in Internet of Things: a review," *IEEE Sensors Journal*, 2022).

- [101] S.H. Martínez, P.O.J. Salcedo, and B.S.R. Daza, "IoT application of WSN on 5G infrastructure". IEEE International Symposium on Networks, Computers and Communications (ISNCC) (pp. 1-6), 2017.
- [102] J.J. Benedetto, C. Heil, and D.F. Walnut, "Gabor systems and the Balian-Low theorem." Gabor analysis and algorithms, pp. 85-122, 1997.
- [103] F. Schaich, "Filterbank based multi carrier transmission (FBMC)—evolving OFDM: FBMC in the context of WiMAX," Wireless Conference , pp. 1051-1058, 2010.
- [104] R. Nissel, S. Schwarz and M. Rupp, "Filter bank multicarrier modulation schemes for future mobile communications," IEEE Journal on Selected Areas in Communications, vol. 35, no. 8, pp.1768-1782, 2017.
- [105] C. Kim, Y.H. Yun, K. Kim and J.Y. Seol, "Introduction to QAM-FBMC: From waveform optimization to system design" IEEE Communications Magazine, 54(11), pp.66-73, 2016.
- [106] M. Schellmann, Z. Zhao, H. Lin, P. Siohan, N. Rajatheva, V. Luecken, and A. Ishaque, "FBMC-based air interface for 5G mobile: Challenges and proposed solutions," 9th International Conference on Cognitive Radio Oriented Wireless Networks and Communications, pp. 102-107, 2014.
- [107] Y. Qi and M. Al-Imari, "An enabling waveform for 5G—QAM-FBMC: Initial analysis," IEEE Conference on Standards for Communications and Networking, pp. 1-6, 2016.
- [108] V. Vakilian, T. Wild, F. Schaich, S. ten Brink and J.F. Frigon, "Universal-filtered multi-carrier technique for wireless systems beyond LTE," IEEE Globecom Workshops, pp. 223-228, 2013.
- [109] F. Schaich, T. Wild and Y. Chen, "Waveform contenders for 5G-suitability for short packet and low latency transmissions," IEEE 79th Vehicular Technology Conference, pp. 1-5, 2014.
- [110] T. Wild, F. Schaich and Y. Chen, "5G air interface design based on universal filtered (UF-) OFDM," 19th IEEE International Conference on Digital Signal Processing, pp. 699-704, 2014.

- [111] X. Zhang, M. Jia, L. Chen, J. Ma, and J. Qiu, "Filtered-OFDM-enabler for flexible waveform in the 5th generation cellular networks," IEEE Global Communications Conference, pp. 1-6, 2015.
- [112] J. Abdoli, M. Jia and J. Ma, "Filtered OFDM: A new waveform for future wireless systems," IEEE 16th International Workshop on Signal Processing Advances in Wireless Communications, pp. 66-70, 2015.
- [113] G. Fettweis, M. Krondorf, and S. Bittner, "GFDM-generalized frequency division multiplexing," IEEE 69th Vehicular Technology Conference, pp. 1-4. 2009.
- [114] B. Farhang-Boroujeny and H. Moradi, "OFDM inspired waveforms for 5G" IEEE Communications Surveys & Tutorials, 18(4), pp.2474-2492, 2016.
- [115] X. Zhang, L. Chen, J. Qiu and J. Abdoli, "On the waveform for 5G," IEEE Communications Magazine, 54(11), pp.74-80, 2014.
- [116] M. Murad, I.A. Tasadduq and P. Otero, "Towards multicarrier waveforms beyond OFDM: Performance analysis of GFDM modulation for underwater acoustic channels," IEEE Access, 2020.
- [117] N. Michailow, M. Matth e, I.S. Gaspar, A.N. Caldevilla, L.L. Mendes, A. Festag and G. Fettweis, "Generalized frequency division multiplexing for 5th generation cellular networks," IEEE Transactions on Communications, vol. 62, no. 9, pp.3045-3061, 2014.
- [118] A. Kumar , M. Magarini, "On the modeling of inter-sub-symbol interference in GFDM transmission," IEEE Communication Letters, 1730–1734, 2019.
- [119] Y. Liu, Z. Qin, M. ElKashlan, Z. Ding, A. Nallanathan and L. Hanzo, "Nonorthogonal Multiple Access for 5G and Beyond," Proceedings of the IEEE, 105(12), pp.2347-2381, 2017.
- [120] H. Lee, S. Kim, and J.H. Lim, "Multiuser superposition transmission (MUST) for LTE-A systems," IEEE International Conference on Communications (ICC), pp. 1-6, 2017.
- [121] L. Anxin, L. Yang, C. Xiaohang, and J. Huiling, "Non-orthogonal multiple access (NOMA) for future downlink radio access of 5G," China Communications, 12(Supplement), pp.28-37, 2015.

- [122] L. Dai, B. Wang, Y. Yuan, S. Han, I. Chih-Lin and Z. Wang, "Non-orthogonal multiple access for 5G: solutions, challenges, opportunities, and future research trends," *IEEE Communications Magazine*, 53(9), pp.74-81, 2015.
- [123] A.S. Marcano and H.L. Christiansen, "Performance of Non-Orthogonal Multiple Access (NOMA) in mmWave wireless communications for 5G networks," *International Conference on Computing, Networking and Communications*, pp. 969-974, 2017.
- [124] F. Schaich, and T. Wild, "Waveform contenders for 5G—OFDM vs. FBMC vs. UFMC," *6th International Symposium on Communications, Control and Signal Processing*, pp. 457-460. 2014.
- [125] J. Vihriala, N. Ermolova, E. Lahetkangas, O. Tirkkonen and K. Pajukoski, "On the waveforms for 5G mobile broadband communications," *IEEE 81st Vehicular Technology Conference*, pp. 1-5, 2015.
- [126] V. Vasconcellos, G.C. Ornelas and A.N. Barreto, "Performance of 5G candidate waveforms with non-linear power amplifiers," *IEEE 9th Latin-American Conference on Communications*, pp. 1-5, 2017.
- [127] H. Wang, A.A. Zaidi, X. Chen, J. Luo and M. Dieudonne, "Evaluation of 5G Waveform Candidates Considering Hardware Impairments and above 6 GHz Operation," *IEEE 85th Vehicular Technology Conference*, pp 1-5, 2017.
- [128] S. Dikmese, M. Abdelaziz, L. Anttila, M. Renfors, and M. Valkama, "Dynamic and Flexible Spectrum Use with Frequency Localized Waveforms under Transmitter Nonidealities," *IEEE 82nd Vehicular Technology Conference*, pp. 1-6, 2015.
- [129] S.R. Biyabani, R. Khan, M.M. Alam, A.A. Biyabani, and E. McCune, "SS5G: Energy Efficiency Evaluation of Linear Transmitters for 5G NR Wireless Waveforms," *IEEE Transactions on Green Communications and Networking*, 2019.
- [130] A. Bedou and M. Et-tolba, "A comparative analysis of filter bank multicarrier (FBMC) as 5G multiplexing technique," *International Conference on Wireless Networks and Mobile Communications*, pp. 1-7, 2017.

- [131] O. Font-Bach, N. Bartzoudis, X. Mestre, D. López-Bueno, P. Mege, L. Martinod, V. Ringset and T.A. Myrvoll, "When SDR meets a 5G candidate waveform: agile use of fragmented spectrum and interference protection in PMR networks," *IEEE Wireless Communications*, 22(6), pp.56-66, 2015.
- [132] Y. Zeng, Y.C. Liang, M.W. Chia and T.H. Pham, "Fast Algorithms for FBMC and GFDM in Dynamic Spectrum Access," *Wireless Communications and Networking Conference*, pp. 1-6, 2017.
- [133] I.B. Almeida, L.L. Mendes, J.J. Rodrigues, and M.A. da Cruz, "5G Waveforms for IoT Applications," *IEEE Communications Surveys & Tutorials*, 2019.
- [134] V. Berg, J.B. Doré and D. Noguét, "A flexible radio transceiver for TVWS based on FBMC," *Microprocessors and Microsystems*, 38(8), pp.743-753, 2014.
- [135] V. Anis, J. Guo, S. Weiss and L.H. Crockett, "FPGA implementation of a TVWS up-and downconverter using non-power-of-two FFT modulated filter banks," *27th European Signal Processing Conference*, pp. 1-5, 2019.
- [136] R. Nissel, E. Zöchmann, M. Lerch, S. Caban, and M. Rupp, "Low-latency MISO FBMC-OQAM: It works for millimeter waves!," *IEEE MTT-S International Microwave Symposium*, pp. 673-676, 2017.
- [137] K. Roth, L.G. Baltar, M. Faerber, and J.A. Nossek, "Performance analysis of FBMC and CP-OFDM in the presence of phase noise," *European Conference on Networks and Communications*, pp. 1-5, 2017.
- [138] N. Al-Falahy and O.Y. Alani, "Millimetre wave frequency band as a candidate spectrum for 5G network architecture: a survey," *Physical Communication*, 32, pp.120-144, 2019.
- [139] H.M. Abdel-Atty, W.A. Raslan, and A.T. Khalil, "Evaluation and analysis of FBMC/OQAM systems based on pulse shaping filters," *IEEE Access*, 55750-55772, 2020.
- [140] I. Galdino, R. Zakaria, D. Le Ruyet and M.L. de Campos, "Short prototype filter design for OQAM-FBMC modulation," *IEEE Transactions on Vehicular Technology* 69, no. 8, pp. 9163-9167, 2020.

- [141] H. Han and H. Park, "CFO estimation for QAM-FBMC systems considering non-orthogonal prototype filters," IEEE 28th Annual International Symposium Personal, Indoor, and Mobile Radio Communications, pp. 1-5, 2017.
- [142] H. Kim, H. Han, and H. Park, "Waveform design for QAM-FBMC systems," IEEE 18th International Workshop on Signal Processing Advances in Wireless Communications, pp. 1-5, 2017.
- [143] J. Wen, J. Hua, F. Li, D. Wang, and J. Li, "Design of FBMC waveform by exploiting a NPR prototype filter," Advances in Wireless and Optical Communications (RTUWO), pp. 156-161, 2017.
- [144] Z. He, L. Zhou, Y. Chen, and X. Ling, "Filter optimization of out-of-band emission and BER analysis for FBMC-OQAM system in 5G," IEEE 9th International Conference on Communication Software and Networks, pp. 56-60, 2017.
- [145] G.I. Baskara and M. Suryanegara, "Study of filter-bank multi carrier (FBMC) utilizing mirabbasi-martin filter for 5G system," 15th International Conference on Electrical and Computer Engineering, pp. 457-461, 2017.
- [146] J. Wen, J. Hua, S. Li, K. Zhou and D. Wang, "Interference-driven designs of nonlinear-phase FIR filter with application in FBMC system," China Communications, 13(12), pp.15-24, 2016.
- [147] K.W. Martin, "Small sidelobe filter design for multitone data-communication applications," IEEE Transactions on Circuits and Systems, CAS-II, vol.45, pp.1155-1161, 1998.
- [148] R. Nissel and M. Rupp, "On pilot-symbol aided channel estimation in FBMC-OQAM," IEEE International Conference on Acoustics, Speech and Signal Processing, pp. 3681-3685, 2016.
- [149] R. Haas, and J.C. Belfiore, "A time-frequency well-localized pulse for multiple carrier transmission", Wireless personal communications, 5(1), pp.1-18, 1997.

- [150] M. Renfors, T. Ihalainen and T.H. Stitz, "A block-Alamouti scheme for filter bank based multicarrier transmission," in European Wireless Conference, pp. 1031-1037, 2010.
- [151] L.S. Gordon, "Principles of mobile communication" Springer, 2017.
- [152] A. T. Abou-Elkheir, E. F. Badran and O. Y. Alani, "Performance Evaluation of OQAM-FBMC System with STBC/SM MIMO over Rayleigh Fading Channel," in 11th IEEE Annual Info. Tech., Electronics and Mobile Com. Conf., Virtual, pp. 0854-0859, 2020.
- [153] V. Tarokh, H. Jafarkhani and A.R. Calderbank, "Space-time block codes from orthogonal designs," IEEE Transactions on Information theory, 45(5), pp.1456-1467, 1999.
- [154] M. Rupp and C.F. Mecklenbrauker, "On extended Alamouti schemes for space-time coding," The 5th international symposium on wireless personal multimedia communications Vol. 1, pp. 115-119, 2002.
- [155] B. Sklar, "Digital Communications: Fundamentals and Applications," Englewood Cliffs, NJ, USA: Prentice Hall, 1988.
- [156] F. Farrukh, S. Baig and M. J. Mughal, "Performance Comparison of DFT-OFDM and Wavelet-OFDM with Zero-Forcing Equalizer for FIR Channel Equalization," in Inter. Conf. on Electrical Eng., Lahore, Pakistan, pp. 1-5, 2007.
- [157] K. Cho and D. Yoon, "On the general BER expression of one- and two-dimensional amplitude modulations," IEEE Trans. Commun., vol. 50, no. 7, pp. 1074–1080, Jul. 2002.
- [158] P. Singh, H. B. Mishra, A. K. Jagannatham, and K. Vasudevan, "Semiblind, training, and data-aided channel estimation schemes for MIMO FBMC-OQAM systems," IEEE Trans. Signal Process., vol. 67, no. 18, pp. 4668–4682, Sep. 2019.
- [159] S. Haykin, "Digital Communications," Wiley, New York, 1988.
- [160] P. Duhamel and M. Vetterli, "Fast Fourier transforms: A tutorial review and a state of the art", Signal Process., vol. 19, no. 4, pp. 259-299, 1990.
- [161] E. Badran, A. Alamri, M. Mokhtar and E. El-Badawy, "A Space Wavelet Block Codes MIMO SC-WDMA Systems," Physical Communications, vol. 36, 2019.
- [162] 3GPP Release 15. Available at: <https://www.3gpp.org/release-15>

- [163] K. V. S. Hari, "Channel Models for Wireless Communication Systems," in *Wireless Network Design*, USA: Springer, 2011.
- [164] P. Sharma, A. Shankar and X. Cheng, "Reduced PAPR Model Predictive Control based FBMC/OQAM signal for NB-IoT paradigm," in *International Journal of Machine Learning and Cybernetics*, Springer, vol. 12, no. 11, pp. 3309-3323, 2021.
- [165] P. Kabilamani and C. Gomathy, "Implementation of Downlink Physical Channel Processing Architecture for NB-IoT Using LTE/5G Networks" in *Wireless Personal Communications*, Springer, vol.116, no.4, pp.3527-3551, 2021.
- [166] P. Singh, E. Sharma, K. Vasudevan and R. Budhiraja, " CFO and channel estimation for frequency selective MIMO-FBMC/OQAM systems," in *IEEE Wireless Communications Letters*, vol.7, no.5, pp.844-847, 2018.
- [167] K. Raghunath and A. Chockalingam, "SC-FDMA versus OFDMA: Sensitivity to large carrier frequency and timing offsets on the uplink," *IEEE Global Telecommunications Conference*, pp. 1-6, 2009.
- [168] C. Rapp, "Effects of HPA nonlinearity on a 4-DPSK/OFDM signal for a digital sound broadcasting system," in *Proc. 2nd European Conf. on Satellite Commun.*, Liège, Belgium, pp. 179–184, Oct. 1991.
- [169] S.A. Aburakhia, E.F. Badran, and D.A. Mohamed, "Linear companding transform for the reduction of peak-to-average power ratio of OFDM signals," *IEEE Transactions on Broadcasting* 55, no. 1, pp. 155-160, 2009.

APPENDIX A: PUBLICATIONS

- Abou-Elkheir, A.T., Badran, E.F. and Alani, O.Y., “Performance Evaluation of OQAM-FBMC System with STBC/SM MIMO over Rayleigh Fading Channel”, in 2020 11th IEEE Annual Information Technology, Electronics and Mobile Communication Conference (IEMCON) (pp. 0854-0859), November, 2020.
- A. T. Abou-Elkheir, E. F. Badran and O. Y. Alani, “A Hybrid Structure Offset-QAM Filter Bank Multi-Carrier MIMO System” (*under review of IEEE Transactions on Signal and Information Processing over Networks*)
- A. T. Abou-Elkheir, E. F. Badran and O. Y. Alani, “A Single Carrier Offset-QAM Filter Bank Multi-Carrier MIMO System: A Low PAPR solution for uplink” (*under review of Elsevier International Journal of Electronics and Communications*)

APPENDIX B: ATTENDED TRAINING SESSIONS

Date	Title	Key Learning Points
28 Sep 2016	Introduction to EndNote X7	Managing electronic references.
20 Jun 2018	Using the Library	How to find academic information using the library.
20 Mar 2019	How to reference and avoid plagiarism (Online)	What is plagiarism and how to avoid it. How to properly reference information sources.
4 Apr 2019	Excel: Analyzing Data	Sorting and filtering data, using Pivot tables and charts, VLOOKUP and Get and Transform tools.
8 Apr 2019	Introduction to Critical and Analytical Skills	How to critically analyze resources
3-4 Jul 2019	SPARC 2019	Poster discussion & presentation of: "Optimization of Waveforms & Modulation for Green 5G Networks"
10 May 2021	PGR Student Vox Coaching Development Sessions Application: Interview/Viva Training	<i>(Applied for attending the session)</i>

APPENDIX C: SAMPLE MATLAB CODE

1. Hybrid OQAM/FBMC SFBC MIMO FDE vs. OFDM BER (Chapter 4)

```
clc
clear all
N = 128; % Number of FFT points
K = 4; % Overlapping symbols, one of 2, 3, or 4
M=4; % QAM Modulation order
numFrames =10000; % Number of Monte Carlo simulations
snrdB = 0:3:27; % SNR in dB
tap=7; % Number of multipath channel taps
% Prototype filter coefficients
switch K
    case 2
        HkOneSided = sqrt(2)/2;
    case 3
        HkOneSided = [0.911438 0.411438];
    case 4
        HkOneSided = [0.971960 sqrt(2)/2 0.235147];
    otherwise
        return
end
% Build symmetric filter
Hk = [fliplr(HkOneSided) 1 HkOneSided];
% Impulse response for polyphase implementation in transmitter
H1=HkOneSided(1); H2=HkOneSided(2); H3=HkOneSided(3);
factech=1+2*(H1+H2+H3);
hef(1:4*N)=0;
for i=1:4*N-1
    hef(1+i)=1-2*H1*cos(pi*i/(2*N))+2*H2*cos(pi*i/N)-2*H3*cos(pi*i*3/(2*N));
end
hef=hef/factech;
%%
KN = K*N;
SubCar1 = zeros(N, 1);
SubCarUp1 = zeros(KN, 1);
SubCar2 = zeros(N, 1);
SubCarUp2 = zeros(KN, 1);
ber=zeros(numFrames,length(snrdB));
xber=zeros(numFrames,length(snrdB));
yber=zeros(numFrames,length(snrdB));
zber=zeros(numFrames,length(snrdB));
xx=N;
Ncp=xx/8;
inpSymbols = randi([0 M-1], N/2, numFrames);
yinpSymbols = randi([0 M-1], xx, numFrames);
currSym11=zeros(1,K*N);
currSym22=zeros(1,K*N);
Ant1=zeros(N/2,1);
Ant2=zeros(N/2,1);
yAnt1=zeros(xx,1);
yAnt2=zeros(xx,1);
dec1=zeros(N/2,1); %FBMC ZF
dec2=zeros(N/2,1);
ydec1=zeros(xx,1); %FBMC MMSE
ydec2=zeros(xx,1);
zdec1=zeros(xx,1); %OFDM ZF
zdec2=zeros(xx,1);
xdec1=zeros(N/2,1); %OFDM MMSE
xdec2=zeros(N/2,1);
%%
for frame = 1:numFrames
    frame
    mod = qammod(inpSymbols(:, frame),M);
    % STBC
    Ant1(1:2:end)=mod(1:2:end);
```

```

Ant1(2:2:end)=-conj(mod(2:2:end));
Ant2(1:2:end)=mod(2:2:end);
Ant2(2:2:end)=conj(mod(1:2:end));
%OFDM
ymod = qammod(yinpSymbols(:, frame),M);
yAnt1(1:2:end)=ymod(1:2:end);
yAnt1(2:2:end)=-conj(ymod(2:2:end));
yAnt2(1:2:end)=ymod(2:2:end);
yAnt2(2:2:end)=conj(ymod(1:2:end));
yf1 = (ifft((yAnt1)).')*sqrt(xx);
yf2 = (ifft((yAnt2)).')*sqrt(xx);
CP1=yf1(end-Ncp+1:end); % Cyclic Prefix Insertion
CP2=yf2(end-Ncp+1:end);
ycurrSym1= [CP1 yf1];
ycurrSym1=ycurrSym1/sqrt(sum(abs(ycurrSym1).^2)/numel(ycurrSym1));
ycurrSym2= [CP2 yf2];
ycurrSym2=ycurrSym2/sqrt(sum(abs(ycurrSym2).^2)/numel(ycurrSym2));
%FBMC
% OQAM Modulator : alternate real and imaginary parts
if rem(frame,2)==1 % Odd symbols
    SubCar1(1:2:N) = real(Ant1);
    SubCar1(2:2:N) = 1i*imag(Ant1);
    SubCar2(1:2:N) = real(Ant2);
    SubCar2(2:2:N) = 1i*imag(Ant2);
else % Even symbols
    SubCar1(1:2:N) = 1i*imag(Ant1);
    SubCar1(2:2:N) = real(Ant1);
    SubCar2(1:2:N) = 1i*imag(Ant2);
    SubCar2(2:2:N) = real(Ant2);
end
end
%Polyphase FBMC implementation (filter in time domain)
x1=(ifft(SubCar1)*sqrt(N)).';
%Duplication of the signal
x41=[x1 x1 x1 x1];
%We apply the filter on the duplicated signal
txSymb1=x41.*hef;
currSym11=txSymb1+[currSym11(1+N/2:end) zeros(1,N/2)];%
currSym1=currSym11./sqrt(sum(abs(currSym11).^2)/numel(currSym11));
x2=(ifft(SubCar2)*sqrt(N)).';
x42=[x2 x2 x2 x2];
%We apply the filter on the duplicated signal
txSymb2=x42.*hef;
currSym22=txSymb2+[currSym22(1+N/2:end) zeros(1,N/2)];%
currSym2=currSym22./sqrt(sum(abs(currSym22).^2)/numel(currSym22));
%Multipath Channel
h = (1/sqrt(tap))* (randn(4,tap)+sqrt(-1)*randn(4,tap))/sqrt(2);
h1 = h(1,:);h2 = h(2,:);h3 = h(3,:);h4 = h(4,:);
H11 = fft(h1,KN);H12 = fft(h2,KN);H21 = fft(h3,KN);H22 = fft(h4,KN);
%OFDM
yx11=filter(h1,1,ycurrSym1); yx12=filter(h2,1,ycurrSym2);
yx21=filter(h3,1,ycurrSym1); yx22=filter(h4,1,ycurrSym2);
ys1=yx11+yx12;
ys2=yx21+yx22;
yH11 = fft(h1,xx);yH12 = fft(h2,xx);yH21 = fft(h3,xx);yH22 = fft(h4,xx);
yA1 = diag(yH11);yA2 = diag(yH12);yA3 = diag(yH21);yA4 = diag(yH22);
yAT = [yA1 yA2;yA3 yA4];
%FBMC
H11 = fft(h1,KN);H12 = fft(h2,KN);H21 = fft(h3,KN);H22 = fft(h4,KN);
x11=filter(h1,1,currSym1); x12=filter(h2,1,currSym2);
x21=filter(h3,1,currSym1); x22=filter(h4,1,currSym2);
s1=x11+x12;
s2=x21+x22;
A1 = diag(H11);A2 = diag(H12);A3 = diag(H21);A4 = diag(H22);
AT = [A1 A2;A3 A4];
for ii=1:length(snrdB)
PdB1=10.*log10(sum((abs(currSym1)).^2)/numel(currSym1));
PdB2=10.*log10(sum((abs(currSym2)).^2)/numel(currSym2));
yn1=awgn(s1,snrdB(ii),PdB1);
yn2=awgn(s2,snrdB(ii),PdB2);
%OFDM
yPdB1=10.*log10(sum((abs(ycurrSym1)).^2)/numel(ycurrSym1));

```

```

yPdB2=10.*log10(sum((abs(ycurrSym2)).^2)/numel(ycurrSym2));
yyn1=awgn(ys1,snrdB(ii),yPdB1);
yyn2=awgn(ys2,snrdB(ii),yPdB2);
%MMSE Equalization Matrices
yC=(yAT'*yAT+10^(-snrdB(ii)/10)*eye(2*xx))\yAT';
C=(AT'*AT+10^(-snrdB(ii)/10)*eye(2*KN))\AT';
%FDE OFDM
yr1=yyn1(Ncp+1:end); % remove CP
yr2=yyn2(Ncp+1:end);
yrf1 = fft((yr1))/sqrt(length(yr1)); % Perform FFT
yrf2 = fft((yr2))/sqrt(length(yr2));
%ZF
yY_equal = yAT\([yrf1 yrf2].');
yre1=yY_equal(1:end/2);
yre2=yY_equal(end/2+1: end);
ydl=yre1.';
yd2=yre2.';
% MMSE
zY_equal=(yC*[yrf1 yrf2].');
zre1=zY_equal(1:end/2);
zre2=zY_equal(end/2+1: end);
zdl=zre1.';
zd2=zre2.';
%FDE FBMC
rf1 = fft(fftshift(yn1))/sqrt(length(yn1)); % Perform FFT
rf2 = fft(fftshift(yn2))/sqrt(length(yn2));
%ZF
Y_equal = AT\([rf1;rf2]);
re1=Y_equal(1:end/2);
re2=Y_equal(end/2+1: end);
% MMSE
xY_equal=(C*[rf1;rf2]);
xre1=xY_equal(1:end/2);
xre2=xY_equal(end/2+1: end);
%ZF
rxf1 = filter(Hk, 1, re1); % Matched filtering with prototype filter
rx1 = [rxf1(K:end); zeros(K-1,1)]; % Remove K-1 delay elements
rxf2 = filter(Hk, 1, re2); % Matched filtering with prototype filter
rx2 = [rxf2(K:end); zeros(K-1,1)]; % Remove K-1 delay elements
%MMSE
xrx1 = filter(Hk, 1, xre1); % Matched filtering with prototype filter
xrx1 = [xrx1(K:end); zeros(K-1,1)]; % Remove K-1 delay elements
xrx2 = filter(Hk, 1, xre2); % Matched filtering with prototype filter
xrx2 = [xrx2(K:end); zeros(K-1,1)]; % Remove K-1 delay elements
% OQAM post-processing
% Downsample by 2K, extract real and imaginary parts
if rem(frame, 2) % Imaginary part is K samples after real one
    r11 = real(rx1(1:2*K:end));
    r21 = imag(rx1(K+1:2*K:end));
    rcomb11 = complex(r11, r21);
    r12 = real(rx2(1:2*K:end));
    r22 = imag(rx2(K+1:2*K:end));
    rcomb12 = complex(r12, r22);
    %MMSE
    xr11 = real(xrx1(1:2*K:end));
    xr21 = imag(xrx1(K+1:2*K:end));
    xrcomb11 = complex(xr11, xr21);
    xr12 = real(xrx2(1:2*K:end));
    xr22 = imag(xrx2(K+1:2*K:end));
    xrcomb12 = complex(xr12, xr22);
else % Real part is K samples after imaginary one
    r11 = imag(rx1(1:2*K:end));
    r21 = real(rx1(K+1:2*K:end));
    rcomb11 = complex(r21, r11);
    r12 = imag(rx2(1:2*K:end));
    r22 = real(rx2(K+1:2*K:end));
    rcomb12 = complex(r22, r12);
    %MMSE
    xr11 = imag(xrx1(1:2*K:end));
    xr21 = real(xrx1(K+1:2*K:end));
    xrcomb11 = complex(xr21, xr11);

```

```

        xr12 = imag(xrx2(1:2*K:end));
        xr22 = real(xrx2(K+1:2*K:end));
        xrcomb12 = complex(xr22, xr12);
    end
    %FBMC ZF
    d1=(1/K)*rcomb11;
    d2=(1/K)*rcomb12;
    dec1(1:2:end)=d1(1:2:end);
    dec1(2:2:end)=-conj(d1(2:2:end));
    dec2(1:2:end)=conj(d2(2:2:end));
    dec2(2:2:end)=(d2(1:2:end));
    rec=(dec1+dec2)/2;
    rxSymbols = qamdemod(rec,M);
    [~,ber(frame,ii)] = biterr(inpSymbols(:,frame),rxSymbols);
    %FBMC MMSE
    xd1=(1/K)*xrcomb11;
    xd2=(1/K)*xrcomb12;
    xdec1(1:2:end)=xd1(1:2:end);
    xdec1(2:2:end)=-conj(xd1(2:2:end));
    xdec2(1:2:end)=conj(xd2(2:2:end));
    xdec2(2:2:end)=(xd2(1:2:end));
    xrec=(xdec1+xdec2)/2;
    xrxSymbols = qamdemod(xrec,M);
    [~,xber(frame,ii)] = biterr(inpSymbols(:,frame),xrxSymbols);
    %OFDM ZF
    ydec1(1:2:end)=yd1(1:2:end);
    ydec1(2:2:end)=-conj(yd1(2:2:end));
    ydec2(1:2:end)=conj(yd2(2:2:end));
    ydec2(2:2:end)=(yd2(1:2:end));
    yrec=(ydec1+ydec2)/2;
    yrxSymbols = qamdemod(yrec,M);
    [~,yber(frame,ii)] = biterr(yinpSymbols(:,frame),yrxSymbols);
    %OFDM MMSE
    zdec1(1:2:end)=zd1(1:2:end);
    zdec1(2:2:end)=-conj(zd1(2:2:end));
    zdec2(1:2:end)=conj(zd2(2:2:end));
    zdec2(2:2:end)=(zd2(1:2:end));
    zrec=(zdec1+zdec2)/2;
    zrxSymbols = qamdemod(zrec,M);
    [~,zber(frame,ii)] = biterr(yinpSymbols(:,frame),zrxSymbols);
end
end
%%
error=mean(ber);
xerror=mean(xber);
yerror=mean(yber);
zerror=mean(zber);
figure,
semilogy(snrdB,error,'-+b',snrdB,xerror,'-ok',snrdB,yerror,'r',snrdB,zerror,'-xg','LineWidth',1)
grid on
xlabel('SNR (dB)')
ylabel('BER')
legend('Hybrid FBMC-ZF','Hybrid FBMC-MMSE','OFDM-ZF','OFDM-MMSE')
set(findall(gcf,'-property','Font'),'Font','Cambria Math')

```

2. Hybrid SC-OQAM/FBMC MIMO BER (Chapter 5)

```

clc
clear all
N=64; % Number of subcarriers
Frame=100000; % Number of Monte Carlo repetitions
K=4; % Overlapping Factor
M=16; % QAM Modulation order
snrdB = 0:3:30; % SNR in dB
tap=20; % Number of multipath channel taps
%%
% Initialization for transmission
KN=K*N;
currSym1a=zeros(1,K*N);

```

```

currSym2a=zeros(1,K*N);
currSym1b=zeros(1,K*N);
currSym2b=zeros(1,K*N);
dataSubCar1a=zeros(N/2,1);
dataSubCar1b=zeros(N/2,1);
dataSubCar2a=zeros(N,1);
dataSubCar2b=zeros(N,1);
ber1=zeros(Frame,length(snrdB));
ber2=zeros(Frame,length(snrdB));
%% Prototype filter coefficients
H1=0.971960; H2=sqrt(2)/2; H3=0.235147;
factech=1+2*(H1+H2+H3);
hef(1:4*N)=0; %Oversampled Impulse response
for i=1:4*N-1
    hef(1+i)=1-2*H1*cos(pi*i/(2*N))+2*H2*cos(pi*i/N)-2*H3*cos(pi*i*3/(2*N));
end
hef=hef/factech;
%% Single Carrier matrix (M)
subcarriermapping='IFDMA'; %interleaved mapping
Q=N/(N/2);
In=eye(N/2);
MM=zeros(N,(N/2));
if subcarriermapping=='IFDMA'
    MM(1:Q:end,:)=In;
else %localized mapping
    MM(1:(N/2),:)=In;
end
Wn1=dftmtx(N/2)/sqrt(N/2);
IWn1=inv(Wn1);
Wm1=dftmtx(N)/sqrt(N);
IWm1=Wm1\MM;
DMWm1=MM.'*Wm1;
papr_FBMC=zeros(1,Frame);
papr_SC=zeros(1,Frame);
ain=zeros(1,Frame);
aout=zeros(1,Frame);
bin=zeros(1,Frame);
bout=zeros(1,Frame);
Adb=10; %As Adb increases the curve becomes more linear
Asat=(10^(Adb/10));
rap=comm.MemorylessNonlinearity('Method','Rapp
model','OutputSaturationLevel',Asat,'Smoothness',1);
%%
for m=1:Frame
    m
    in1=randi([0 M-1], N/4, 1);
    in2=randi([0 M-1], N/2, 1);
    A1=qammod(in1,M);
    A2=qammod(in2,M);
    %Alamouti for SC-FBMC
    Ant1a=zeros(size(A1));
    Ant1b=Ant1a;
    Ant1a(1:2:end)=A1(1:2:end);
    Ant1a(2:2:end)=-conj(A1(2:2:end));
    Ant1b(1:2:end)=A1(2:2:end);
    Ant1b(2:2:end)=conj(A1(1:2:end));
    %Alamouti for FBMC
    Ant2a=zeros(size(A2));
    Ant2b=Ant2a;
    Ant2a(1:2:end)=A2(1:2:end);
    Ant2a(2:2:end)=-conj(A2(2:2:end));
    Ant2b(1:2:end)=A2(2:2:end);
    Ant2b(2:2:end)=conj(A2(1:2:end));
    %OQAM modulation
    if rem(m,2)==1 % Odd symbols
        %for SC
        dataSubCar1a(1:2:end)=real(Ant1a);
        dataSubCar1a(2:2:end)=1i*imag(Ant1a);
        dataSubCar1b(1:2:end)=real(Ant1b);
        dataSubCar1b(2:2:end)=1i*imag(Ant1b);
    %
        %for FBMC

```

```

dataSubCar2a(1:2:end) = real(Ant2a);
dataSubCar2a(2:2:end) = 1i*imag(Ant2a);
dataSubCar2b(1:2:end) = real(Ant2b);
dataSubCar2b(2:2:end) = 1i*imag(Ant2b);
else % Even symbols
    %for SC
    dataSubCar1a(1:2:end) = 1i*imag(Ant1a);
    dataSubCar1a(2:2:end) = real(Ant1a);
    dataSubCar1b(1:2:end) = 1i*imag(Ant1b);
    dataSubCar1b(2:2:end) = real(Ant1b);
    %for fbmc
    dataSubCar2a(1:2:end) = 1i*imag(Ant2a);
    dataSubCar2a(2:2:end) = real(Ant2a);
    dataSubCar2b(1:2:end) = 1i*imag(Ant2b);
    dataSubCar2b(2:2:end) = real(Ant2b);
end
xw1a=Wn1*dataSubCar1a;
x1a=(IWmM1*xw1a)';
xw1b=Wn1*dataSubCar1b;
x1b=(IWmM1*xw1b)';
x2a=ifft(dataSubCar2a)'.*sqrt(length(dataSubCar2a));
x2b=ifft(dataSubCar2b)'.*sqrt(length(dataSubCar2b));
%Duplication of the signal
x1Ka=[x1a x1a x1a x1a];
x1Kb=[x1b x1b x1b x1b];
x2Ka=[x2a x2a x2a x2a];
x2Kb=[x2b x2b x2b x2b];
%We apply the filter on the duplicated signal
txSymb1a=x1Ka.*hef;
txSymb1b=x1Kb.*hef;
txSymb2a=x2Ka.*hef;
txSymb2b=x2Kb.*hef;
% Transmitted signal
currSym1a=txSymb1a+[currSym1a(1+N/2:end) zeros(1,N/2)];%
currSym1b=txSymb1b+[currSym1b(1+N/2:end) zeros(1,N/2)];%
tcurrSym1a=rap(currSym1a)'.';
tcurrSym1b=rap(currSym1b)'.';
currSym2a=txSymb2a+[currSym2a(1+N/2:end) zeros(1,N/2)];%
currSym2b=txSymb2b+[currSym2b(1+N/2:end) zeros(1,N/2)];%
tcurrSym2a=rap(currSym2a)'.';
tcurrSym2b=rap(currSym2b)'.';
%channel
h = (1/sqrt(tap))* (randn(4,tap)+sqrt(-1)*randn(4,tap))/sqrt(2);
h1 = h(1,:);h2 = h(2,:);h3 = h(3,:);h4 = h(4,:);
H11 = fft(h1,KN);H12 = fft(h2,KN);H21 = fft(h3,KN);H22 = fft(h4,KN);
A1 = diag(H11);A2 = diag(H12);A3 = diag(H21);A4 = diag(H22);
AT = [A1 A2;A3 A4];
x1aa=filter(h1,1,tcurrSym1a); x1ab=filter(h2,1,tcurrSym1b);
x1ba=filter(h3,1,tcurrSym1a); x1bb=filter(h4,1,tcurrSym1b);
s1a=x1aa+x1ab;
s1b=x1ba+x1bb;
x2aa=filter(h1,1,tcurrSym2a);x2ab=filter(h2,1,tcurrSym2b);
x2ba=filter(h3,1,tcurrSym2a);x2bb=filter(h4,1,tcurrSym2b);
s2a=x2aa+x2ab;
s2b=x2ba+x2bb;
for ii=1:length(snrdB)
% Demodulator
PdB1a=10.*log10(sum((abs(tcurrSym1a)).^2)/numel(tcurrSym1a));
yn1a=awgn(s1a,snrdB(ii),PdB1a);
PdB1b=10.*log10(sum((abs(tcurrSym1b)).^2)/numel(tcurrSym1b));
yn1b=awgn(s1b,snrdB(ii),PdB1b);
PdB2a=10.*log10(sum((abs(tcurrSym2a)).^2)/numel(tcurrSym2a));
yn2a=awgn(s2a,snrdB(ii),PdB2a);
PdB2b=10.*log10(sum((abs(tcurrSym2b)).^2)/numel(tcurrSym2b));
yn2b=awgn(s2b,snrdB(ii),PdB2b);
%FDE
Y1a=fft(yn1a)/sqrt(length(yn1a));
Y1b=fft(yn1b)/sqrt(length(yn1b));
Y2a=fft(yn2a)/sqrt(length(yn2a));
Y2b=fft(yn2b)/sqrt(length(yn2b));
C=(AT'*AT+10^(-snrdB(ii)/10)*eye(2*KN))\AT';

```

```

Y1=(C*[Y1a.';Y1b.']);
Y1a=Y1(1:end/2);
Y1b=Y1(end/2+1:end);
rela=ifft(Y1a).*sqrt(length(Y1a));
relb=ifft(Y1b).*sqrt(length(Y1b));
Y_equal2=(C*[Y2a.';Y2b.']);
Ye2a=Y_equal2(1:end/2);
re2a=ifft(Ye2a).*sqrt(length(Ye2a));
Ye2b=Y_equal2(end/2+1:end);
re2b=ifft(Ye2b).*sqrt(length(Ye2b));
% SC-FBMC
r1a=(rela).*hef; % We apply the filter
u1a=zeros(1,N);
r1b=(relb).*hef; % We apply the filter
u1b=zeros(1,N);
% FBMC
r2a=(re2a).*hef; % We apply the filter
u2a=zeros(1,N);
r2b=(re2b).*hef; % We apply the filter
u2b=zeros(1,N);
%downsampling
for k=1:K
    u1a=u1a+r1a(1,1+(k-1)*N:k*N);
    u1b=u1b+r1b(1,1+(k-1)*N:k*N);
    u2a=u2a+r2a(1,1+(k-1)*N:k*N);
    u2b=u2b+r2b(1,1+(k-1)*N:k*N);
end
u1a=DMWm1*(u1a./K);
sest1a=(Wn1\u1a).';
u1b=DMWm1*(u1b./K);
sest1b=(Wn1\u1b).';
sest2a=fft(u2a/K)/sqrt(length(u2a));
sest2b=fft(u2b/K)/sqrt(length(u2b));
% OQAM demodulation
if rem(m, 2)
    % Imaginary part is K samples after real one
    y11a = real(sest1a(1:2:end));
    y21a = imag(sest1a(2:2:end));
    rcomb1a = complex(y11a, y21a);
    y11b = real(sest1b(1:2:end));
    y21b = imag(sest1b(2:2:end));
    rcomb1b = complex(y11b, y21b);
    z11a = real(sest2a(1:2:end));
    z21a = imag(sest2a(2:2:end));
    rcomb2a = complex(z11a, z21a);
    z11b = real(sest2b(1:2:end));
    z21b = imag(sest2b(2:2:end));
    rcomb2b = complex(z11b, z21b);
else
    y11a = imag(sest1a(1:2:end));
    y21a = real(sest1a(2:2:end));
    rcomb1a = complex(y21a, y11a);
    y11b = imag(sest1b(1:2:end));
    y21b = real(sest1b(2:2:end));
    rcomb1b = complex(y21b, y11b);
    z11a = imag(sest2a(1:2:end));
    z21a = real(sest2a(2:2:end));
    rcomb2a = complex(z21a, z11a);
    z11b = imag(sest2b(1:2:end));
    z21b = real(sest2b(2:2:end));
    rcomb2b = complex(z21b, z11b);
end
%Alamouti decoding SC
d1a=rcomb1a;
d1b=rcomb1b;
dec1a=zeros(size(d1a));
dec1b=dec1a;
dec1a(1:2:end)=d1a(1:2:end);
dec1a(2:2:end)=-conj(d1a(2:2:end));
dec1b(1:2:end)=conj(d1b(2:2:end));
dec1b(2:2:end)=(d1b(1:2:end));

```

```

rec1=(dec1a+dec1b)/2;
%Alamouti decoding no SC
d2a=rcomb2a;
d2b=rcomb2b;
dec2a=zeros(size(d2a));
dec2b=dec2a;
dec2a(1:2:end)=d2a(1:2:end);
dec2a(2:2:end)=-conj(d2a(2:2:end));
dec2b(1:2:end)=conj(d2b(2:2:end));
dec2b(2:2:end)=(d2b(1:2:end));
rec2=(dec2a+dec2b)/2;
p=sum(abs(rec1).^2)/length(rec1);
p2=sum(abs(rec2).^2)/length(rec2);
rx1 = qamdemod(sqrt(10)*rec1./sqrt(p),M);
[~,ber1(m,ii)]= biterr(in1,rx1);
rx2 = qamdemod(sqrt(10)*rec2./sqrt(p2),M);
[~,ber2(m,ii)]= biterr(in2,rx2);
    end
end
error1=mean(ber1);
error2=mean(ber2);
figure,semilogy(snrdB,error1,'b',snrdB,error2,'r','LineWidth',1)
grid on
xlabel('SNR (dB)')
ylabel('BER')
legend('SC-OQAM/FBMC','OQAM/FBMC')
set(findall(gcf,'-property','Font'),'Font','Cambria Math')

```